AN EXPERIMENTAL INVESTIGATION OF A VORTEX STABILIZED ARC IN AN AXIAL MAGNETIC FIELD

Gordon L. Cann

Technology, Incorporated

Prepared for:

Aerospace Research Laboratories

March 1973

DISCLAIMER NOTICE

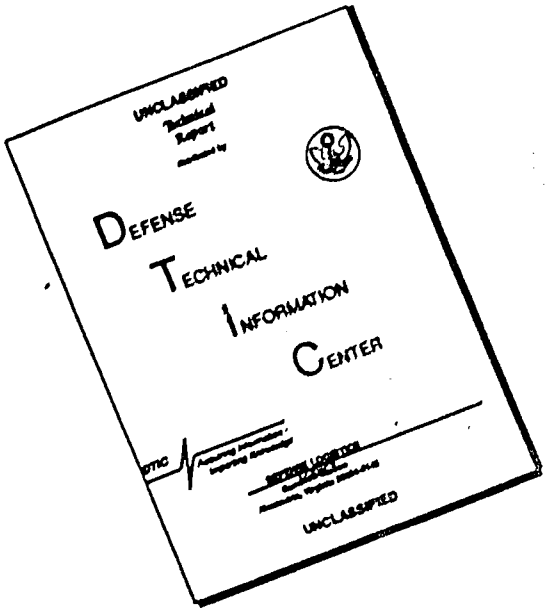

THIS DOCUMENT IS BEST QUALITY AVAILABLE. THE COPY FURNISHED TO DTIC CONTAINED A SIGNIFICANT NUMBER OF PAGES WHICH DO NOT REPRODUCE LEGIBLY.

ARL 73-0043
MARCH 1973

Aerospace Research Laboratories

AN EXPERIMENTAL INVESTIGATION OF A VORTEX STABILIZED ARC IN AN AXIAL MAGNETIC FIELD

GORDON L. CANN

TECHNOLOGY, INCORPORATED
DAYTON, OHIO

CONTRACT F33615-71-C-1463
PROJECT 7065

Approved for public release; distribution unlimited.

AIR FORCE SYSTEMS COMMAND
United States Air Force

NOTICES

When Government drawings, specifications, or other data are used for any purpose other than in connection with a definitely related Government procurement operation, the United States Government thereby incurs no responsibility nor any obligation whatsoever; and the fact that the Government may have formulated, furnished, or in any way supplied the said drawings, specifications, or other data, is not to be regarded by implication or otherwise as in any manner licensing the holder or any other person or corporation, or conveying any rights or permission to manufacture, use, or sell any patented invention that may in any way be related thereto.

Agencies of the Department of Defense, qualified contractors, and other Government agencies may obtain copies from:

Defense Documentation Center
Cameron Station
Alexandria, VA 22314

This document has been released (for sale to the public) to:

National Technical Information Services
Clearinghouse
Springfield, VA 22151

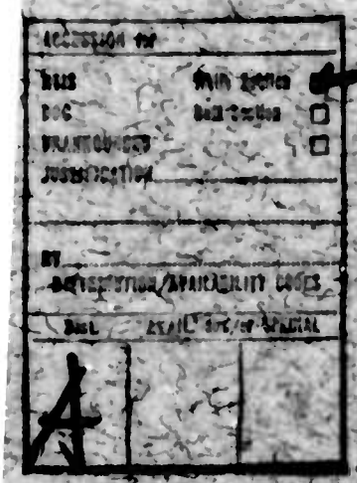

Copies of ARL Technical Reports should not be returned to the Aerospace Research Laboratories unless return is required by security considerations, contractual obligations, or notices on a specific document.

AIR FORCE/56780/25 April 1973 — 100

UNCLASSIFIED
Security Classification

DOCUMENT CONTROL DATA - R & D

(Security classification of title, body of abstract and indexing annotation must be entered when the overall report is classified)

1. ORIGINATING ACTIVITY (Corporate author) Technology Incorporated Dayton, Ohio	2a. REPORT SECURITY CLASSIFICATION Unclassified 2b. GROUP

3. REPORT TITLE

AN EXPERIMENTAL INVESTIGATION OF A VORTEX STABILIZED ARC IN AN AXIAL MAGNETIC FIELD

4. DESCRIPTIVE NOTES (Type of report and inclusive dates)

Scientific - Final

5. AUTHOR(S) (First name, middle initial, last name)

Gordon L. Cann

6. REPORT DATE	7a. TOTAL NO. OF PAGES	7b. NO. OF REFS
March 1973	~~101~~ 105	12

8a. CONTRACT OR GRANT NO	9a. ORIGINATOR'S REPORT NUMBER(S)
F33615-71-C-1463 b. PROJECT NO 7065 c. DoD Element 61102F d. DoD Subelement 681307	ARL 73-0043 9b. OTHER REPORT NO(S) (Any other numbers that may be assigned this report)

10. DISTRIBUTION STATEMENT

Approved for public release; distribution unlimited.

11. SUPPLEMENTARY NOTES	12. SPONSORING MILITARY ACTIVITY
TECH OTHER	Fluid Dynamics Facilities Rsch Lab Aerospace Research Laboratories (AFSC) Wright-Patterson AFB, Ohio 45433

13. ABSTRACT

An experimental program has been conducted to investigate the physical processes occurring in vortex stabilized arcs, with and without an applied axial magnetic field. Arc temperature measurements indicate centerline temperature to be insensitive to arc current and chamber pressure. Centerline temperature was found to decrease when arc length was increased, when orifice area was decreased and when axial magnetic field strength was increased. Magnetic field strength could only be increased to a "critical" value, at which point the discharge moved off the centerline line of the chamber and attached to its walls. A "stability criterion" has been derived to estimate the strength of the "critical" magnetic field. Experimental data agrees very well with the derived expression. Measurements have been made to determine arc "optical" diameter. There was an "apparent" increase in arc diameter when the magnetic field was applied which got larger as the field strength was increased. However, high speed resolution of light intensity from the arc indicated that arc diameter did, in fact, not increase but that the arc went into a helix. Helix diameter increased as magnetic field strength increased. Heat flux measurements indicate that it is possible to reduce conduction and convection losses from the arc to zero except at the electrodes and in the nozzle. The radiation measurements indicate that it is possible to reduce radiation losses from an arc by increasing arc length, making the flow through the orifice a minimum and by using as strong an axial magnetic field as is possible.

DD FORM 1 NOV 68 1473

UNCLASSIFIED
Security Classification

14 KEY WORDS	LINK A		LINK B		LINK C	
	ROLE	WT	ROLE	WT	ROLE	WT
gas heaters						
electric arcs						
vortex stabilized						
arc temperature/radiation						
arc stability criterion						
axial magnetic fields						

*U.S.Government Printing Office: 1973 — 759-492/464

ARL 73-0043

AN EXPERIMENTAL INVESTIGATION OF A VORTEX STABILIZED ARC IN AN AXIAL MAGNETIC FIELD

GORDON L. CANN

TECHNOLOGY INCORPORATED
DAYTON, OHIO

MARCH 1973

CONTRACT NO. F33615-71-C-1463
PROJECT NO. 7065

AEROSPACE RESEARCH LABORATORIES
AIR FORCE SYSTEMS COMMAND
UNITED STATES AIR FORCE
WRIGHT-PATTERSON AIR FORCE BASE, OHIO

ic

FOREWORD

This technical report documents the results of a program at ARL for investigating the interaction of an electric arc with an applied magnetic field. The program was executed by Dr. G. L. Cann, in the capacity of a Visiting Scientist at Aerospace Research Laboratories through Technology Incorporated, and was part of an overall effort to understand the processes occurring in high power, high pressure electric discharges interacting with g 6 flows where parallel or transverse magnetic fields may or may not be cpplied. The work was initiated in the Thermomechanics Research Laboratory by Mr. E. Soenghen and Mr. Kenneth Cramer and completed in the Fluid Dynamics Facilities Research Laboratory under the technical cognizance of Mr. Elmer Johnson.

The author is indebted to numerous colleagues within ARL who contributed to this research. Among them are Messrs. Herbert Schrade, James Miller, Frank Jarvis and Larry Burden, and Capts. Charles Miller, James Radley and Alan Hunter.

ABSTRACT

An experimental program has been conducted to investigate the physical processes occurring in vortex stabilized arcs, with and without an applied axial magnetic field. Arc temperature measurements indicate centerline temperature to be insensitive to arc current and chamber pressure. Centerline temperature was found to decrease when arc length was increased, when orifice area was decreased and when axial magnetic field strength was increased. Magnetic field strength could only be increased to a "critical" value, at which point the discharge moved off the centerline line of the chamber and attached to its walls. A "stability criterion" has been derived to estimate the strength of the "critical" magnetic field. Experimental data agrees very well with the derived expression. Measurements have been made to determine arc "optical" diameter. There was an "apparent" increase in arc diameter when the magnetic field was applied which got larger as the field strength was increased. However, high speed resolution of light intensity from the arc indicated that arc diameter did, in fact, not increase, but that the arc went into a helix. Helix diameter increased as magnetic field strength increased. Heat flux measurements indicate that it is possible to reduce conduction and convection losses from the arc to zero except at the electrodes and in the nozzle. The radiation measurements indicate that it is possible to reduce radiation losses from an arc by increasing arc length, making the flow through the orifice a minimum and by using as strong an axial magnetic field as is possible.

TABLE OF CONTENTS

LIST OF TABLES

LIST OF ILLUSTRATIONS

LIST OF ILLUSTRATIONS (Continued)

LIST OF ILLUSTRATIONS (Continued)

LIST OF ILLUSTRATIONS (Concluded)

LIST OF SYMBOLS

A_o	orifice cross-sectional area
A_1	reference cross-sectional area of orifice = $\pi/4 \times 10^{-6}$ meters
B	magnetic field strength
$C(T_{\mathfrak{C}_L}, p)$	$\frac{u_{\mathfrak{C}_L}}{\sigma_{\mathfrak{C}_L}} = \frac{P_r V}{I(L + L_o)L}$ = column correlation function
d_T	"optical" diameter of arc as determined from the temperature measurement
$d_{S.D.}$	"optical" diameter of arc as determined from the slow disc
$d_{F.D.}$	"optical" diameter or arc as determined from the fast disc
E	electric field strength in arc column
F	radial force on arc
f*	setting on mass flow rate control orifice
f†	observed frequency of light intensity when magnetic field points toward cathode
f-	observed frequency of light intensity when magnetic field points toward the anode
$f(\gamma/\gamma_o)$	radial distribution function of specific radiation
I_m	magnet current
I	arc current
i	light intensity
i_o	$\pi/3(4y-)^2 \gamma_o \, u_{\mathfrak{C}_L}$ reference light intensity
j	current density in arc
k	universal gas constant
L	arc length
L_o	distance arc extends into anode

m	gas mass flow rate
m_a	mass of gas molecula
$P_\gamma = P_w$	power radiated from arc = power absorbed in chamber wall
P	gas pressure
P_a	atmospheric pressure
P_w	pressure at chamber wall
γ_o	arc radius
R	radius of helix
R_d	radius on the spinning disc at which hole is drilled
t	time
T	temperature in degrees Kelvin
T_w	wall temperature
u	specific radiation from arc
$u_{\mathfrak{C}_L}$	specific radiation from arc centerline
V	arc potential drop
w	axial gas velocity
x_o	length of observation path through arc
y	distance of observation point from center of symmetry
Δy	diameter of hole in spinning disc
δ	inlet slit width
ρ	gas density
ρ_A	average gas density in the arc
ρ_o	gas density near wall
σ	electrical conductivity
$\sigma_{\mathfrak{C}_L}$	electrical conductivity at arc centerline

λ	wave length of helix
ω_d	angular velocity of spinning disc
ω_v	angular velocity of vortex core

SECTION I

INTRODUCTION

Designing arc heaters that can maintain an average gas enthalpy level of over 5×10^7 kJoule/kg while producing a gas flow with an impact pressure of over 100 atmospheres provides one of the most difficult challenges to arc scientists and engineers at the present time.

Arc heaters of the Linde design are capable of operation in this pressure regime, but they produce enthalpies of under 0.75×10^7 kJoule/kg (see Refs. 1,2). Constricted arc heaters have not been operated reliably at pressure levels of over 100 atms and even then, their enthalpy has been less than 1.5×10^7 kJoule/kg (Refs. 3,4). Scaling laws for constricted arc heaters (Ref. 5) indicate that an "optimum" constricted arc heater can perhaps operate at enthalpies of close to 2×10^7 kJoule/kg when the stagnation pressure is about 150 atmospheres. The major problem in the design of any coaxial arc heater is to keep the power loss from the arc, due to radiation, lower than the power transferred to the gas. Since at a given enthalpy, the power radiated from the arc increases at least linearly with pressure, it is obvious that techniques to keep the radiation as low as possible provide the clues to the design of high pressure arc heaters. The added fact that for a given pressure the radiation increases exponentially with temperature allows one to define the optimization needed. It is best described as a "mini-max" problem and can be stated as follows: an arc, interacting with a coaxial gas flow in a cylindrical chamber where the stagnation pressure is p_o and the Mach number is low, should heat the gas to an average enthalpy h_o without allowing the enthalpy in the arc to rise significantly above h_o at any axial or radial position. To accomplish this, the discharge must be made to remain diffused and the mass must <u>all</u> flow through the arc channel, i.e., mixing of the gas flow <u>and</u> arc must occur, at least near the outled end.

The phenomena that promote mixing of the gas in the arc with the external flow remains unclear. For this reason, techniques of estimating or controlling the arc radius in heater designs are unreliable. It seems clear that the turbulence level, the vorticity of the flow and the circulation in the gas, as well as the geometry of the heater, all play important roles in the "mixing" process. Very large temperature and velocity gradients exist in the arc heated gas. This gas therefore contains a high vorticity level. The exterior flow, even though it may be turbulent and spinning can often be considered as a potential flow. A very general law states that these two flows cannot mix. The potential flow can feed into the flow of high vorticity but material from this region cannot enter the region of potential flow. The result of the principle is very important: Arc heated gas cannot be mixed with the surrounding gas at any position along the arc

even though the turbulence level is high. The effect of free stream gas dynamic turbulence is thus reduced to increasing the rate of mass injection into the arc and thus causing the diameter to increase more rapidly than would occur in laminar flows.

In constricted arcs, it seems likely that the vorticity produced in the wake of the cathode and in the wall boundary layers is instrumental in promoting strong mixing of the whole flow with the arc. This has the advantage of allowing large mass flow rates to be heated in relatively short distances at the expense, however, of very large wall heat loads due to turbulent convection. In the Linde type heaters the size of the vortex core, in which the vorticity in the gas is concentrated, probably has the strongest influence upon the arc size. There is likely a one to one correspondence between the two diameters.

To maintain reasonably sized flow fields in which to test models at high stagnation pressure, the power level becomes very high. Once levels of over 20 Megawatts in the gas flow are required, the efficiency with which the gas is heated becomes a major economic consideration. Every effort, therefore, must be expended in obtaining the best efficiency possible in the arc heater. This requires minimizing the conduction heat losses as well as the radiation losses. For this reason, it is important to vortex stabilize the arc on the centerline of a large diameter chamber, so that conduction losses are reduced to near zero in this portion of the heater.

The conditions under which it is possible to stabilize the arc on the centerline of the device are not well understood. The first problem caused by arc instability occurred very early in the history of arc heaters. It was found that if the arc channel was much smaller than the constrictor diameter, the arc did not stay on the centerline, but moved about in an apparently random manner, causing severe local heating and often wall erosion, especially near the inlet. Examples of this can be found in Ref. 6. This problem was solved experimentally by introducing the gas tangentially to the heater column, thus vortex stabilizing the arc. The only disadvantage of this procedure was that under certain conditions gas recirculations would occur; i.e., the vortex would become unstable and break down into secondary flows. These secondary flows would often carry hot gas to critical structural components and cause local burning. Some knowledge of how the vortex stabilizes the arc and under what conditions secondary flows develop is needed for adequate design of the gas injection flow system.

A second type of arc instability was found to occur when an axial magnetic field was applied along the column. This instability has been studied extensively by Yuen (Ref. 7). He found that the arc assumed a corkscrew shape and was convected through the column by the gas flow. His studies also

indicated that the arc could be stabilized by both the radial temperature and velocity gradients in the column. Provided that the corkscrew arc does not touch the wall, there is reason to believe that this arc could be more effective than the axially stabilized arc for heating the gas. The technique to analyze this process is not immediately apparent; hence, some experiments could be of value in clarifying the parameters of the problem.

In this report, the results of a group of experiments aimed at investigating some of the fundamental physical processes discussed above of the arc-gas flow interaction are presented. The experiments were conducted in a device where wall interactions with the processes were eliminated by vortex stabilizing the arc near the centerline of a large diameter chamber.

SECTION II

NATURE AND SCOPE OF THE INVESTIGATION

This experimental program had several objectives. The first was to study the flow field in a vortex chamber with divided flow, part exiting through a central orifice, the remainder through an exit slit. The distribution of circulation, pressure and turbulence was to be determined by probes. The occurrence and nature of any vortex breakdown phenomena was also to be investigated. Secondly, the behavior of an arc in the flow was to be studied. Several specific questions were considered most relevant. One was concerned with the arc path. It is known that in some vortex chambers at a high enough Reynold's number (based on throughflow), the vortex core "breaks down"; i.e., it can move off the centerline and forms a helix (Ref. 8). Whether the arc follows this helical path or takes some intermediate path is a question of importance to arc heater design.

Another question of importance is that of determining the arc radius and centerline temperature. Also, the parametric manner in which they change with arc current, gas flow rate, chamber pressure, etc. needs to be known. It has been found extremely difficult to formulate this problem analytically because no fixed "boundary" occurs in the vortex core at which temperature and velocity values can be applied. It was hoped that some experimental data could be of value in determining

the nature of the boundaries values to this problem so that some reliable analytic technique could be developed for investigating this type of arc-gasflow interaction.

Lastly, some interesting phenomena had been observed to occur by the author and co-workers when an axial magnetic field was applied to an axial arc in a constrictor (Ref. 6); e.g., the arc radiation was observed to decrease as the magnetic field was increased at low arc currents but little effect occurred at high arc currents. Also at low arc currents the wall heat flux increased considerably. It was hoped that the nature of the phenomena occurring could be determined with the equipment at Aerospace Research Laboratories.

SECTION III

EXPERIMENTS

Over the past few years an impressive array of experimental equipment has been accumulated in the Thermomechanics Laboratory at Aerospace Research Laboratories for investigating electric discharge phenomena. Because of this it was possible to conduct this project using existing equipment with only minor modifications. The specific device used had been assembled for investigations into the feasibility of reducing the radial thermal conduction from a vortex stabilized arc by using an axial magnetic field. This concept was promoted by Alfven (Ref. 9) and tests in an annular configuration have been conducted by PieKaar, et al. (Ref. 10).

The major change that was made in the equipment was to remove a rod anode and replace it by a cylindrical anode with the orifice being 1.0 cm or 0.5 cm in diameter. This equipment was designed by F. Jarvis and fabricated by Technology Incorporated.

1. EXPERIMENTAL EQUIPMENT

A schematic diagram of the experimental equipment used in the arc interaction investigations is shown in Figure 1. It consists of the following components:

a) A water cooled copper cylinder with an internal diameter of 8.6 cm and length of 51 cm. The chamber is designed so that gas can be injected azimuthally over its entire length through a slit which communicates with a pressure inlet manifold. Similarly, gas is removed from the chamber at the outer periphery through another slit. The gap of this inlet slit is 1 mm, that of the outlet 2 mm. Access for viewing the discharge is provided by a quartz end-wall on the cathode end of the chamber. Six viewing windows are also provided in 3 diagonally opposed sets along the body of the chamber.

b) A conical tungsten cathode is mounted on a water cooled copper rod. The rod passes through a seal in the quartz end plate of the chamber and can be moved throughout the length of the chamber. The drive mechanism permits axial motion back and forth at a speed of about 2 cm/sec. The arc length can thus be varied over a range of 5 cm to over 35 cm while the discharge current is flowing.

c) An anode assembly is mounted on the end plate opposite to that of the cathode. It consists of a water-cooled copper dylinder of 1 cm internal diameter that is 15 cm in length. During the program another anode of 1/2 cm internal diameter and 6 cm length was also used.

d) A set of 8 Magnion, water-cooled coils are placed along the length of the chamber to provide a fairly uniform axial magnetic field. The coils provide 15 gauss per ampere of magnet current. The magnetic field strength is completely variable from 0 to over 12,000 gauss. Provision is made so that the magnet current can be reversed.

The flow-rate of gas into the chamber is controlled by using a variable area sonic nozzle. The calibration of the sonic orifice in terms of the orifice area control setting (f^*) is shown in Figure 2. The pressure in the chamber can be varied for a fixed f^* by opening or closing a valve on the by-pass gas system which controls the flow through the exit slit of the chamber.

2. ELECTRICAL AND HEAT BALANCE INSTRUMENTATION AND MEASUREMENTS

Provision was made to continuously record eight channels of data. The data recorded was changed periodically but for most of the experiments the following information was recorded:

a) The arc current.

b) The arc voltage.

c) The R.M.S. value of the arc voltage fluctuations in the range 100-1500 kz.

d) The R.M.S. value of the arc voltage fluctuations in the range 1500-10,000 kz.

e) The R.M.S. value of the arc voltage fluctuations in the range 10,000-100,000 kz.

f) The magnet current.

g) The arc length.

h) The radiation intensity as determined by the output from a photo-cell focused on the arc a few millimeters in front of the anode.

The power absorbed by the cooling water was determined by measuring temperature rises in the water and the water flow rate. The following power measurements were made:

a) The power in the anode cooling water.

b) The power in the cathode cooling water.

c) The power in the water circuits that cooled the copper arc chamber.

d) The power in the by-pass gas.

e) The power in the gas exhausted through the central orifice.

Besides these measurements, thermocouples were used to measure the temperature of the gas leaving both the "by-pass" calorimeter that swallowed the orifice gas flow.

Since power levels of from 20 kw to 150 kw were dissipated in the discharge, the instrumentation was designed to measure accurately power levels of over 0.5 kw. Throughout the testing program no measurable power was ever recovered from the by-pass gas and the temperature of the gas remained consistently at values considerably lower than 60°C. This measurement led to the very important conclusion that the by-pass gas was never heated either by conduction or convection from the arc. Also, all of the power collected in the chamber cooling water was due to radiation from the hot gas in the arc. This ability to unambiguously measure the radiated power made it possible to measure some of the fundamental properties of the arc-gas flow and arc-magnetic field interactions.

Even at the highest currents the power in the cathode cooling circuit was always less than 1% of the input power. This meant that the power could practically all be accounted for by measuring:

a) The power radiated to the chamber from the arc.

b) The power radiated and conducted to the anode.

c) The power convected out of the central orifice with the gas flow.

Some curves representing typical values of the arc potential drop, the power radiated, and the anode power loss in argon and nitrogen are presented in Figures 3 through 15.

3. TEMPERATURE MEASUREMENTS

It was decided to try and measure the temperature of the arc using the most easily available technique. A device to scan the arc through a side window was constructed. A slit, a 5460 A filter and a photomultiplier were placed on the scanning device and optics arranged to focus the image of the arc on the slit. A standard lamp was used to obtain an absolute calibration of the intensity. The intensity values were plotted and the best smooth, symmetric profile was drawn through the points. Several of the intensity curves are shown in Figures 16 through 19. The smoothed data was then inverted, using a standard program for the Computer. The "inverted" intensities were then converted into temperatures using the data and extrapolation formulae given by Morris (Ref. 11). The relation between intensity at 5460 A and temperature that was used for argon and nitrogen at 2 atmospheres pressure are shown in Figures 20 and 21. It should be noted that all of the values below 9000°K are extrapolated and hence subject to considerable error.

The measured values of centerline temperature and arc radius are presented in Table I. Several temperature profiles are shown in Figures 22 and 23.

Provision was made for measuring the temperature at two positions. One was just a few millimeters in front of the anode. The other was 17.3 cm upstream of this position.

4. MEASUREMENT OF ARC "OPTICAL" DIAMETER

Three different pieces of equipment were used from which the arc "optical" diameter could be estimated. The first was the device for scanning the arc through the 5460 A filter described in Paragraph III.3. The "optical" diameter in this case will be defined as the diameter at which the intensity measurement is lower than the peak value by a factor of 20. Values of this optical diameter (d_T) are presented in Table II.

The second method of estimating an "optical" arc diameter was by using a "slow disc" device, i.e., one that scanned automatically across the arc 8 times a minute. The disc had 8 holes 0.33 m.m. in diameter drilled in it at a radius of 1.5 cm. It was mounted on the second hand of a clock drive so that it rotated once every minute. An image of the arc was focused on the disc and a photo cell was placed behind the wheel. The signal from the photocell was amplified and recorded on one channel of an Offner recorder. The optical diameter $d_{s.d.}$ was estimated from this measurement by determining the diameter at which the signal had dropped to 5% of its peak value. Some values of this optical diameter $d_{s.d.}$ are shown in Table III.

The third piece of equipment used to estimate an optical diameter was similar to the slow disc. The main difference was that the disc rotated at 30 hz instead of 1/60 hz. The construction of this device is discussed in Paragraph III.5. The optical diameter $d_{F.d.}$ was estimated from the oscilloscope traces obtained from this machine by once again determining the pulse width at which the signal had dropped to 5% of its peak value. Some values of this optical arc diameter $d_{F.d.}$ are presented in Table IV.

5. MAGNETIC FIELD EFFECTS

When an axial magnetic field was superposed along the axis of the arc a number of effects were observed.

In argon:

1) The light intensity and the total radiated power from the arc decreased as the magnetic field strength was increased, Figure 24.

2) The arc voltage remained almost constant or decreased slightly, Figure 25.

3) The luminous area of the discharge increased in cross-sectional area as the magnetic field strength was increased, Figure 26.

4) The electrical noise level did not change significantly over the frequency ranges being studied, Figure 27.

Similar effects were observed in nitrogen gas except that the voltage increased substantially as the magnetic field strength was increased, Figures 28 through 32.

For all cases tested, as the magnetic field was increased a critical magnetic field strength was found at which the arc moved discontinuously from near the centerline of the chamber to the chamber wall. Fastex motion pictures of the transition indicated

that the arc apparently enlarged and then developed a very turbulent appearance for a short period of time. A current filament then appeared extending radially outward from the anode to the chamber wall and rotated clockwise. A similar current filament developed at the cathode end extending from the chamber wall to the cathode. This filament rotated counterclockwise. The arc was never run in this mode for more than a few seconds.

It is postulated that the transition observed occurred at a magnetic field strength high enough such that the gas vortex was no longer strong enough to stabilize the discharge on or near the centerline. This transition point is hence called the stability limit.

In order to study the phenomena associated with the "apparent enlarging" of the arc at weak magnetic field strengths, a special device was constructed. This consisted of a disc 20 cm in diameter mounted on the synchronous motor that spun it at 30 or 60 hz. A hole 0.33 mm in diameter was drilled at a point 76.5 mm from the disc centerline. A photo cell was mounted on the disc behind the hole and the signal from it was brought out through slip rings. The signal was displayed on an oscilloscope that had a time delay built into the sweep so that the signal could be centered. The light from a side port in the arc chamber was focused on the disc, which was placed at a distance of about 2 meters from the discharge. The optical system had an amplification of about a factor of 4.

A series of pictures taken with this device are shown in Figure 33. The magnetic field is aligned in the direction of the cathode and the field strength is progressively increased throughout the series. In Figure 34 a second series of oscilloscope pictures from the rotating disc are shown in which the magnetic field is directed toward the anode.

When no magnetic field is applied the intensity curve is seen to be similar to a gaussian distribution. When a small magnetic field is applied and directed toward the cathode a wave-like structure, superposed on the gaussian, appears. The frequency is approximately 12,000 hz near the centerline and 6,000 hz near the edge and does not change significantly as the magnetic field strength is increased. By reversing the direction of the applied magnetic field the frequency of the oscillations is greatly reduced (compare Figures 33 and 34).

Since the noise generated by the discharge does not increase but rather decreases in argon when the magnetic field strength is increased, the oscillations observed must be "space-like" rather than "time-like." On the basis of these observations it was postulated that the application of the magnetic field drives the arc into a helix. The "effective" arc diameter changes shown in Figure 26 can be explained by the diameter of the helix increasing as the magnetic field is increased.

The frequency change which occurs by reversing the magnetic field can be accounted for by assuming that the vortex is convected with the gas at or near the combined axial and azimuthal velocities.

It is possible to estimate the frequency of the observed light fluctuations by making some simple calculations. The helix will always form in such a manner as to increase the centerline magnetic field strength. Looking toward the anode the gas spins counterclockwise. When the applied magnetic field points toward the cathode the helical arc will be wound counterclockwise progressing toward the cathode. The observed frequency (f_+) at any position would then be given by

$$f_+ = \frac{w}{\lambda} + \frac{\omega_v}{2\pi}$$

where

w = axial velocity a point of observation

ω_v = angular velocity of vortex cove

λ = wave length of helix

f_+ = observed frequency of arc spin.

When the magnetic field points toward the anode, the observed frequency (f_-) would be

$$f_- = \frac{w}{\lambda} - \frac{\omega_v}{2\pi}$$

In Appendix I the light intensity seen by the photo cell on the spinning disc has been computed for an arc with a parabolic profile of radiated power/vol. This expression is

$$i = \frac{\pi}{5} (\Delta y)^2 \gamma_o u_{\mathcal{L}} \left\{1-\left(\frac{R_d \sin\omega_d t + R\cos 2\pi(ft)t}{\gamma_o}\right)^2\right\}^{3/2}$$

where

Δy = diameter of hole in spinning disc

R_d = radius on the disc at which hole is made

ω_d = angular spin frequency of disc

R = radius of helix

$u_{\mathcal{L}}$ = specific radiation at center of arc

γ_o = arc radius

When the angular extension of the arc on the disc is small the approximation that sin $\omega_d t = \omega_d t$ can be made. Hence, when the helix radius R is zero (no applied magnetic field) then the expression for the light intensity becomes

$$i = i_o \left\{ 1 - \left(\frac{R_d \omega_d t}{\gamma_o}\right)^2 \right\}^{3/2}$$

This expression is plotted in Figure 35. Experimental points from a measured intensity profile are shown for comparison. The agreement appears to be quite good.

The curves in Appendix I showing the computed intensity profiles for a spinning and translating helix agree qualitatively with the measured profiles shown in Figures 33 and 34. Discrepancies between the theoretical and experimental curves can probably be explained by one or more of the following:

a) The wavelength of the helical arc path is not constant.

b) The current may break up into two or more helical arc paths.

c) The axial and radial velocities vary both radially and axially and hence the helix may be assymmetric.

d) The attachment points on the anode and cathode may cause the discharge to move relative to the gas by controlling the arc spin rates near the electrodes.

The program schedule did not permit investigations into any of these hypotheses; hence complete correlation between theory and experiment was not feasible.

6. ARC STABILITY INVESTIGATIONS

When the arc was operated in argon it was possible to increase the magnetic field rapidly and have the chamber pressure and arc current remain constant. In nitrogen this was not the case because of the rapid increase of arc voltage with increasing magnetic field. For this reason, the experiments for establishing the arc stability limits were conducted in argon. The procedure followed was to set the injection velocity, chamber pressure and arc current. The magnetic field was then turned on and slowly increased (.2 Tesla/sec.) A high speed recorder (25 mm/sec) traced out continuously and simultaneously on graph paper the values of magnetic current, arc current, arc voltage, arc electrical noise, arc radiation intensity and the optical noise level of the radiation. A sample trace is shown in Figure 36.

The criterion for determining the critical magnetic field strength was to pick the point at which a discontinuity occurred in the arc potential drop. The transition was repeatable and unambiguous over most of the range of parameters investigated. Some difficulty was encountered in obtaining a clean transition at low spin velocities when the arc current was high. Transition was expected at very low values of the applied magnetic field. Electrode erosion and non-steady behavior were often observed in this regime; hence no data was obtained for transition due to the self-magnetic field alone.

The experimental data is plotted in Figure 37. The equation developed in Reference 6 for the stability criterion was used to define the correlation parameters. Some arbitrary assumptions were made in order to express the destabilizing and stabilizing forces in terms of measured quantities. These were:

1) The wavelength or pitch of the helix was equal to the orifice or anode radius R_A.

2) The gas density difference $(\rho_o - \rho_{arc})$ was approximated by using the gas density at 300°K and at the pressure measured near the centerline.

3) The gas spin velocity v_{arc} was approximated by computing the gas injection velocity ($\dot{m}$ RTw/ 6 Lpw) and dividing it by a factor of two and then multiplying it by the radius ratio R_W/R_A, the wall radius divided by the anode radius. This was done on the basis of some experimental information obtained from hot wire measurements in a vortex chamber with no arc, where the spin velocity at the anode radius appeared to be approximately one half of what would occur if it were a potential vortex flow (constant circulation).

Because of these assumptions, the degree of correlation obtained is completely fortuitous. Also, since the transition is from a "stable" helical arc to spinning radial current filaments, there is some doubt as to the applicability of the stability equation used. Until further studies can be conducted it seems best to use the data and the stability criterion only as guides to estimating critical magnetic field strengths in similar configurations.

7. EFFECTS OF PLACING A FILTER CIRCUIT IN SERIES WITH THE ARC

At certain values of arc power it was observed that a rather high 360 hz ripple component occurred in the arc potential drop and in the luminous power radiated from the discharge. For this reason it was decided to construct a filter system and put it in the arc circuit. The filter consisted of a water cooled coil

(inductor)(≈2m.h) in series with the arc and a condenser bank (≈.05f) across the discharge. The procedure used in determining the effectiveness of the filter was as follows:

1) The inductor was always kept in the circuit.

2) The arc was started with the condenser bank disconnected.

3) The condenser bank was charged up to the arc potential by connecting it across the arc electrodes through a charging resistor (1K ohms).

4) Once the condensers were charged to within a few volts of the arc potential drop, the charging resistor was shorted out with a switch.

In argon, when the charging resistor was shorted out, a very significant reduction in the noise level occurred over all the frequency ranges being monitored (see Figure 38). Also, the optical ripple dropped from a value of about 10% to less than 1%.

In nitrogen, on the other hand, whenever the charging resistor was shorted out, the arc immediately extinguished. This occurred even though the condensers were charged up to within a fraction of a volt of the average arc potential. No simple explanation could be found for this behavior. It should be noted, however, that the electrical noise level with nitrogen was many factors higher than with argon.

8. OSCILLATIONS AND FLUCTUATIONS

There were a wide variety of oscillations and fluctuations observed in the arc potential drop, the luminous intensity and in the arc chamber pressure.

a. Low Frequency Effects

(1) Pulsing 1/10 - 15 hz

When the applied magnetic field was increased, a value was reached at which large amplitude, low frequency pulses sometimes occurred. An example of the pulsing mode is shown in Figure 39 where the fluctuations in voltage, light intensity and 2 k hz noise are displayed. This pulsing could be stopped by making any one of the following changes:

(a) Reducing the arc length.
(b) Increasing the chamber pressure.
(c) Decreasing the magnet current.
(d) Decreasing the arc current.

It was possible to adjust the parameters of the test, so that pulsing would occur at rates as low as 1 every 10 seconds. Measurements with a piezo electric pressure gauge indicated that pressure fluctuations were occurring in phase with the voltage fluctuation.

(2) Low Frequency Oscillations 20-100 hz

Under similar circumstances to those described above, sometimes regular oscillations would occur in the same quantities. An example of this is shown in Figure 40. These oscillations could also be stopped by making any one of the changes noted above.

Measurements and observations of both these types of oscillations led to the conclusion that they were fundamentally fluctuations in the mass of gas in the volume of the arc chamber and the gas feed system. Calculations indicated that because the inlet slot was not operated sonically, it was possible to set up oscillations in the frequency range observed.

b. Audio Oscillations 1500 - 9000 hz

The vortex was observed to have a characteristic frequency associated with it, independent of whether the arc was running or not. The main effect observed when the arc was turned on was that the amplitude of the sound increased by one or two orders of magnitude. The frequency appeared to be associated primarily with the spin rate of the gas as it left the orifice. Near the device, the noise level was high enough to require ear plugs for the operating personnel. Some spectral distributions of the audio noise as picked up by a microphone are shown in Figures 41 and 42. Figures 43 through 47 also show the audio oscillations occurring at the same time as the low frequency oscillations.

9. CATHODE ATTACHMENT REGION

Using the rapidly spinning disc a few measurements were made on the arc properties near the cathode attachment point. The tests were conducted in argon gas at a pressure of 40 psia and with an arc current of 275 amperes. The discharge path grew in cross-section from a few millimeters at the attachment point to a diameter of about 7.5 mm in less than a millimeter. From then on it increased in diameter slowly to a value of about 9.0 mm at a position two centimeters from the attachment point. The centerline radiation decreased rapidly by moving downstream of the attachment point (see Figure 48). These measurements indicate that the highest temperature in the arc is reached in the cathode attachment region and that the temperature drops rapidly in approaching the column.

SECTION IV

DATA CORRELATION

The measurements of temperature indicated that the arc temperature remained remarkably constant throughout its length except within a few millimeters of the cathode attachment region. This makes it possible to neglect axial gradients to first order and to analyze the data using the assumption of constant centerline temperature. As pointed out in Reference 5, when this occurs a quantity can be obtained, using the overall measurements of arc voltage, current, and arc length that is a unique function of the arc centerline temperature and the chamber pressure. The only assumption needed is that the radial profiles of specific radiation u and the electric conductivity σ are similar. We then find that

$$\frac{P_V V}{IL(L+L_o)} = \frac{u_{\ell}}{\sigma_{\ell}} = C(T_{\ell}, p) = \frac{P_W V}{IL(L+L_o)}$$

where L_o is the distance that the discharge extends into the anode before it attaches to the anode surface. Now, the temperature measurement data and the arc optical diameter measurements both indicate that the arc centerline temperature does not increase significantly as the arc current is increased. Rather, the cross-sectional area of the arc increases proportionally with the arc current so that the centerline current density remains constant. For this reason the parameter $P_W V/IL(L+L_o)$ is expected to be independent of the arc current if the pressure is maintained constant. See Figure 49.

In order to try and get an estimate of the value of L_o, the measured quantity $P_W V/I$ was plotted vs. the arc length L in Figure 50 for tests conducted at a constant pressure of 30 psia in nitrogen and with orifice diameters d_A of 1 cm and 1/2 cm. The result is rather surprising: first, instead of being quadratic in the arc length as expected, the function is linear with an intercept giving a value of $L_o \approx 6$ cm; second, the value of $P_W V/I$ appears to be approximately proportional to the cross-sectional area of the orifice.

The conclusion to be drawn from this is that the arc centerline temperature decreases as the arc length is increased and as the orifice area is decreased. Also it does so in a manner to keep the quantity $u_{\ell} L/\sigma_{\ell} A$ constant.

The next question of interest is that of determining the manner in which the quantity $u_{\ell} L/\sigma_{\ell} A$ changes with pressure.

Theory (Reference 12) indicates that the electrical conductivity changes little with pressure and that the specific radiation increases with pressure at a rate that varies between linear and quadratic at constant temperature. The temperature measurements shown in Section III.2 indicate that the arc temperature does not change significantly as the pressure in the arc chamber is varied. Therefore, a plot of the parameter $P_wV/I(L+L_o)$ vs. chamber pressure should indicate approximately the relation between u_ℓ and pressure. Such a plot is shown in Figure 51 for nitrogen with orifice areas of 1 cm and 1/2 cm. The data correlates well using the relation that $P_wV/I(L+L_o)$ is proportional to $(p/p_a)^{3/2}$. These two plots indicate that when there is no applied magnetic field the following quantity should be constant:

$$\frac{P_wV}{IL_1(L+L_o)} \frac{A_1}{A} \left(\frac{p_a}{p}\right)^{3/2} - \frac{u_\ell}{\sigma_\ell} \frac{A_1}{A} \frac{L}{L_1} = \langle C_a \rangle_o$$

The function will be called the column function. Some representative points are presented in Table V and Figures 52, 53, and 54 to indicate the scatter in the experimental values of $\langle C_a \rangle_o$.

Some discrepancy exists between the measured centerline temperature and the estimated temperature using the specific radiation and electrical conductivity data from Reference 13. A plot of the function as computed from the data in Reference 13 is shown in Figure 55. For an arc in nitrogen at 2 atmospheres pressure, 20 cm long, carrying 100 amperes of current and operating with a 1 cm diameter orifice the measured temperature is 12,600°K. The temperature as estimated from Figure 55 and the data in Table V is 12,100°K.

The data shown in Figure 24 indicate that the radiation from the arc decreases by several factors as the strength of the applied magnetic field is increased. Using the information gained from the stability investigation in Section III.6 a parameter which characterizes the magnetic field interaction with the arc and the flow field was derived. This parameter can be expressed as

$$\frac{L}{L_1} \frac{I_A I_M \, p/p_a}{(f^\theta)^2}$$

and is similar to the terms in the stability criterion, except for the length terms (L/L_1). The C function is plotted vs. this parameter in Figure 56. Although there is considerable scatter, the correlation can be of considerable value in estimating magnetic field strengths necessary to effect a significant reduction in the "normal" amount of arc radiation.

SECTION V

CONCLUSIONS

The "arc physics" of a vortex stabilized arc operating over the restricted range of parameters encompassed in this study can be summarized as follows:

1) The arc centerline temperature is relatively constant over its length. Near the cathode the temperature rises about 1000-2000°K.

2) The arc centerline temperature does not change significantly with changes in the arc current. The arc channel area increases approximately proportional to the arc current so that the centerline current density remains relatively constant.

3) The arc centerline temperature is relatively insensitive to the pressure in the arc chamber. Even though the centerline current density rises (arc channel diameter decreases) as the pressure increases, it appears that the increase in radiated power and in the mass flow of gas being heated helps to keep the arc temperature relatively constant.

4) The arc centerline temperature decreases as the arc length is increased, as the orifice area is decreased and as the strength of the axial magnetic field is increased. The effect of the first two can be explained qualitatively as resulting from the change in the amount of gas per unit length being injected radially into the region of arc heated gas. The latter effect can be due to the centripedal forces on the heated gas in the helical arc. This force convects the hot gas out of the arc channel and drives it toward the centerline of the chamber, thus causing cool gas to enter the arc and reduce the centerline temperature of the arc.

The application of an axial magnetic field to an axial vortex stabilized arc causes the arc to follow a helical path. As the strength of the magnetic field is increased the following things occur:

1) The radius of the helical arc path increases.

2) The centerline temperature of the arc decreases.

3) The power radiated from the arc decreases.

4) In nitrogen the arc potential drop increases. In argon gas the arc potential drop remains constant or decreases slightly.

5) The arc eventually is driven unstable and strikes over to the chamber wall.

6) When the magnetic field strength is slightly less than the critical value for driving the arc unstable, pulsations and/or oscillations in the arc voltage, the radiation intensity and the chamber pressure can occur. These are a very low frequency phenomena and are probably associated with fluctuations in the mass in the arc chamber.

The "optical" diameter of the arc was measured and found to vary in the following manner.

1) The arc diameter is larger near the cathode end than it is near the anode end by a factor of about 1.27.

2) The arc channel area increases proportional to the arc current, so that the centerline current density remains relatively constant.

3) The arc channel area decreases as the chamber pressure increases.

4) The arc channel area increases as the arc length is increased.

Putting a filter into the arc electrical circuit caused a significant reduction in the noise and ripple of the anode to cathode voltages in argon gas. The arc would not operate in nitrogen gas when the filter was in the circuit.

TABLE I

MEASURED ARC TEMPERATURES AND RADII

Gas	I Amps	p psia	Position	L cm.	d mm	T°K
N_2	100	30	cath	20	4.30	13,300
N_2	100	30	anode	20	3.40	12,600
N_2	100	30	anode	20	3.37	12,100
N_2	150	30	anode	20	4.35	12,400
N_2	175	30	anode	20	5.18	12,200
N_2	100	60	anode	20	2.71	12,400
N_2	100	75	anode	20	2.70	13,000

TABLE II

OPTICAL DIAMETER (d_T) OF ARC AS DETERMINED FROM TEMPERATURE MEASURING EQUIPMENT

Gas	I Amps	p psia	L cm.	Position	d_T mm
N_2	100	30	20	anode	3.37
N_2	150	30	20	anode	4.35
N_2	175	30	20	anode	5.18
N_2	100	30	20	anode	3.40
N_2	100	60	20	anode	2.71
N_2	100	75	20	anode	2.77
N_2	150	30	25	anode	4.30
N_2	150	30	25	cathode	5.70

TABLE III

OPTICAL DIAMETER ($d_{S.D.}$) OF ARC AS DETERMINED FROM MEASUREMENTS WITH THE SLOW DISC

Gas	I Amps	p psia	L cm.	Position	$d_{S.D.}$ mm
A	100	30	30	anode	6.6
A	150	30	30	anode	7.6
A	200	30	30	anode	9.7
A	250	30	30	anode	10.4
A	300	30	30	anode	11.4
A	200	30	10	anode	7.3
A	300	30	10	anode	8.8
A	400	30	10	anode	9.9
A	450	30	10	anode	10.5
A	500	30	10	anode	11.1
N_2	100	30	20	anode	3.4
N_2	100	60	20	anode	3.0
N_2	100	75	20	anode	2.9
N_2	150	30	20	anode	4.3
N_2	200	30	20	anode	5.4

TABLE IV

OPTICAL DIAMETER ($d_{F.S.}$) OF ARC AS DETERMINED FROM MEASUREMENTS WITH THE FAST DISC

Gas	I Amps	p psia	L cm.	Position	$d_{F.D.}$ m.m.
A	100	30	9	anode	5.0
A	100	30	18	anode	5.4
A	100	30	36	anode	6.2
A	200	30	36	anode	8.1
A	200	30	18	anode	7.4
A	200	30	9	anode	6.7
A	300	30	36	anode	10.8
A	300	30	18	anode	8.1
A	300	30	9	anode	7.3
A	300	43	9	anode	6.4
A	300	43	18	anode	6.9
A	300	43	36	anode	8.3
A	275	40	19	17.3 upstream of anode	8.6
N_2	100	30	20	"	3.8
N_2	100	30	30	"	4.3
N_2	100	30	36	"	4.6
N_2	100	30	10	anode	3.1
N_2	100	30	20	anode	3.4
N_2	100	30	30	anode	3.7

TABLE V

TABULATED DATA FOR NITROGEN SHOWING
AMOUNT OF SCATTER IN CORRELATION FUNCTION

f*	I Amps	V Volts	P k.w.	L cm.	p psia	d cm.	$\langle C_a \rangle_o^2$ Volts^2
.8	100	584	4.93	10	30	1.0	3.16×10^5
.8	100	633	7.00	20	30	1.0	3.12×10^5
.8	100	717	8.49	30	30	1.0	3.00×10^5
.8	100	625	7.34	20	30	1.0	3.12×10^5
.8	100	707	9.05	30	30	1.0	3.14×10^5
.8	100	770	9.53	36	30	1.0	3.10×10^5
1.0	100	699	7.75	20	35	1.0	2.80×10^5
1.0	150	609	14.3	20	35	1.0	3.00×10^5
1.0	200	553	21.0	20	35	1.0	3.00×10^5
2.0	100	581	6.17	20	25	1.0	3.17×10^5
2.0	100	739	8.65	20	35	1.0	3.30×10^5
2.0	100	874	10.6	20	45	1.0	3.42×10^5
2.0	100	948	12.3	20	55	1.0	3.15×10^5
1.5	100	592	6.4	40	40	0.5	3.78×10^5
1.5	100	680	9.5	40	50	0.5	4.60×10^5
2.0	100	406	4.0	30	30	0.5	3.20×10^5
2.0	150	320	7.05	30	30	0.5	2.95×10^5
1.5	100	450	4.23	20	35	0.5	4.00×10^5
1.5	100	546	5.60	20	45	0.5	4.50×10^5
1.5	100	605	6.42	20	55	0.5	4.15×10^5
1.5	100	670	7.15	20	65	0.5	4.10×10^5

$$\frac{P_r V}{\Gamma L_1 (L+L_o)} \frac{A_1}{A} \left(\frac{p_a}{p}\right)^{3/2} = \langle C_a \rangle_o \qquad L = .20 \quad L_o = .06 \quad A_1 = \frac{\pi}{4} 10^{-4}$$

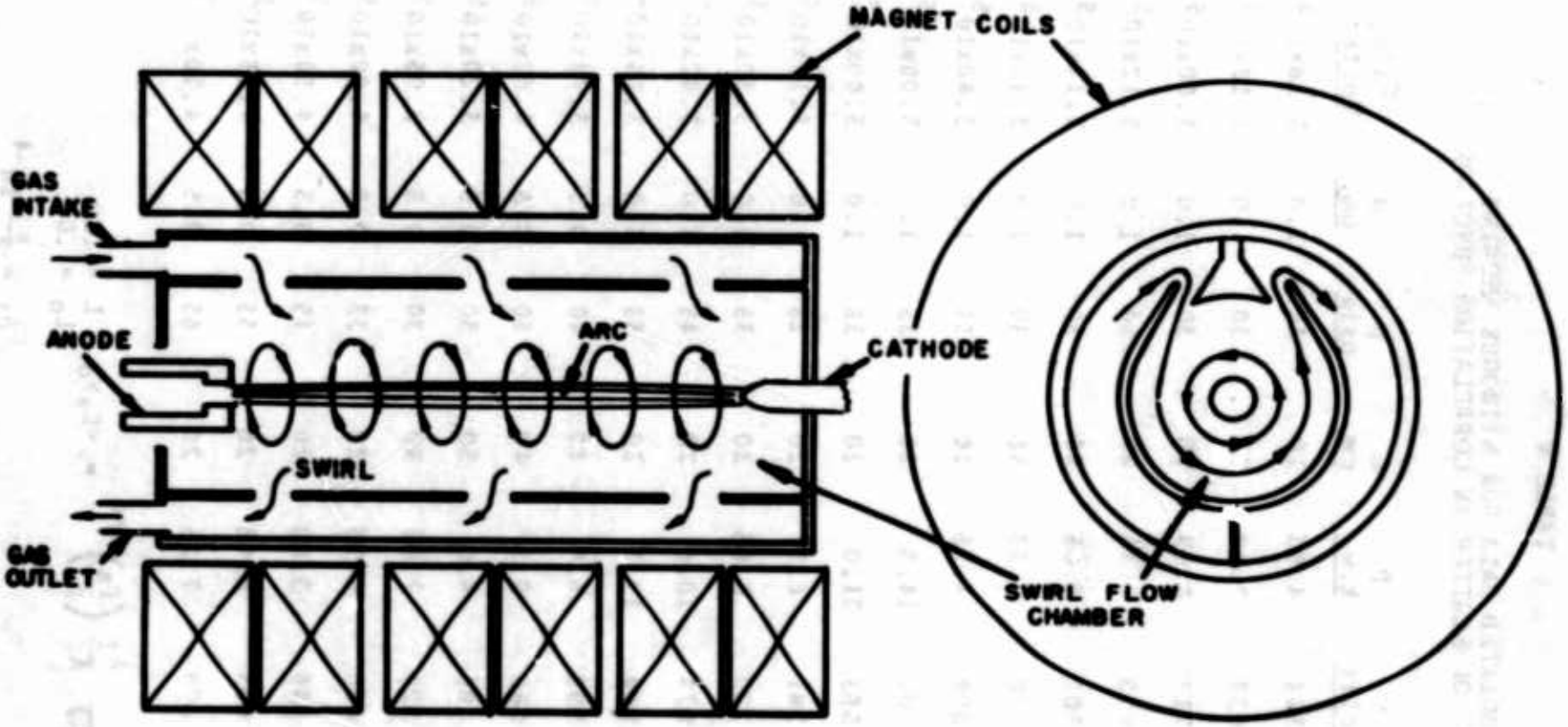

Fig. 1. Schematic View of Swirl Stabilized Arc Experiment

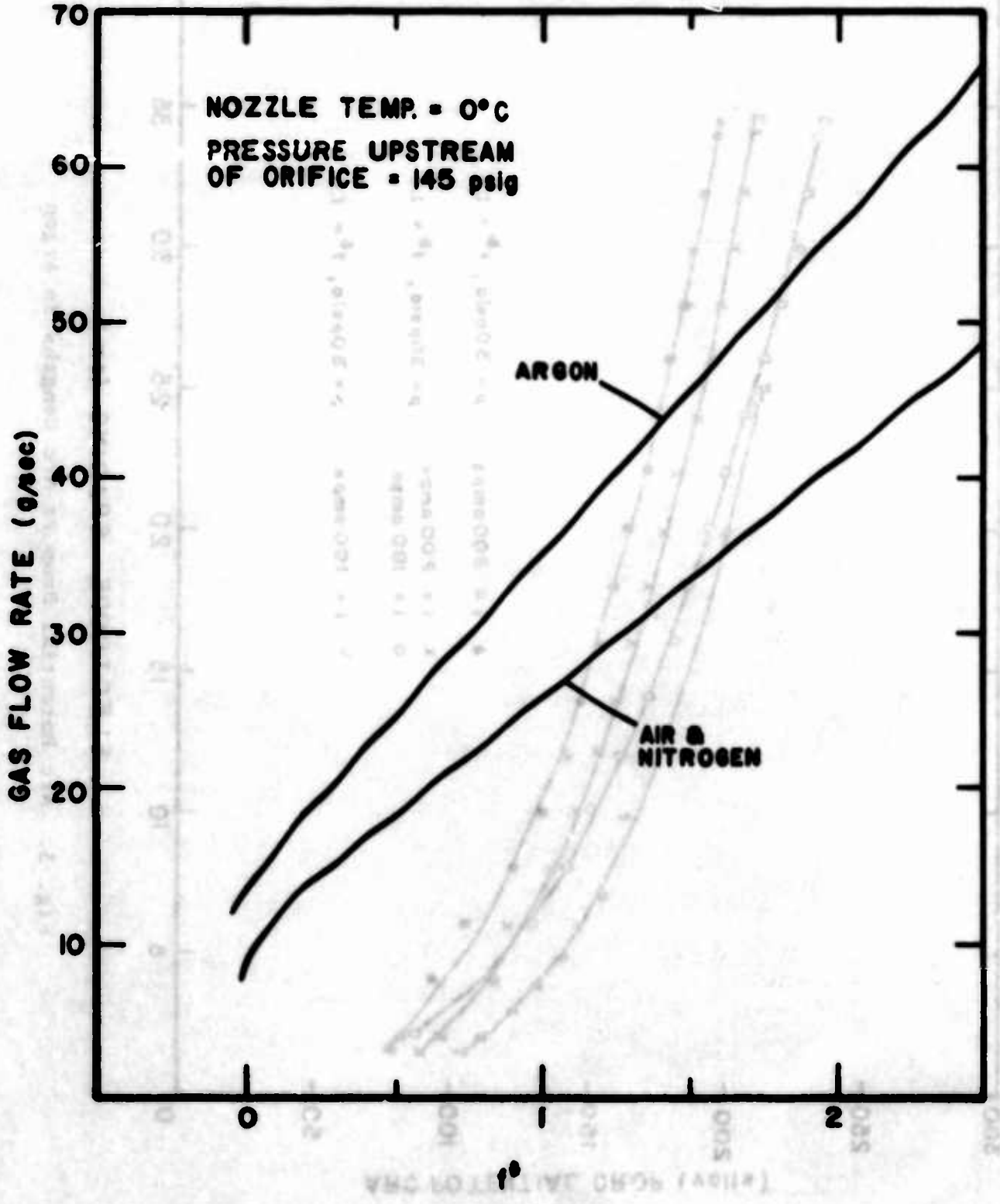

Fig. 2. Calibration of Sonic Nozzle

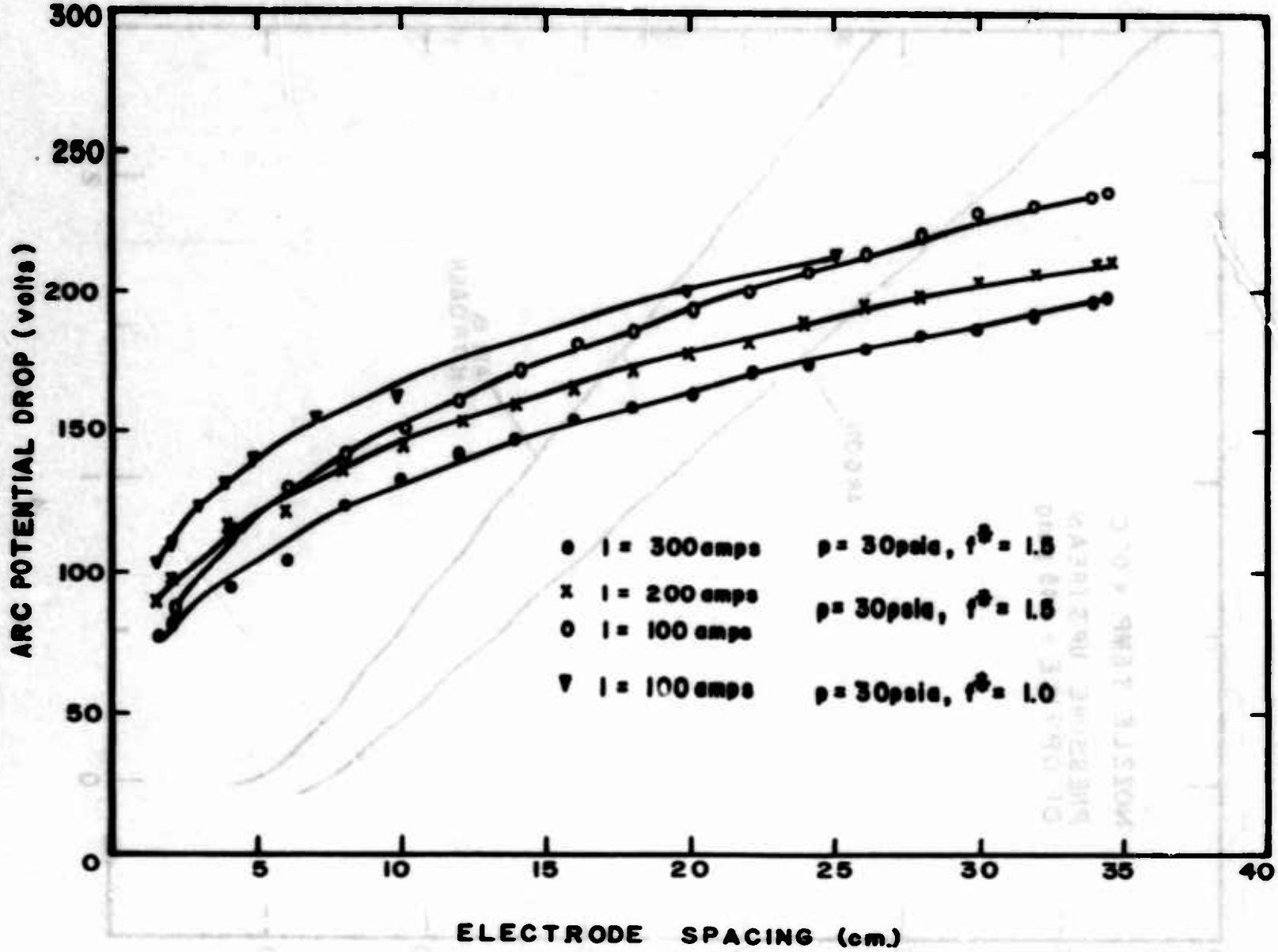

Fig. 3. Arc Potential Drop vs Arc Lengths in Argon

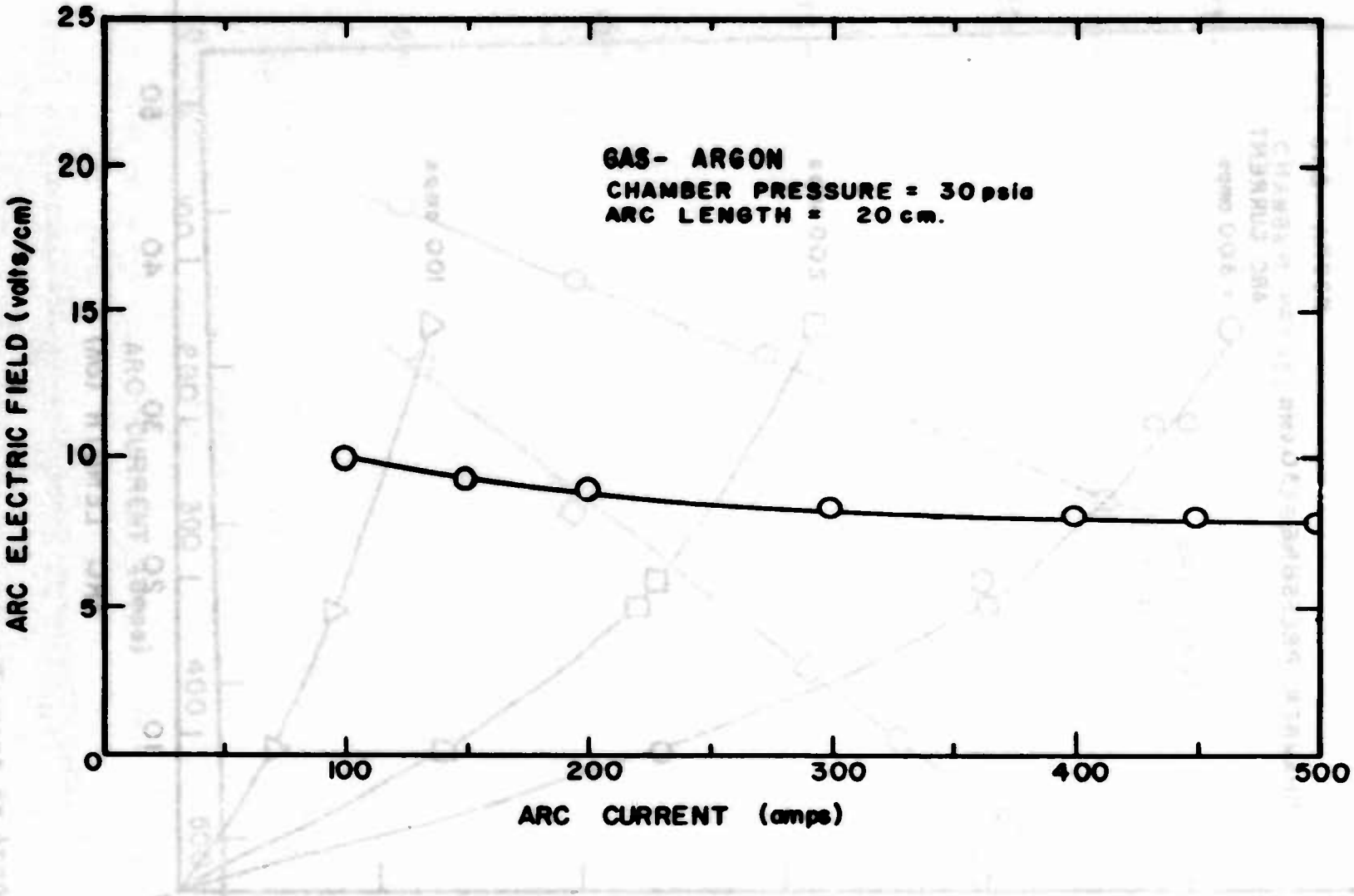

Fig. 4. Arc Electric Field vs Arc Current in Argon

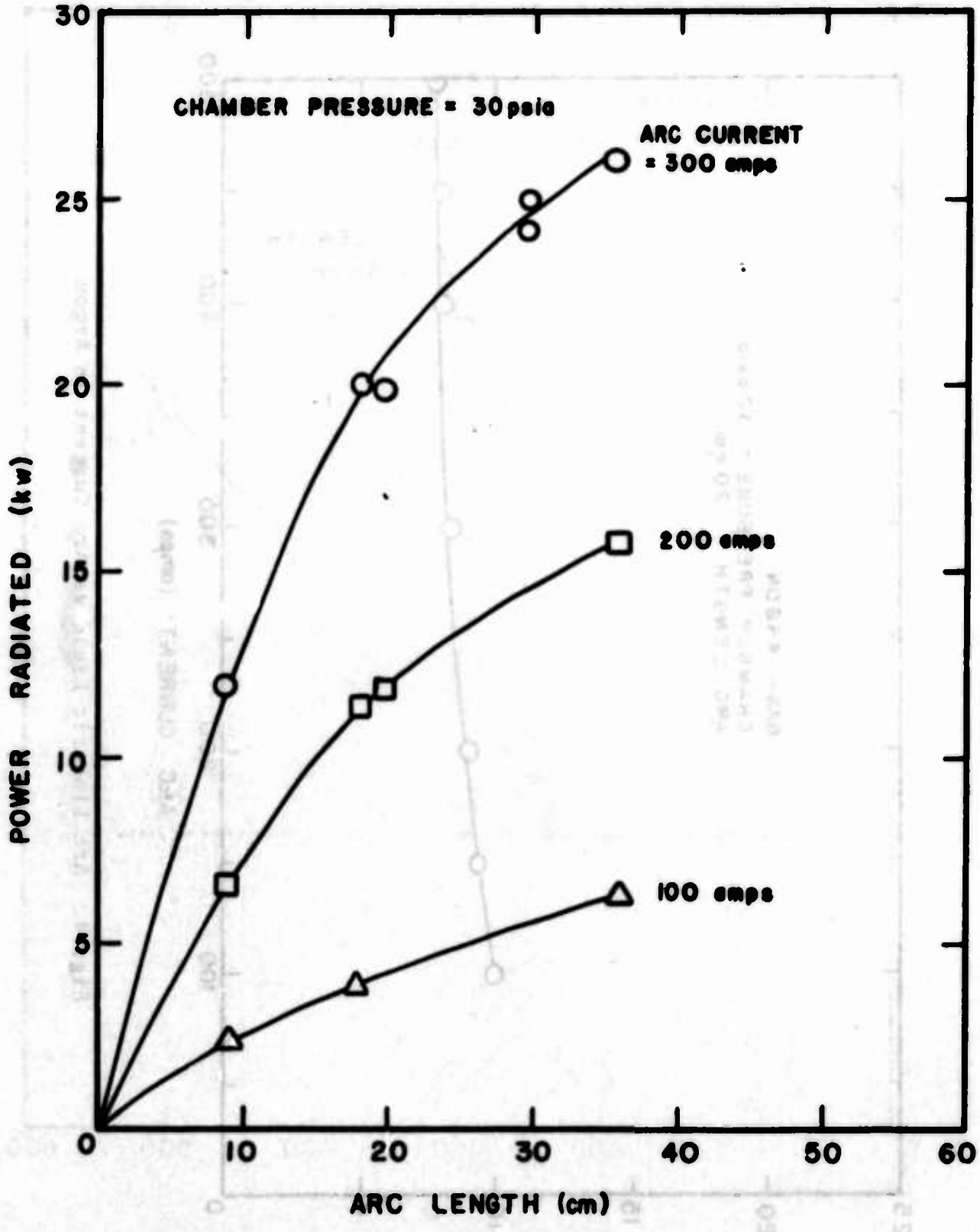

Fig. 5. Power Radiated vs Arc Length in Argon

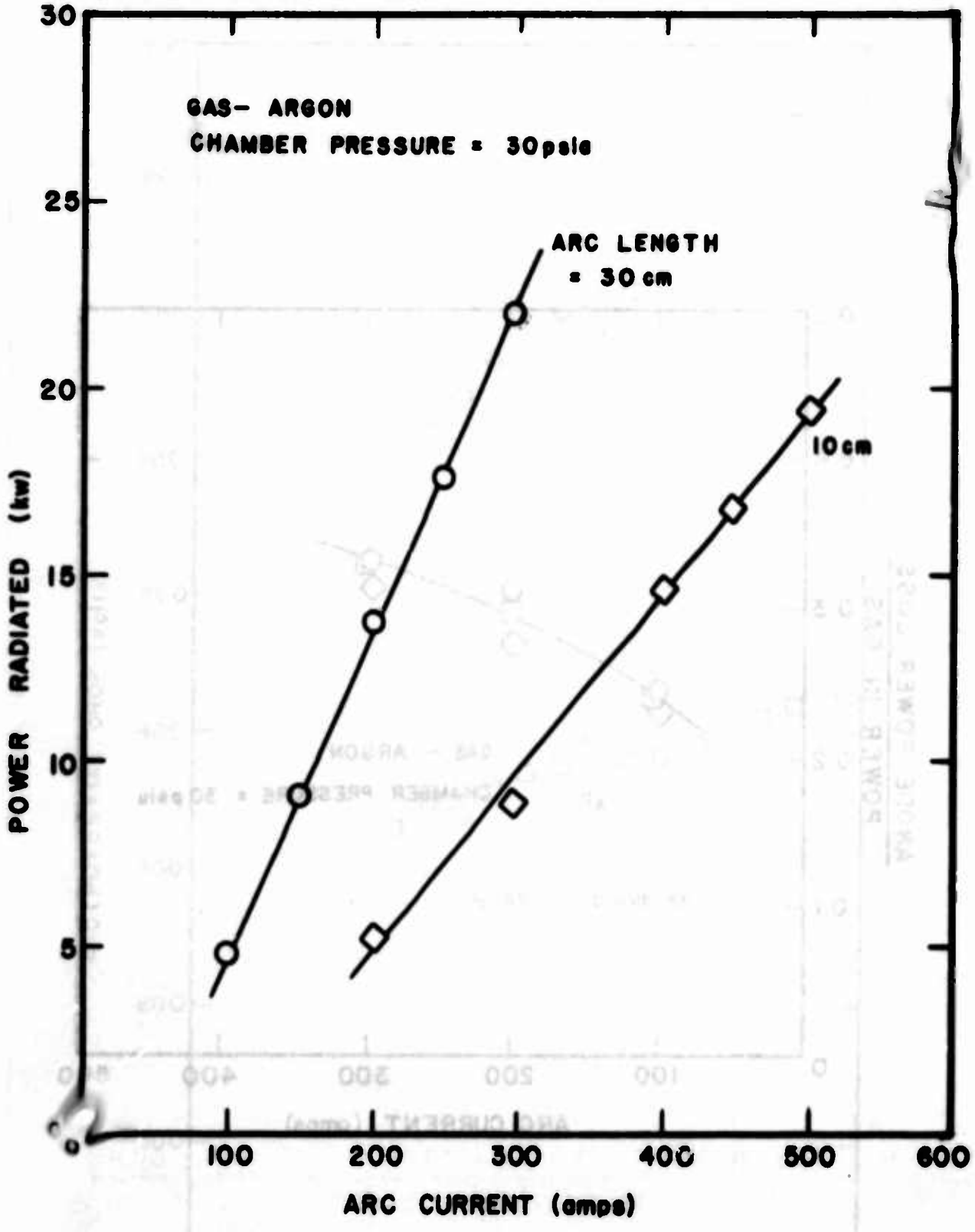

Fig. 6. Power Radiated vs Arc Current in Argon

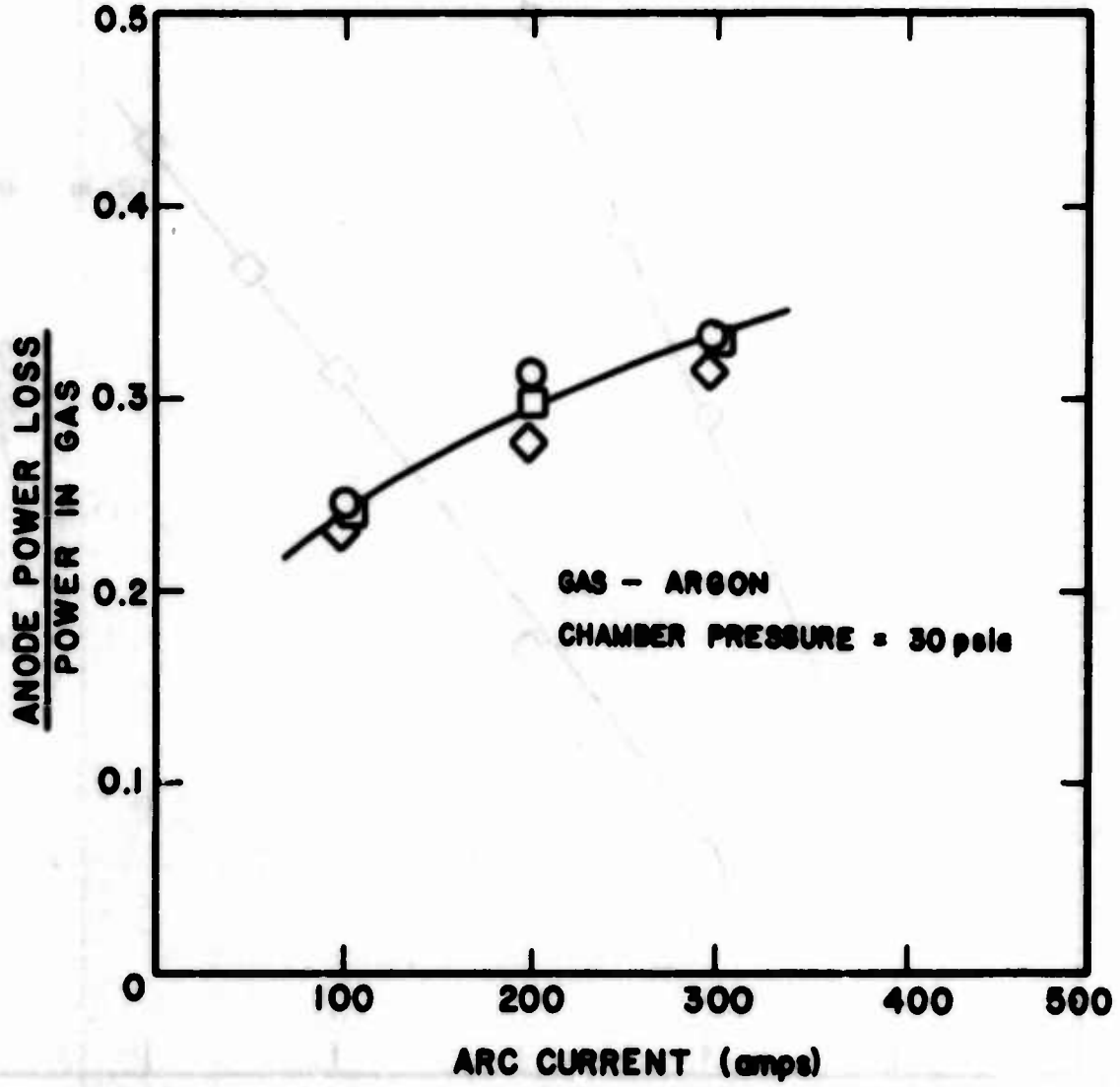

Fig. 7. Anode Power Loss vs Arc Current in Argon

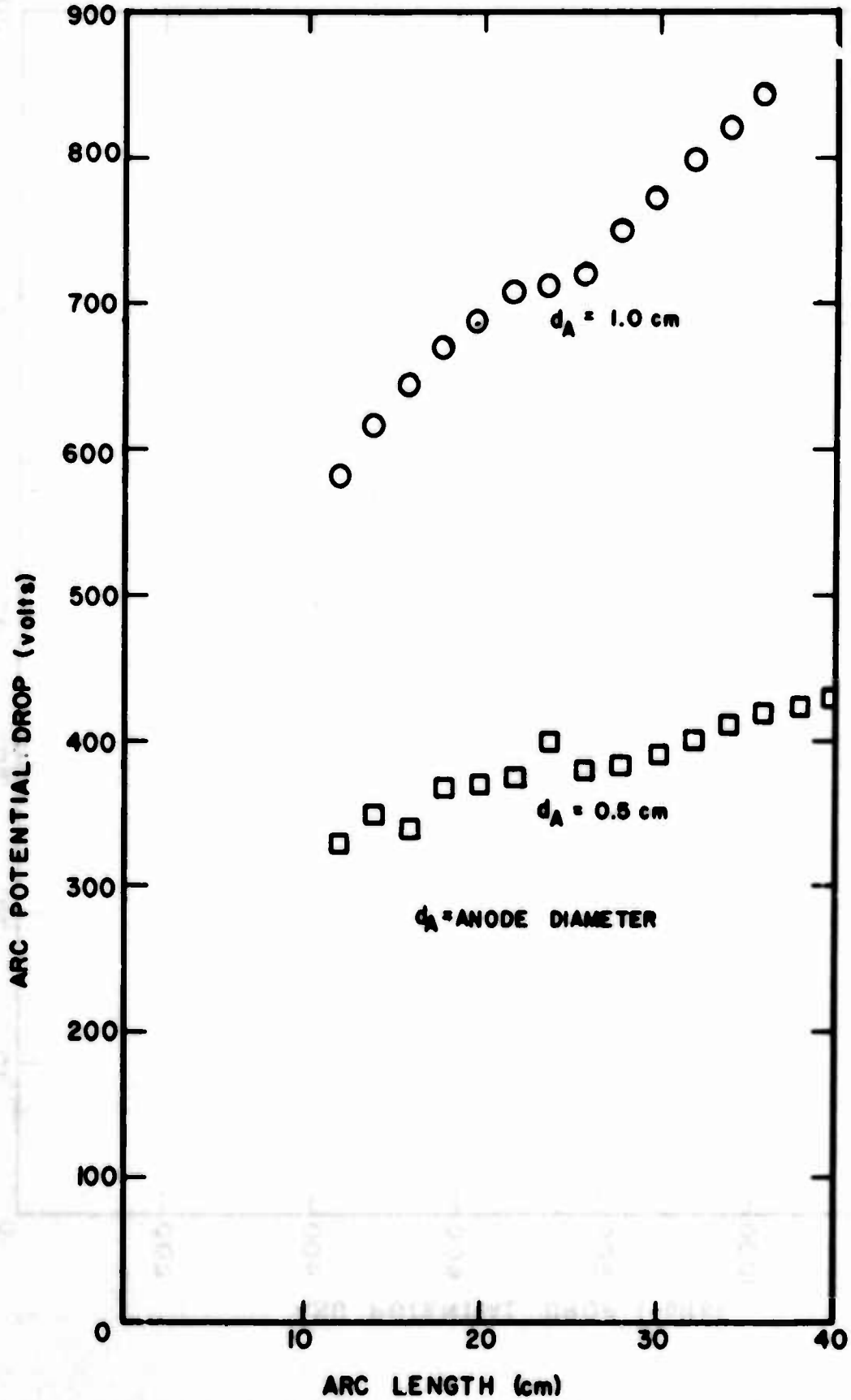

Fig. 8. Arc Potential Drop vs Arc Length in Nitrogen

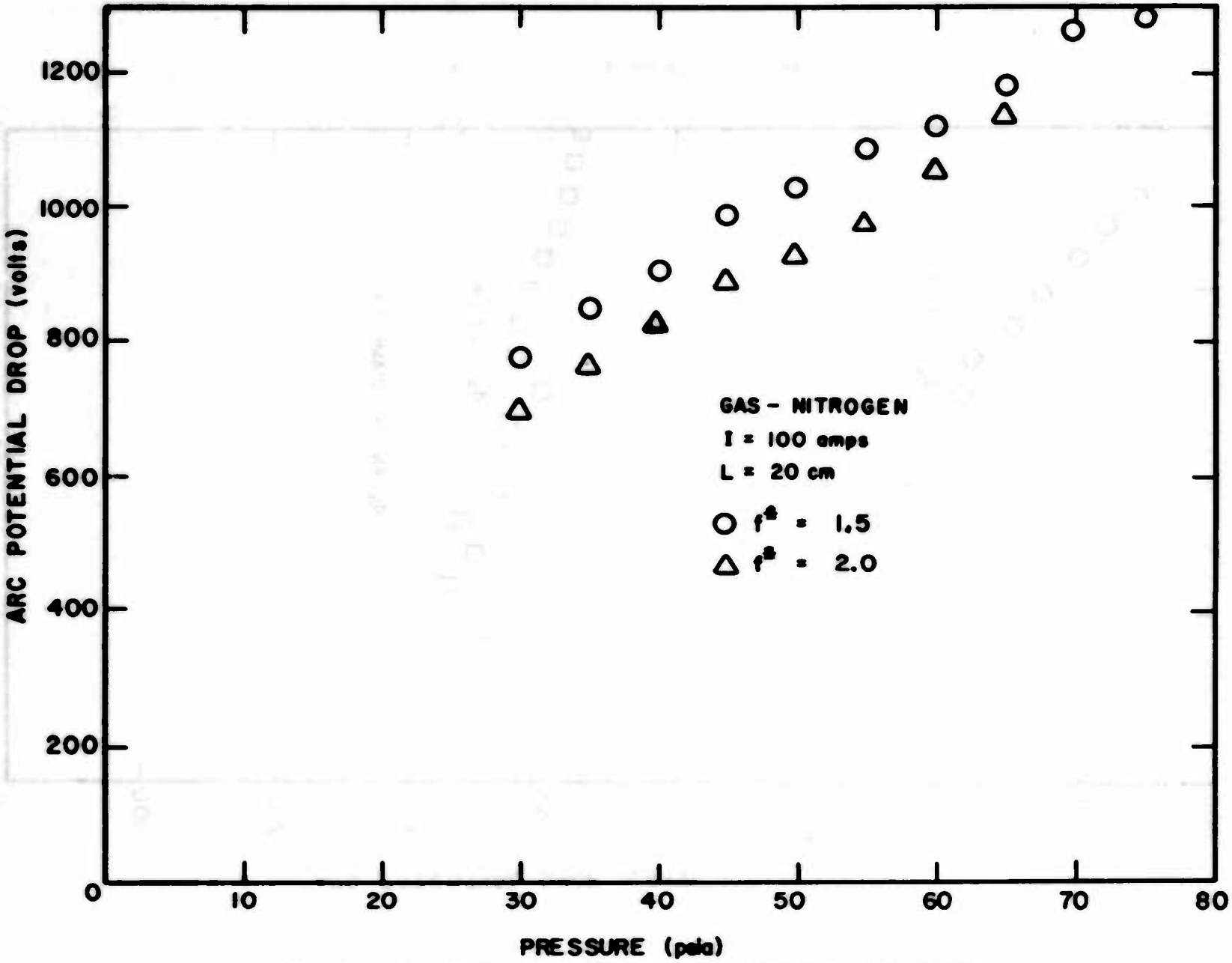

Fig. 9. Arc Potential Drop vs Pressure in Nitrogen

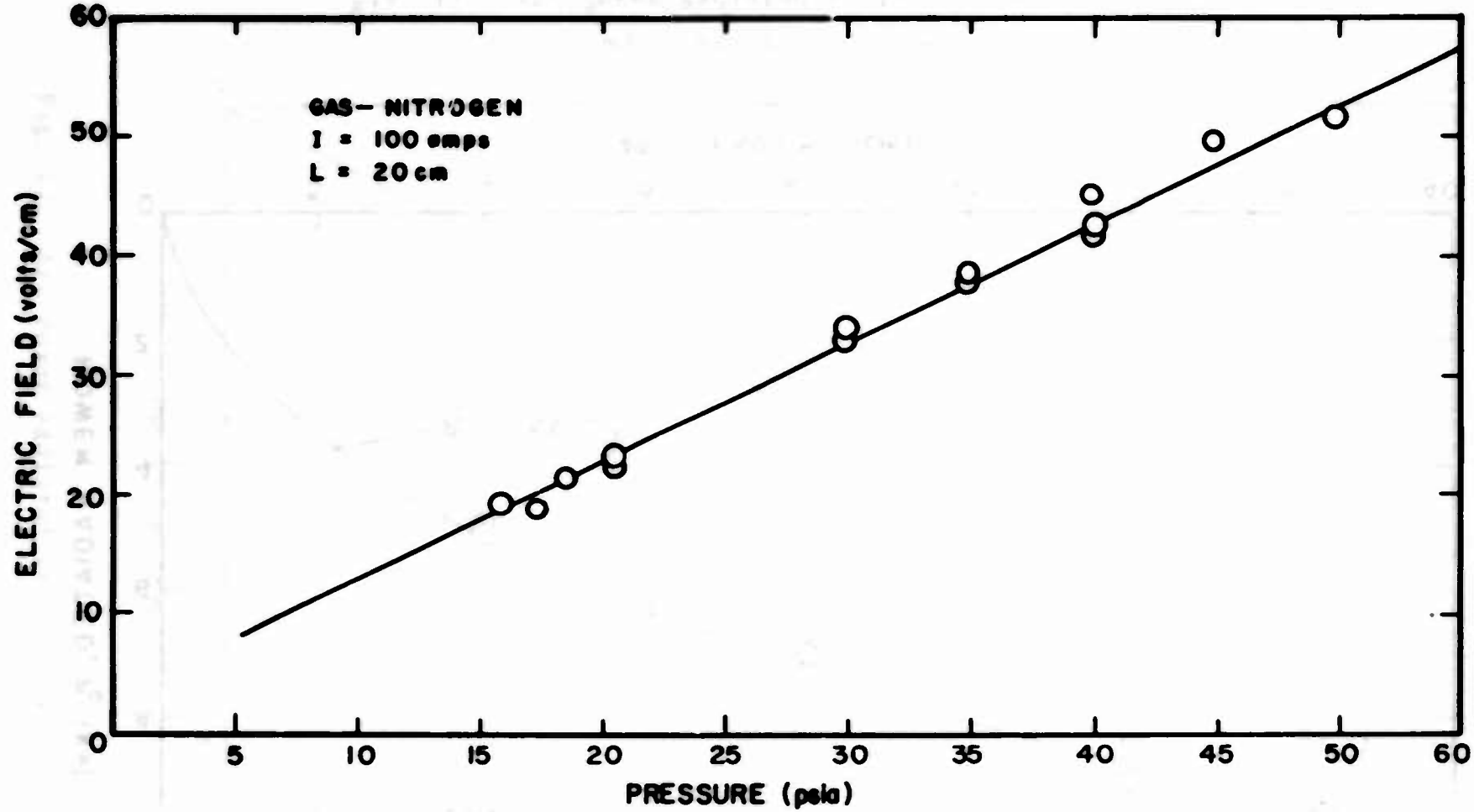

Fig. 10. Arc Electric Field vs Pressure in Nitrogen

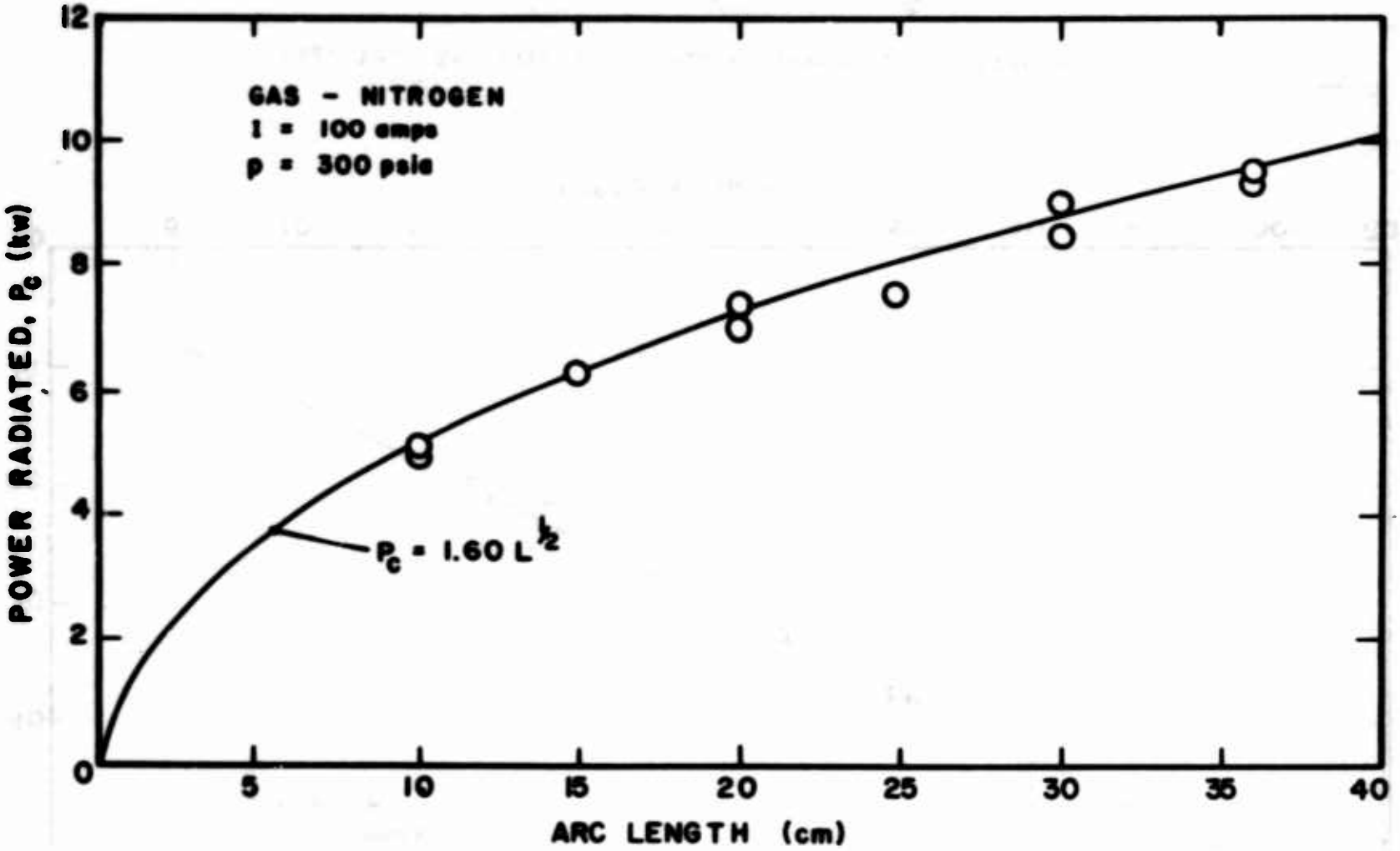

Fig. 11. Arc Power Radiated vs Arc Length in Nitrogen

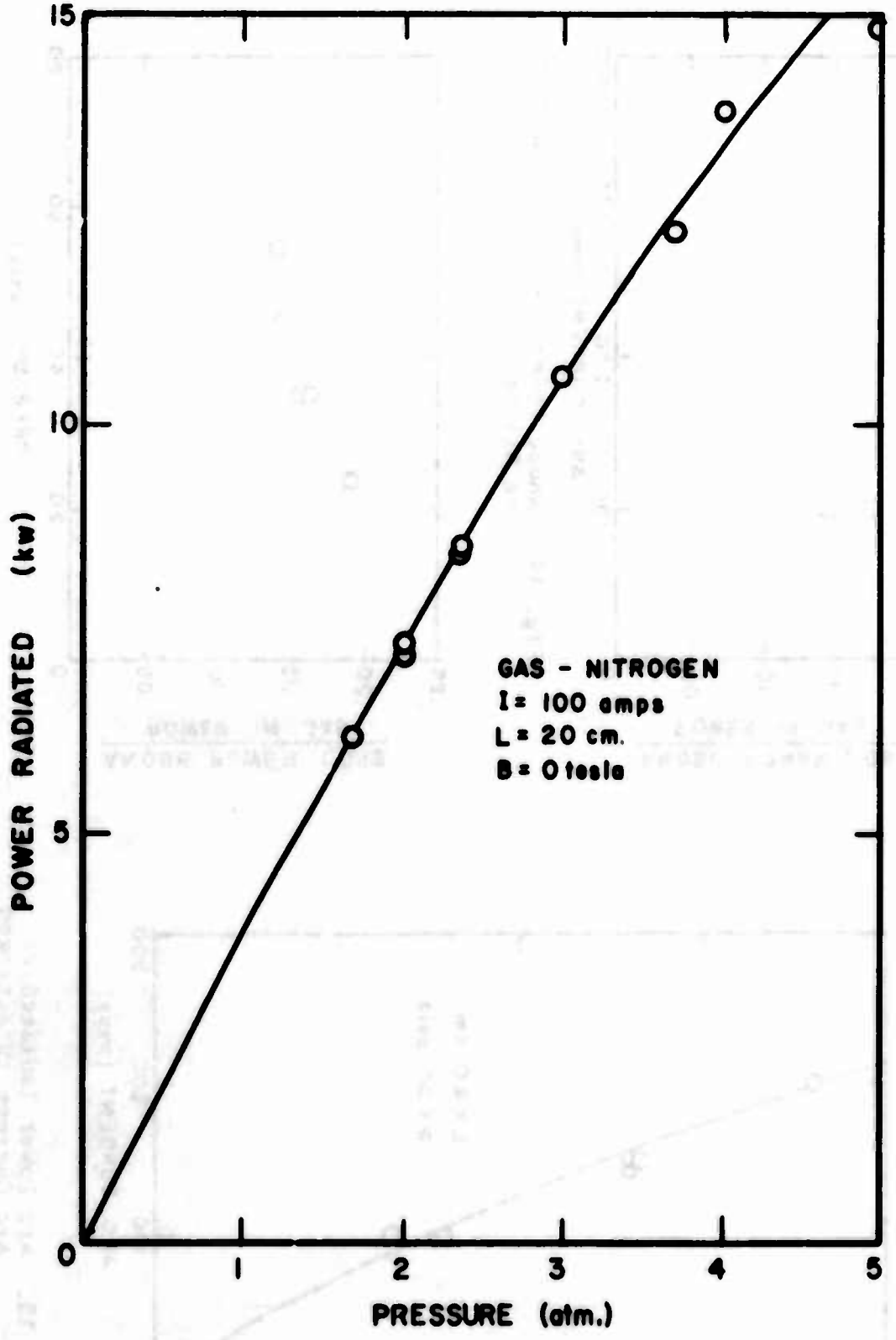

Fig. 12. Arc Power Radiated vs Pressure in Nitrogen

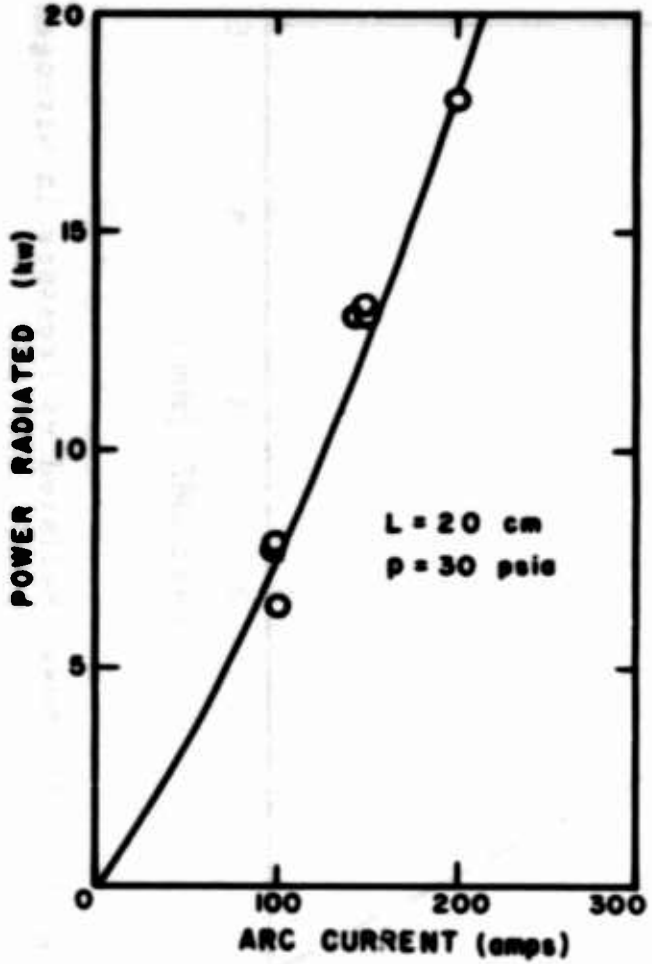

Fig. 13. Arc Power Radiated vs Arc Current in Nitrogen

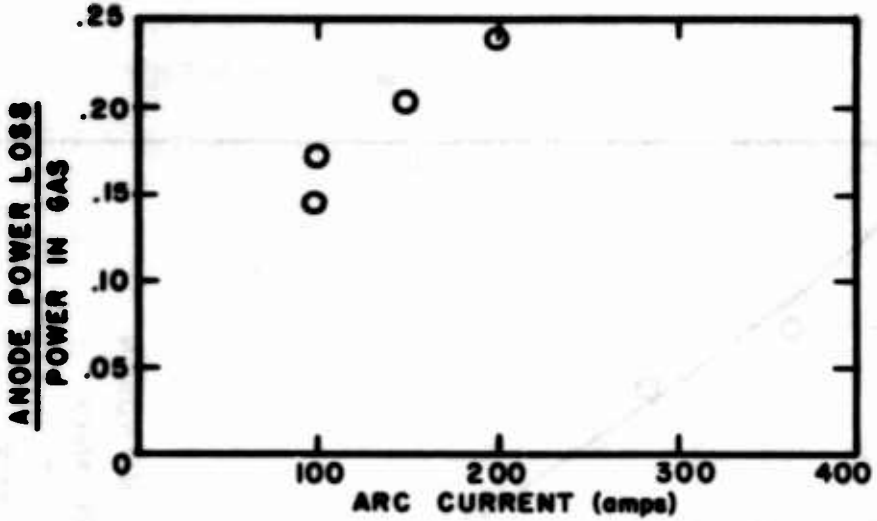

Fig. 14. Anode Power Loss vs Arc Current in Nitrogen

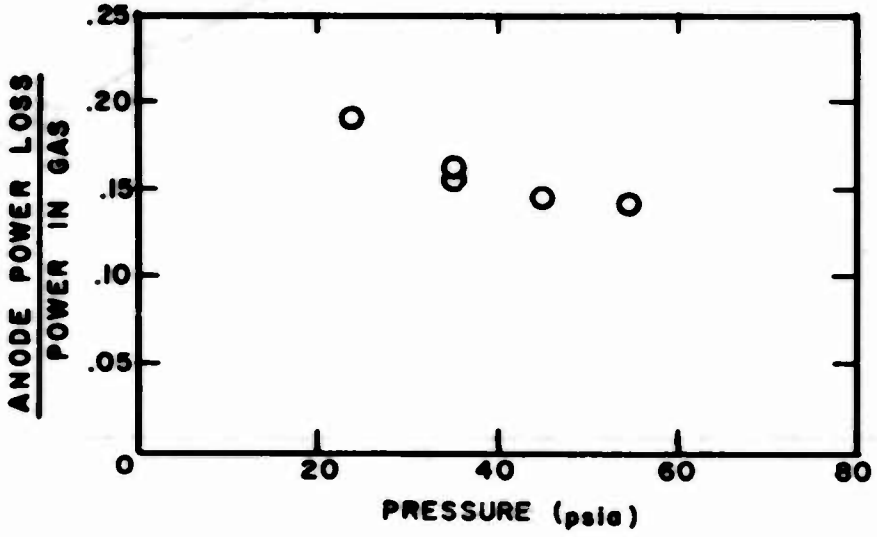

Fig. 15. Anode Power Loss vs Pressure in Nitrogen

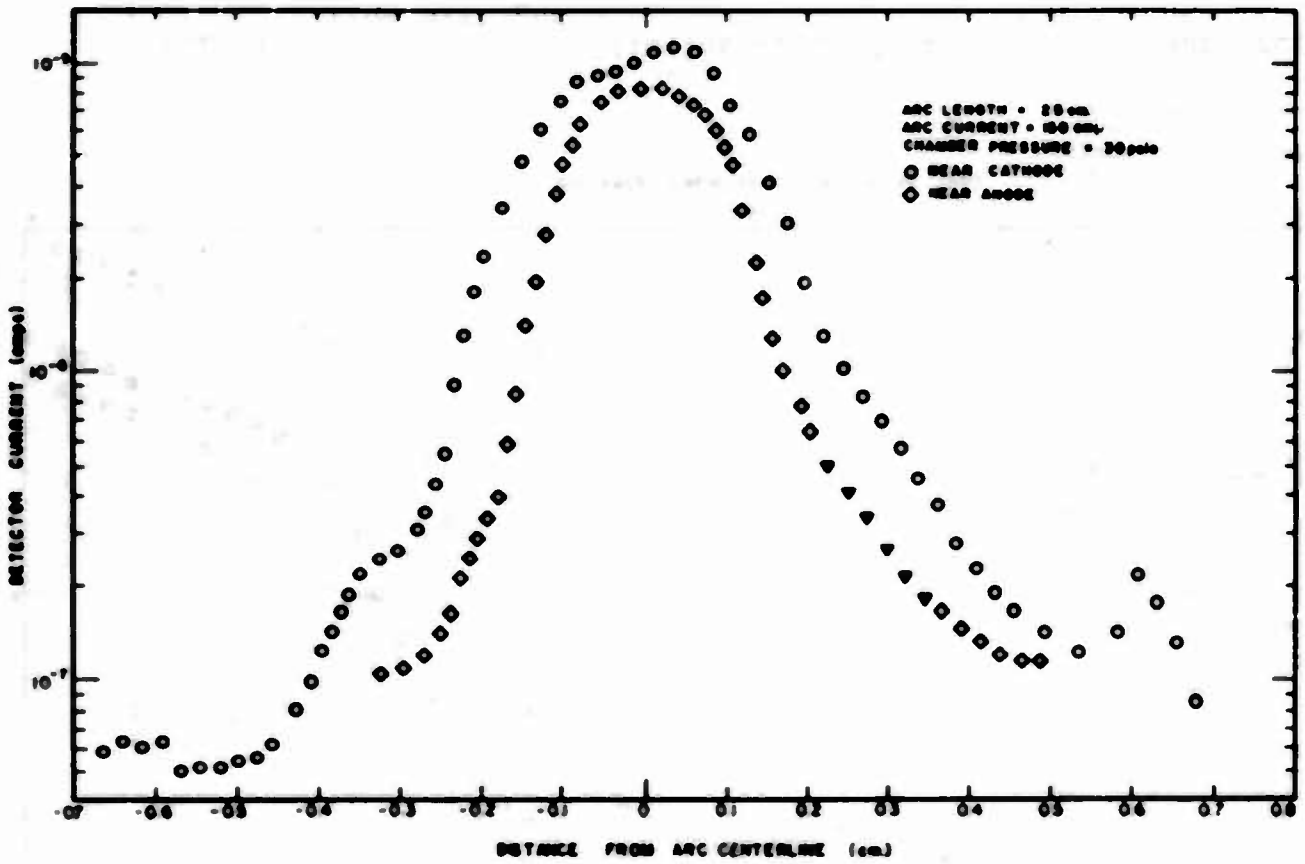

Fig. 16. Intensity of Radiation at 5460A and at Two Axial Positions from Nitrogen

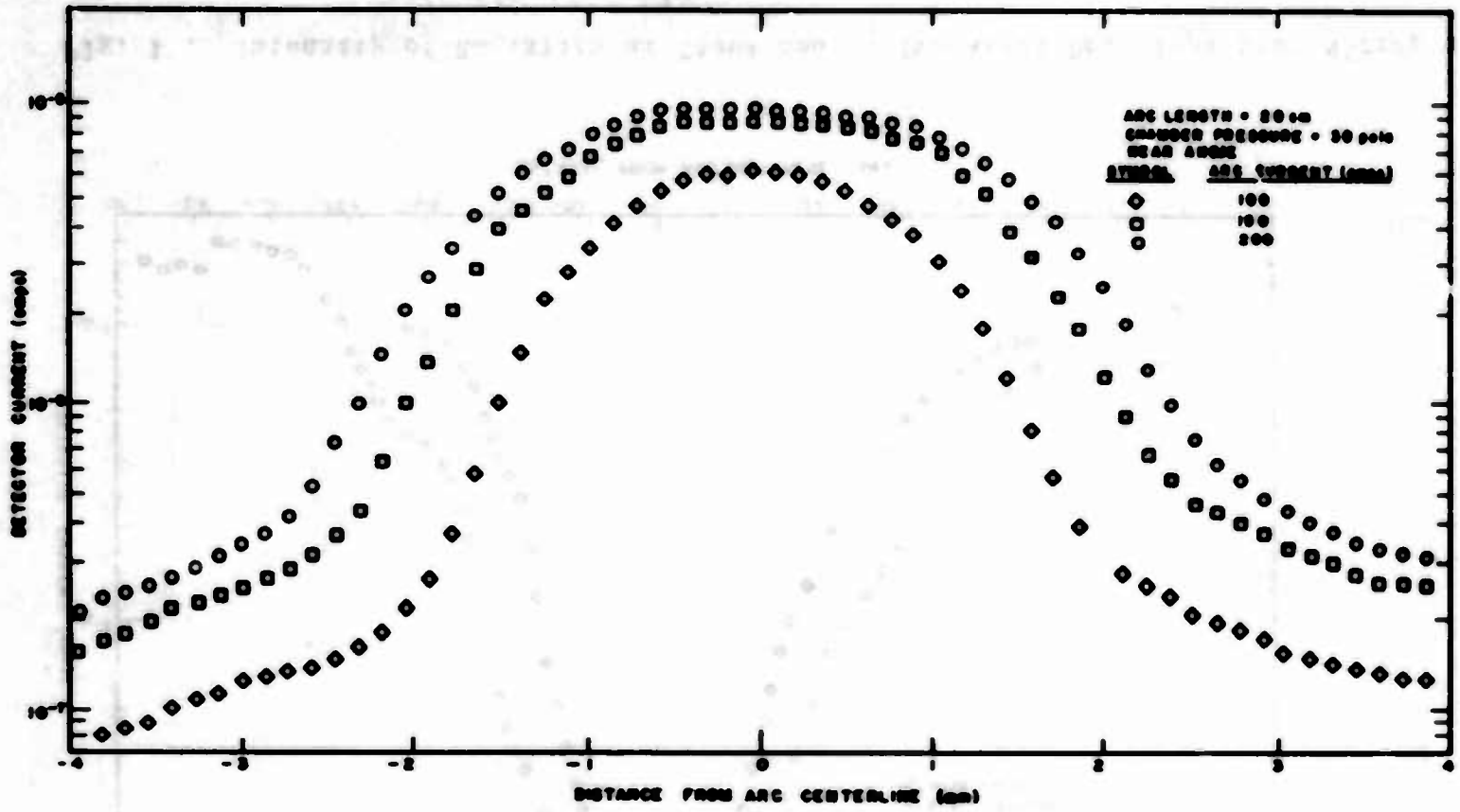

Fig. 17. Intensity of Radiation at 5460A and at Different Arc Currents from Nitrogen

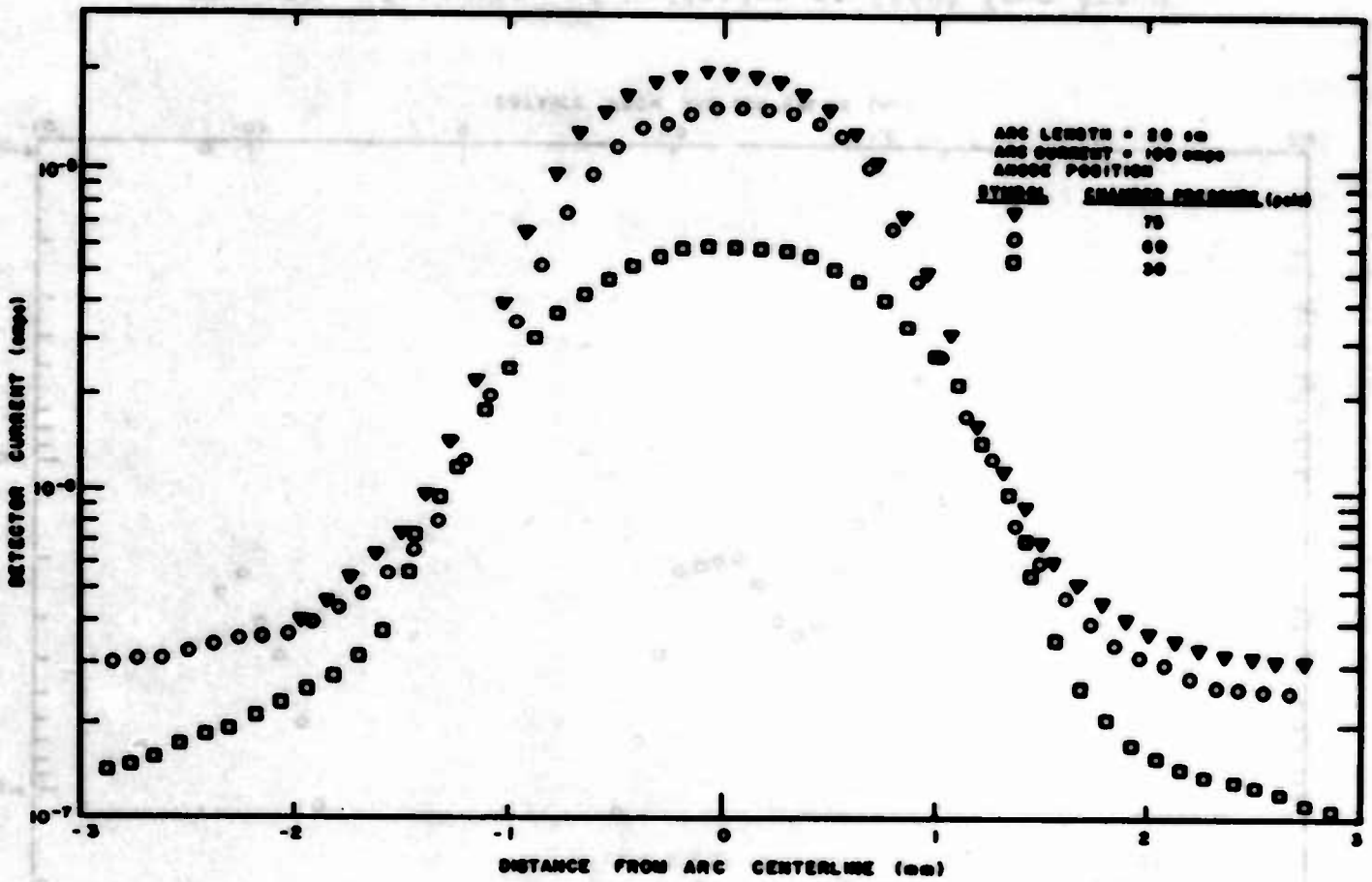

Fig. 18. Intensity of Radiation at 5460A and at Different Chamber Pressures from Nitrogen

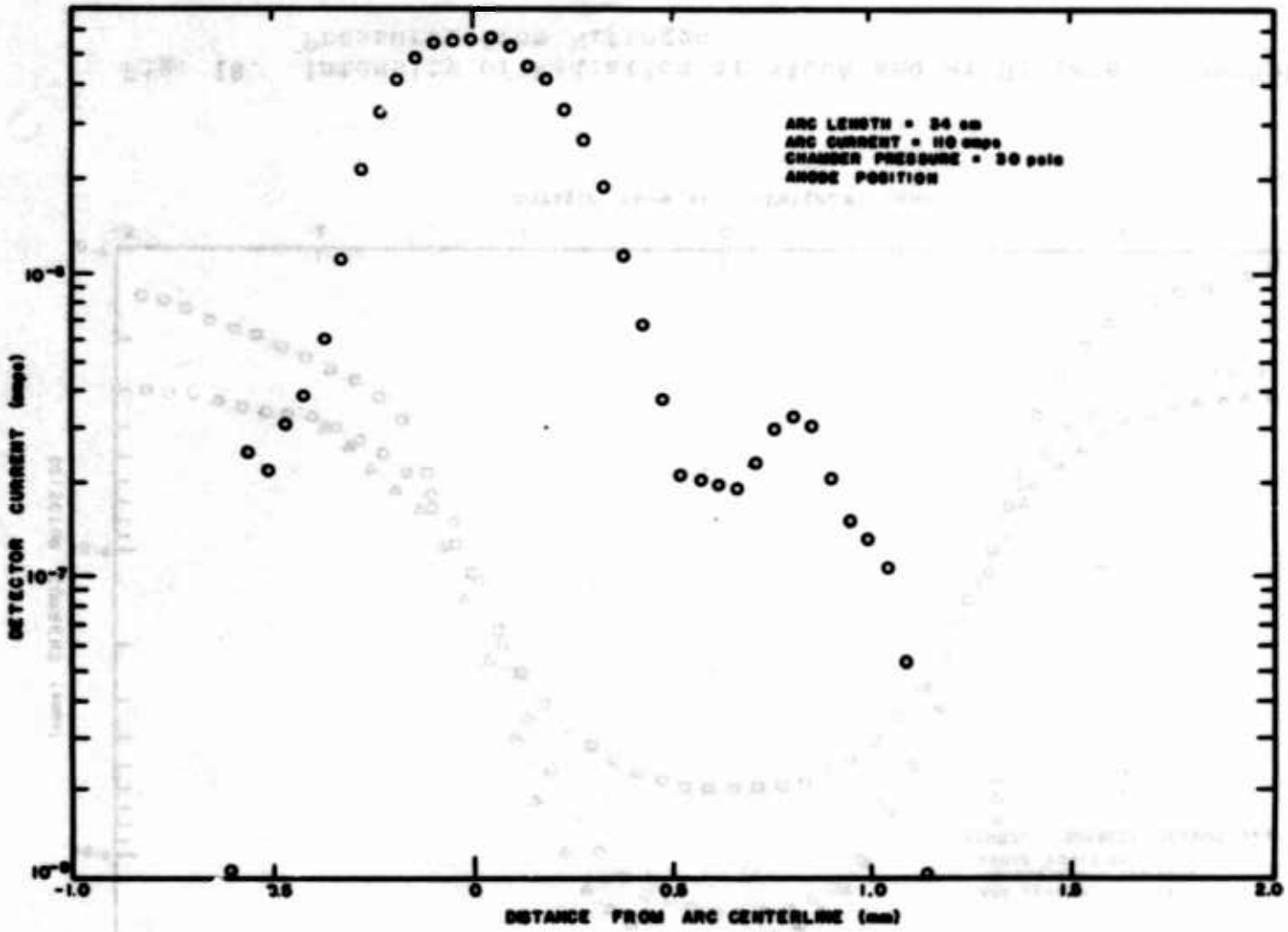

Fig. 19. Intensity of Radiation at 5460A from Argon

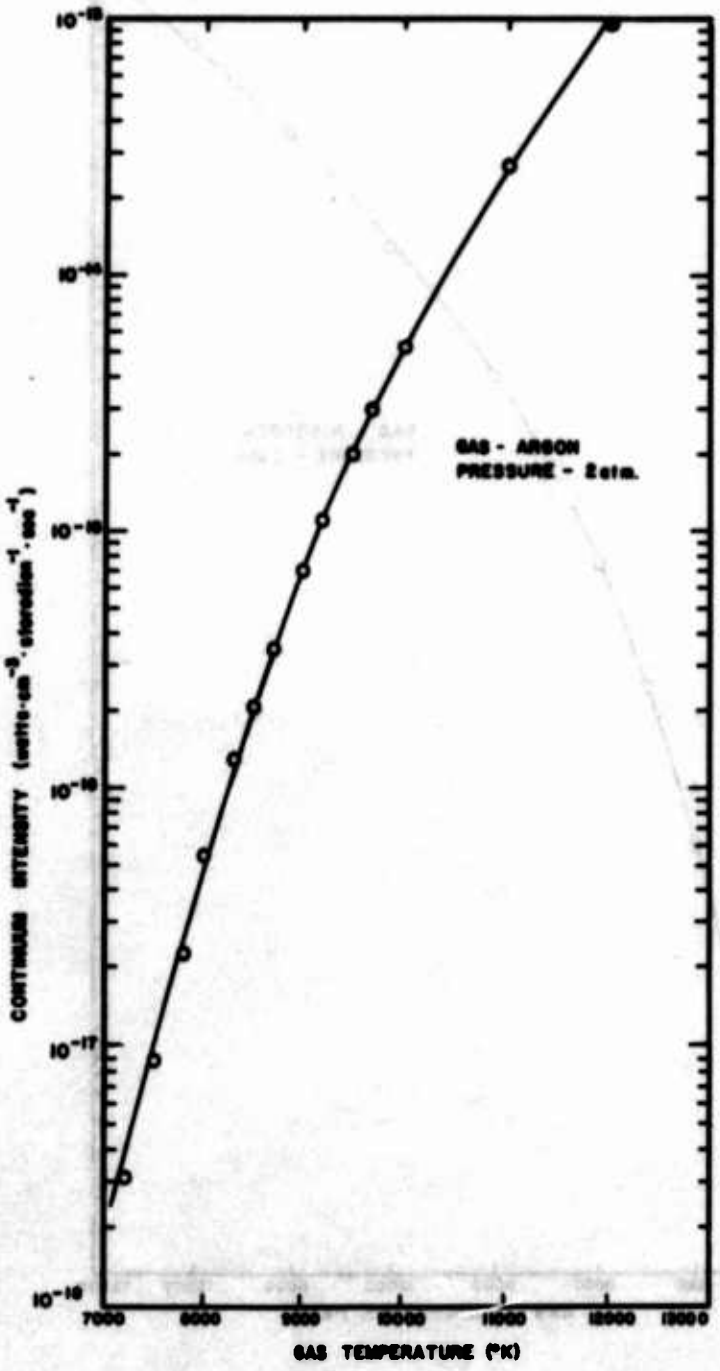

Fig. 20. Relation Between Radiated Power at 5455A and Temperature for Argon

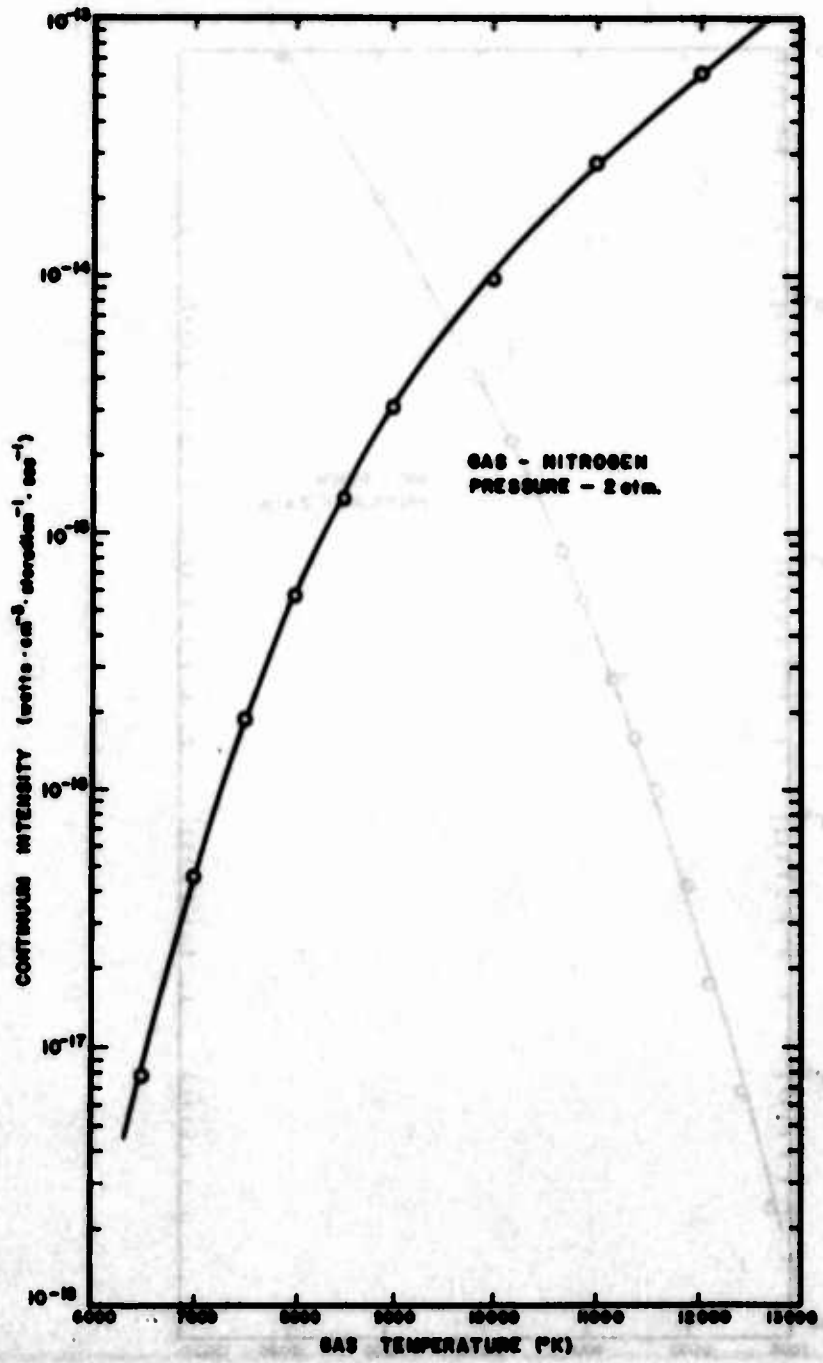

Fig. 21. Relation Between Radiated Power at 5455A and Temperature for Nitrogen

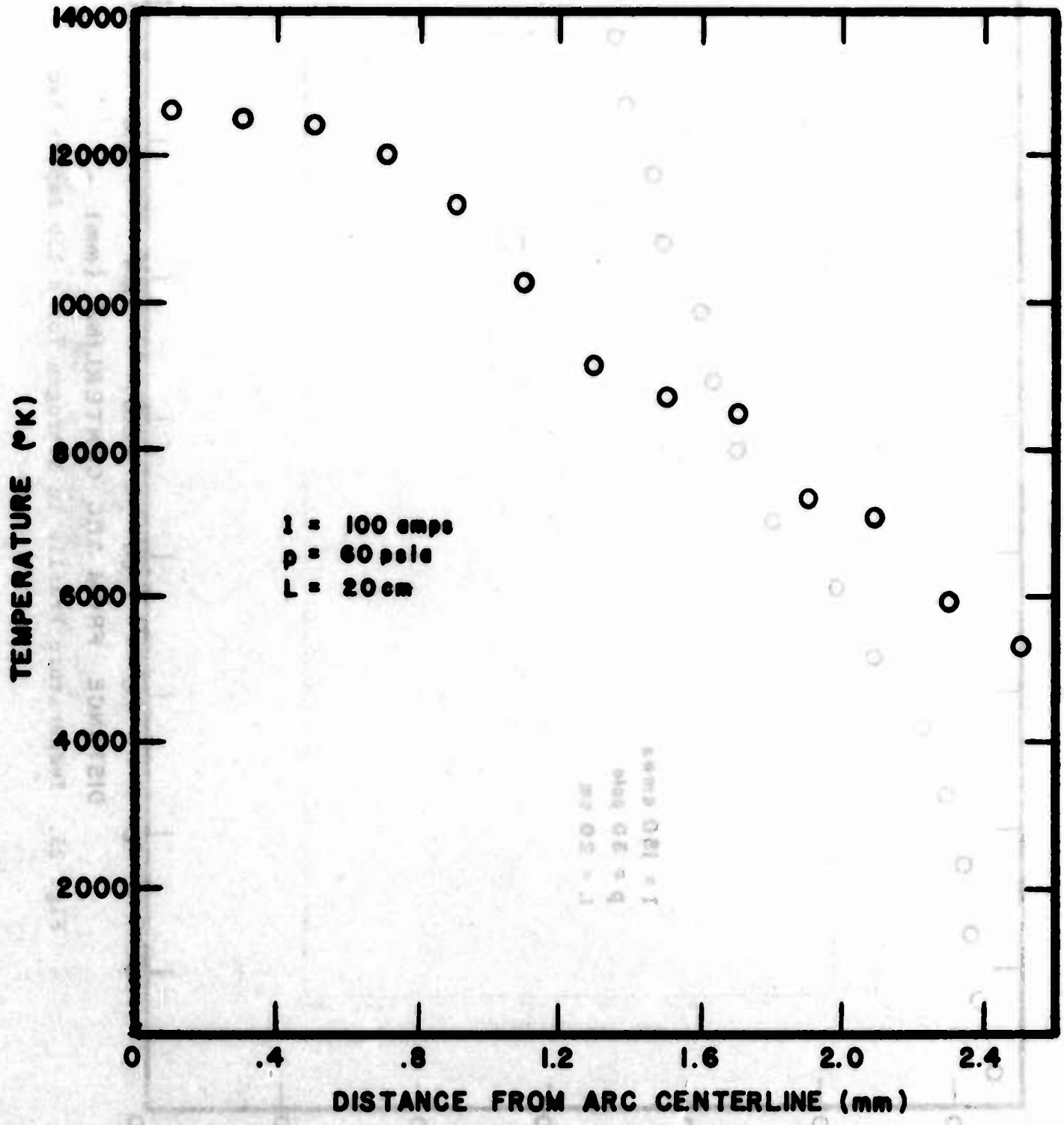

Fig. 22. Temperature Profile in Nitrogen for a 100 Ampere Arc

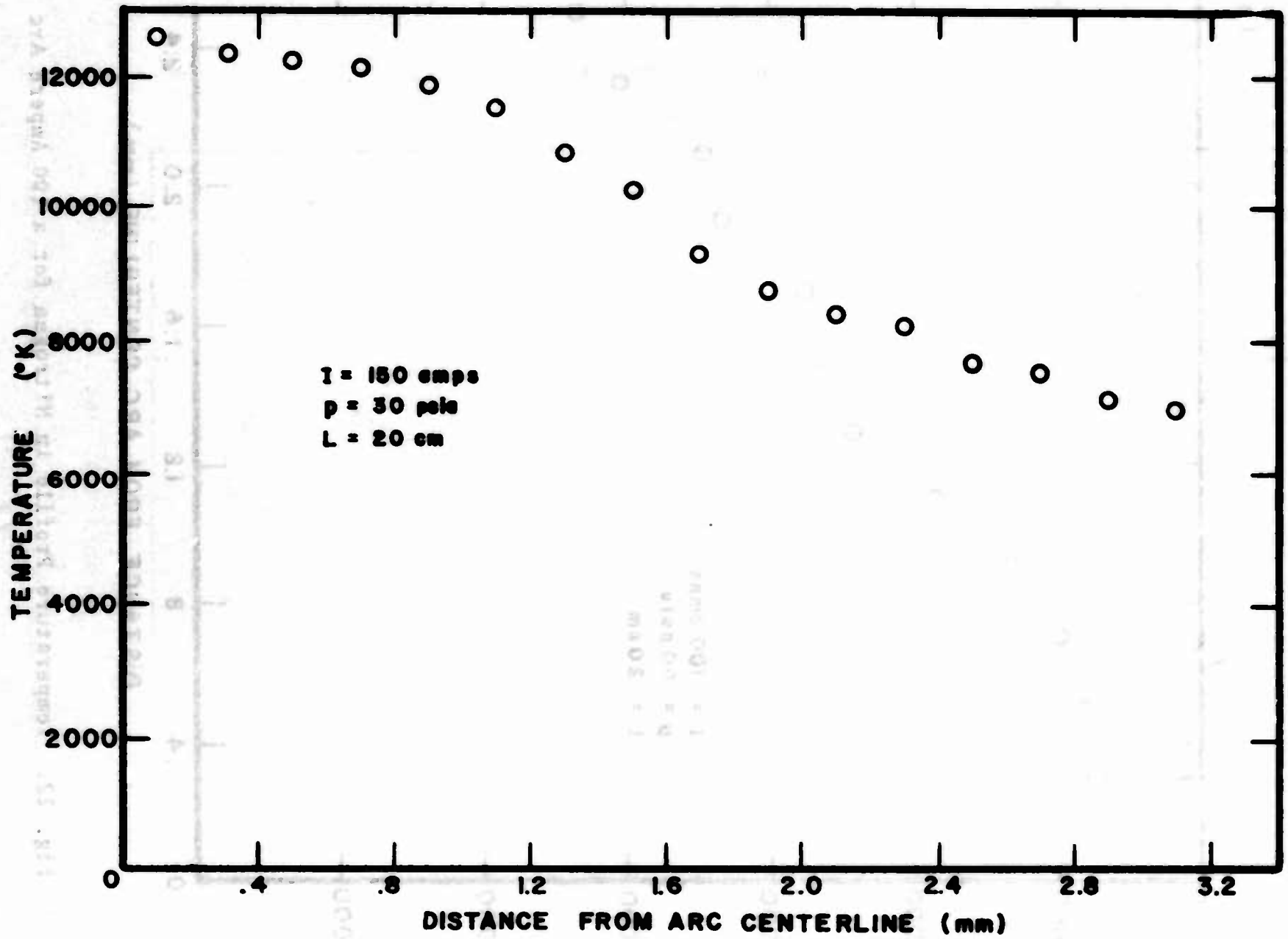

Fig. 23. Temperature Profile in Nitrogen for a 150 Ampere Arc

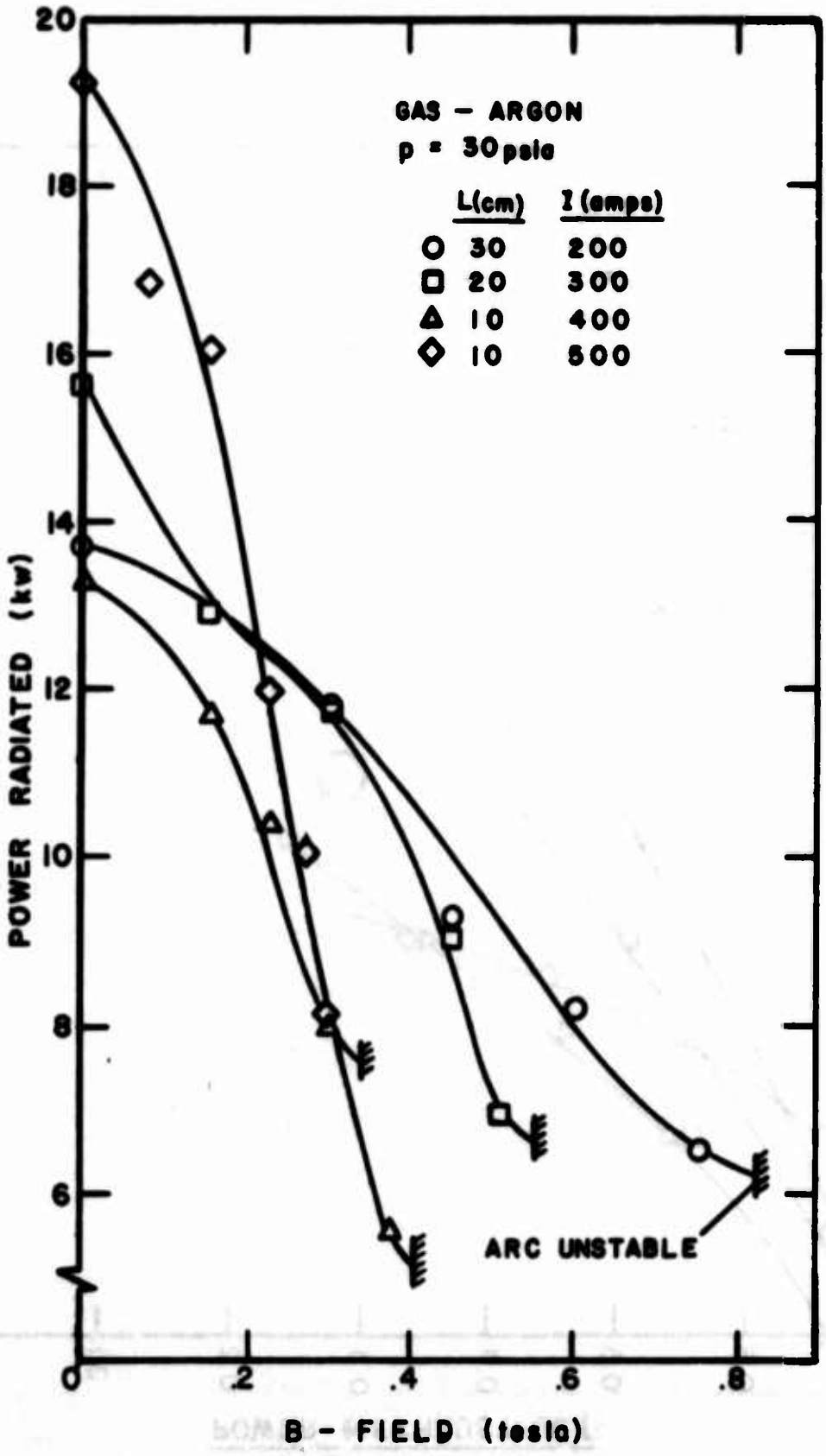

Fig. 24a. Power Radiated from an Arc in Argon vs the Applied Magnetic Field Strength

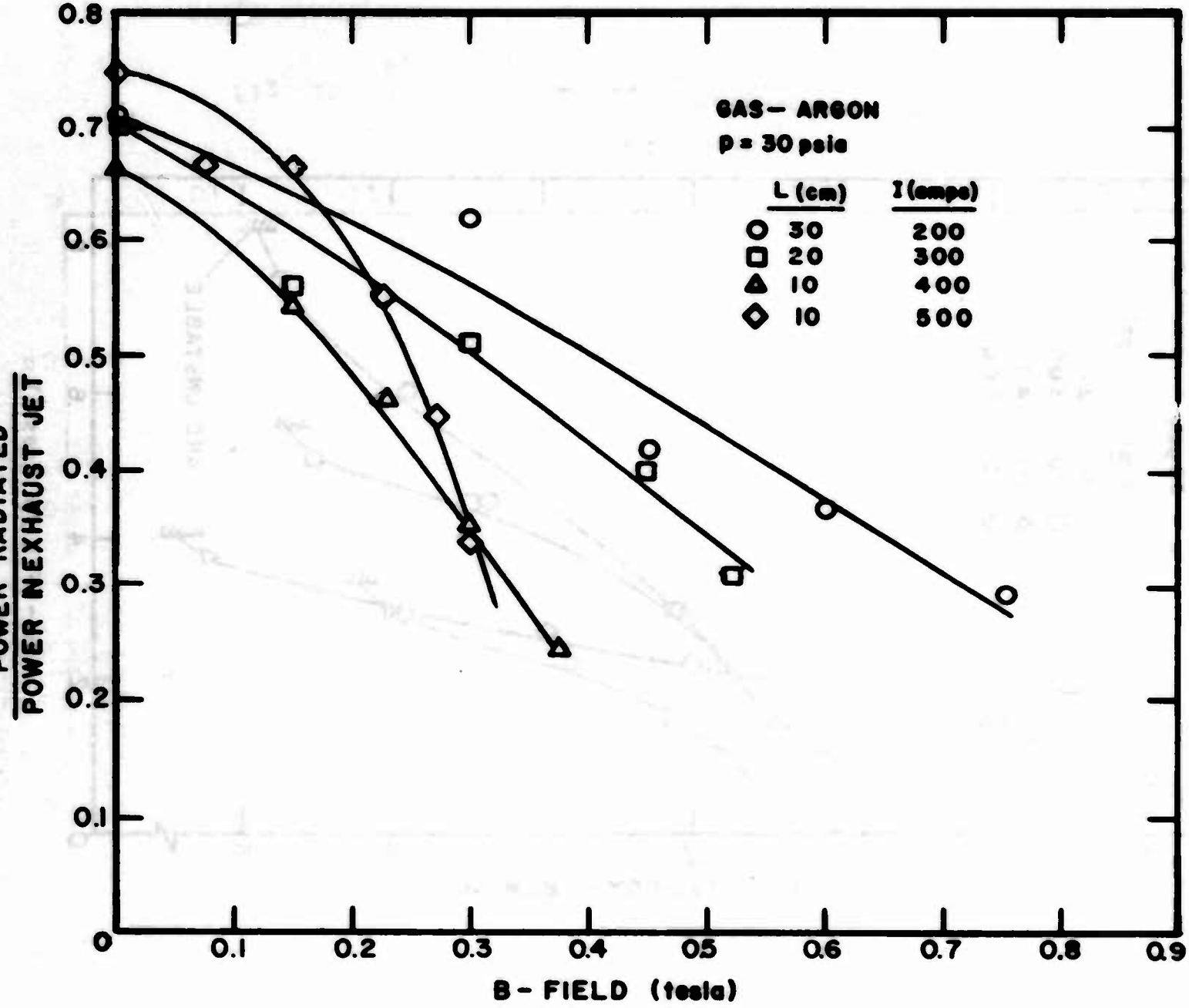

Fig. 24b. Ratio of Power Radiated to Power in Gas in Argon vs the Applied Magnetic Field Strength

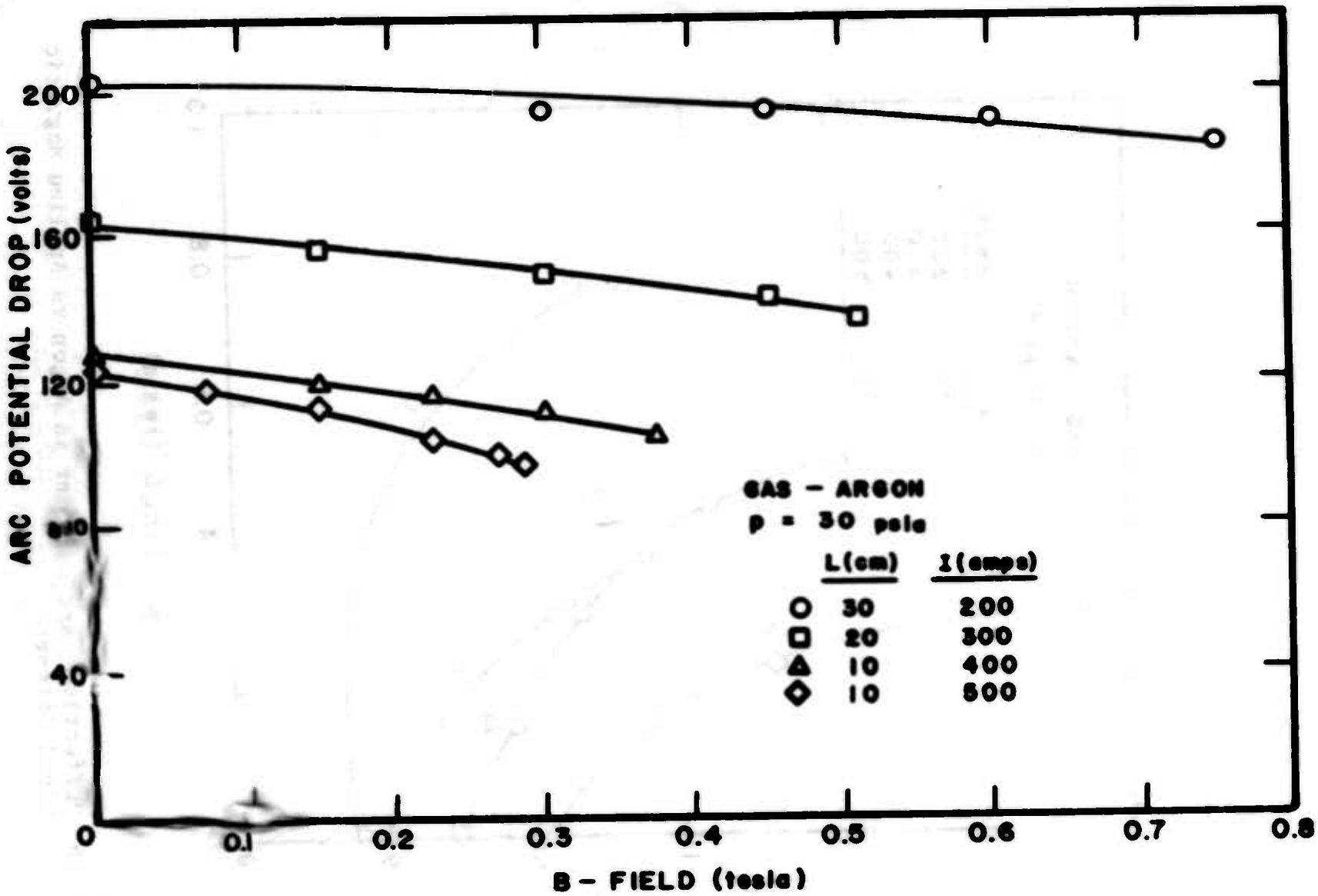

Fig. 25. Arc Potential Drop in Argon vs the Applied Magnetic Field Strength

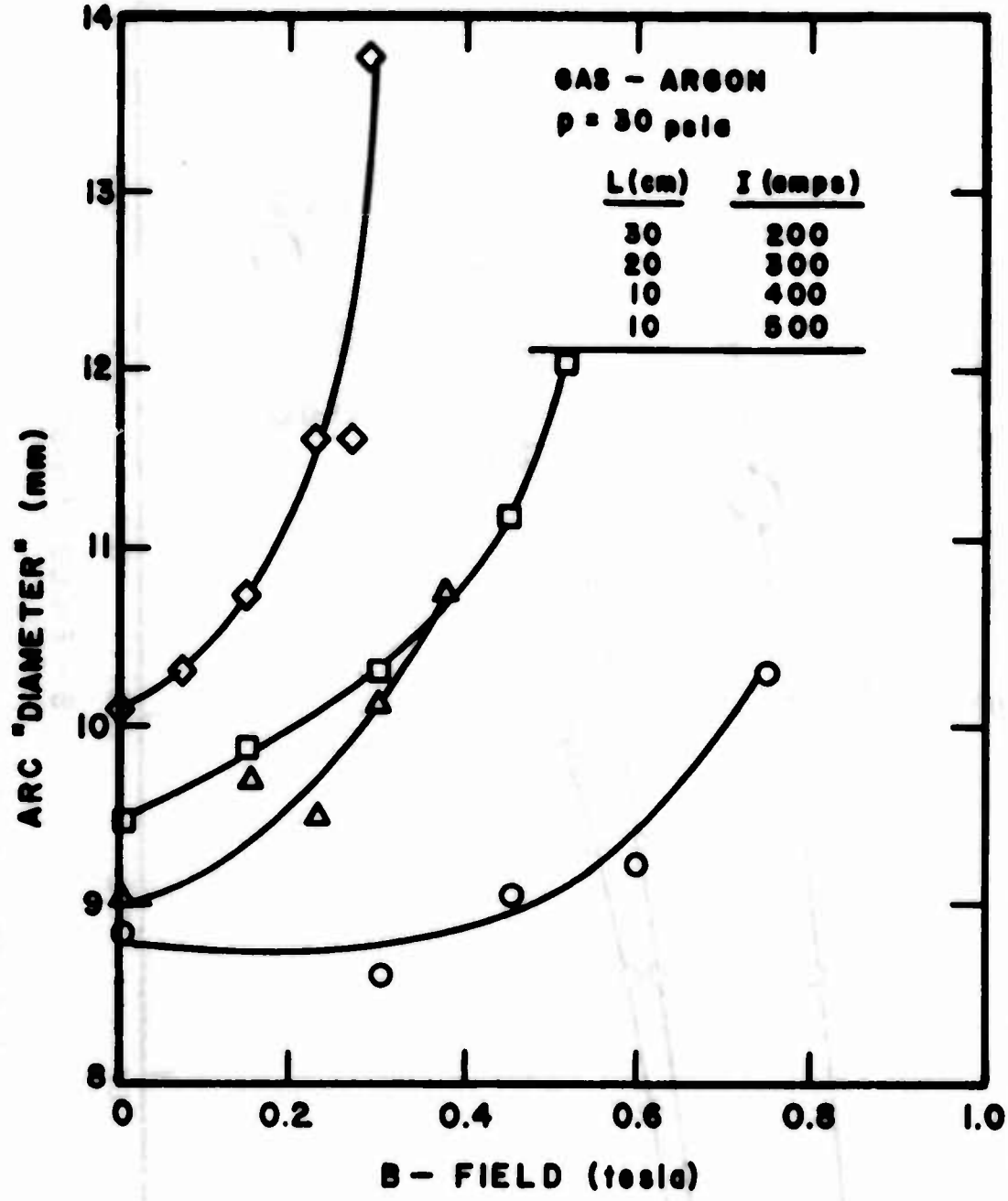

Fig. 26 "Effective" Arc Diameter in Argon vs Applied Magnetic Field Strength

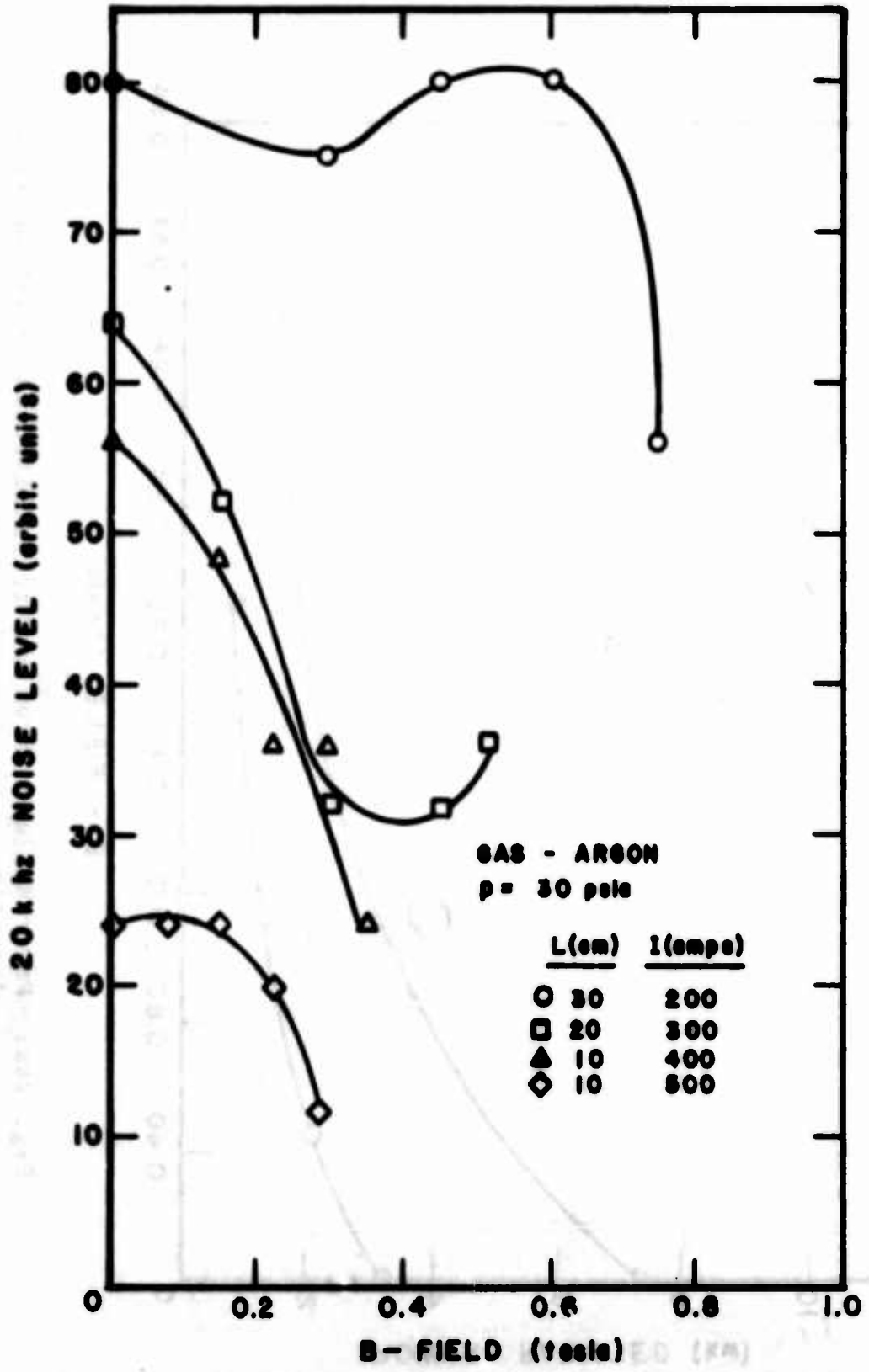

Fig. 27. Electrical Noise Level Around 20K Hz in Argon vs Applied Magnetic Field Strength

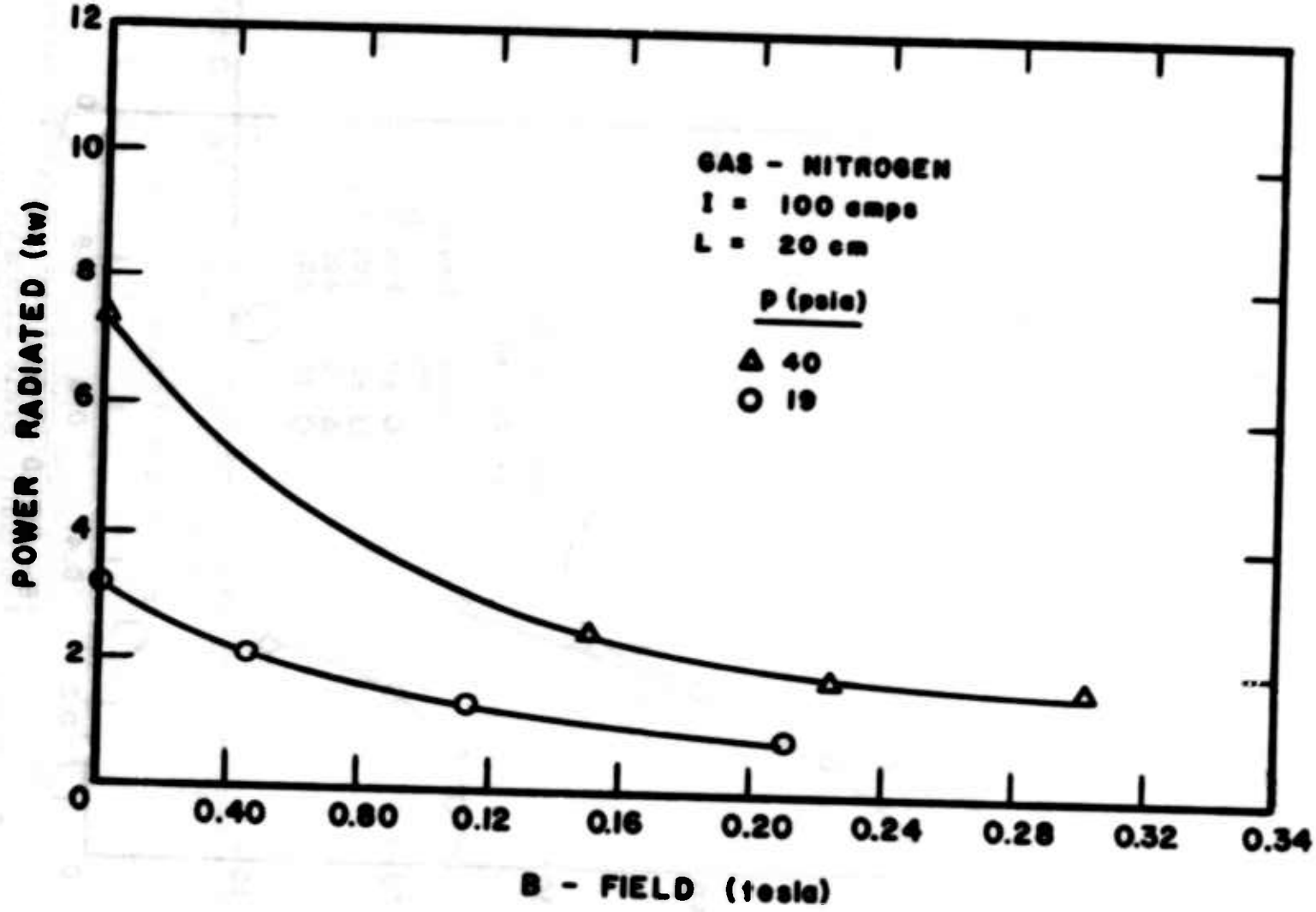

Fig. 28a. Power Radiated from an Arc in Nitrogen vs the Applied Magnetic Field Strength

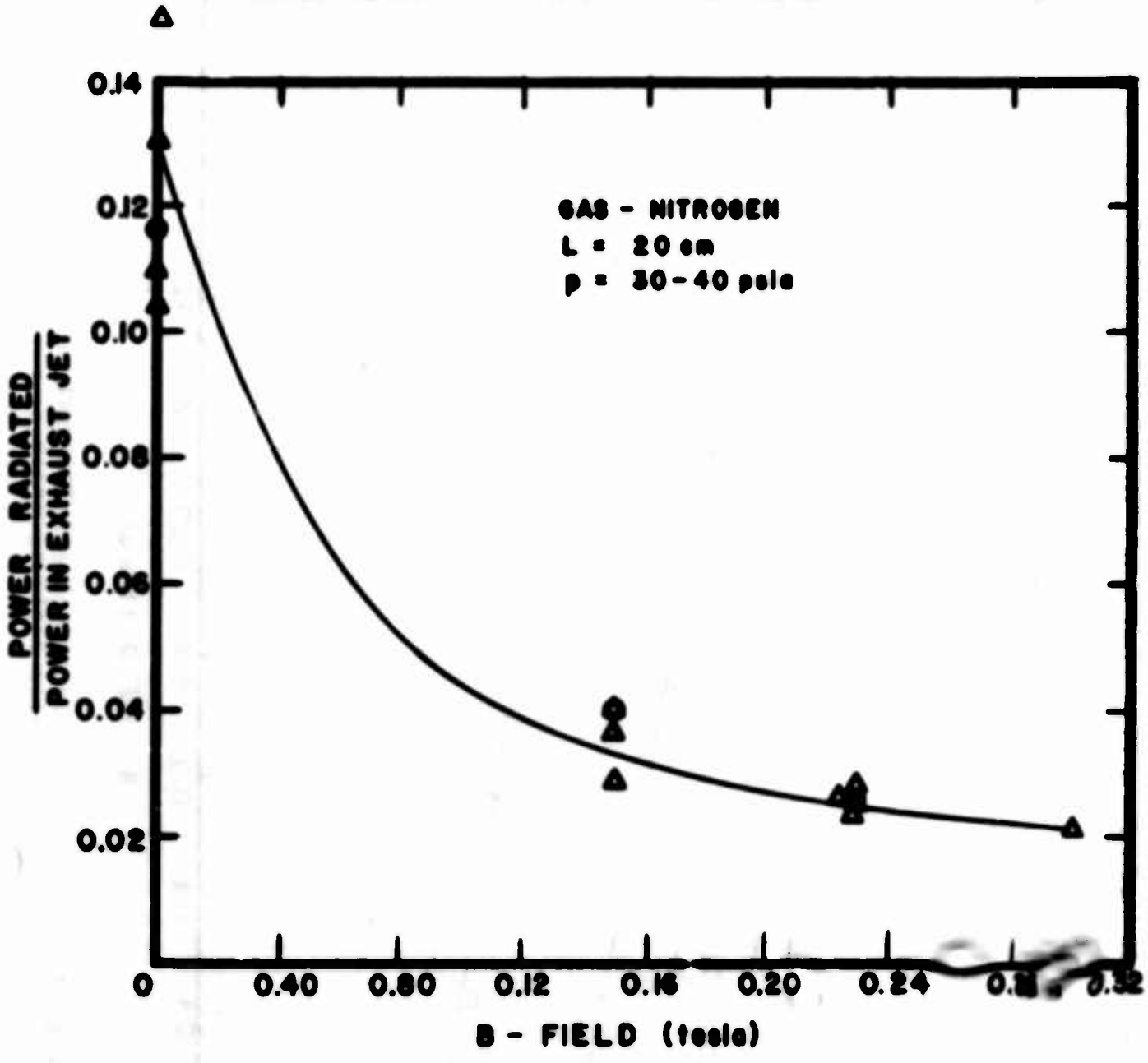

Fig. 28b. Ratio of Power Radiated to Power in Gas in Nitrogen vs the Applied Magnetic Field Strength

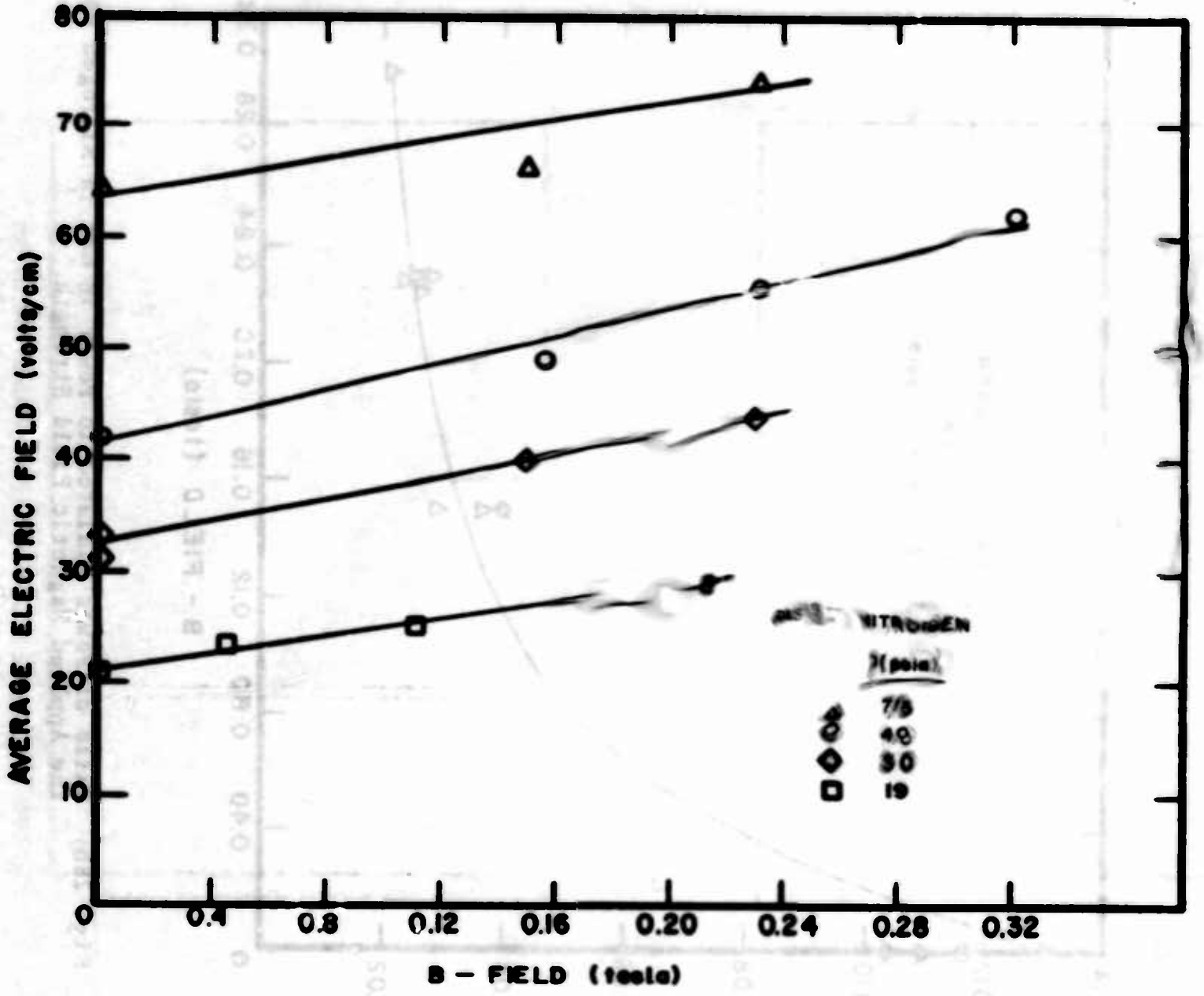

Fig. 29. Average Arc Electric Field Strength in Nitrogen vs the Applied Magnetic Field Strength

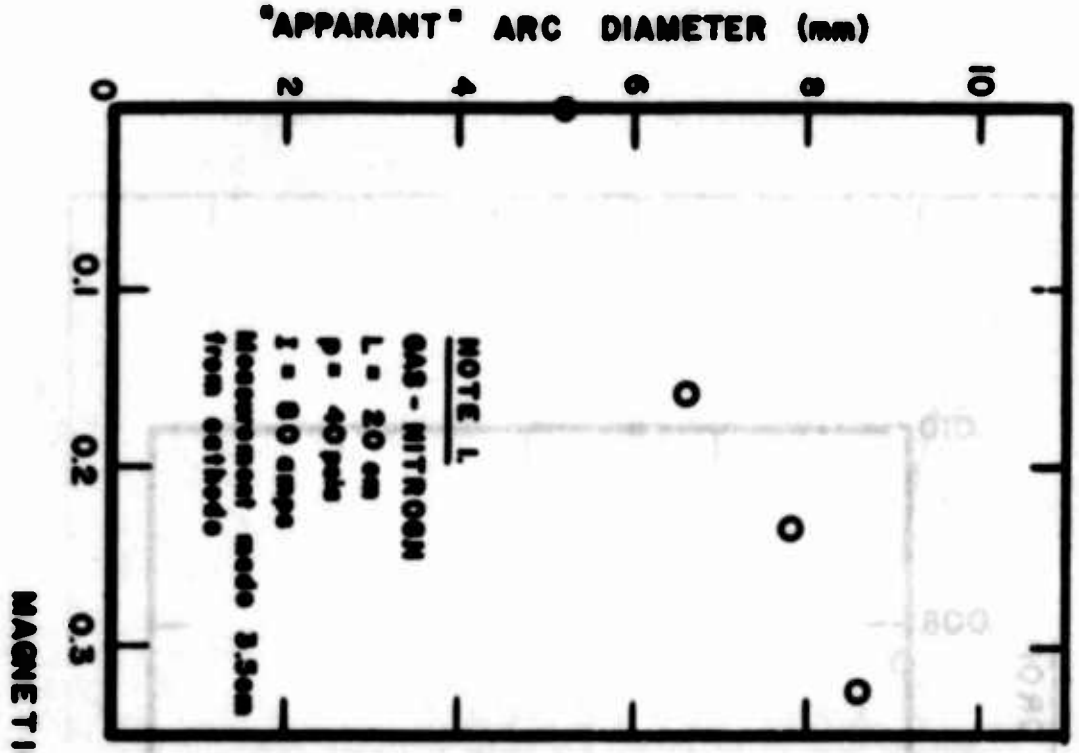

Fig. 30. "Effective" Arc Diameter in Nitrogen vs the Applied Magnetic Field Strength

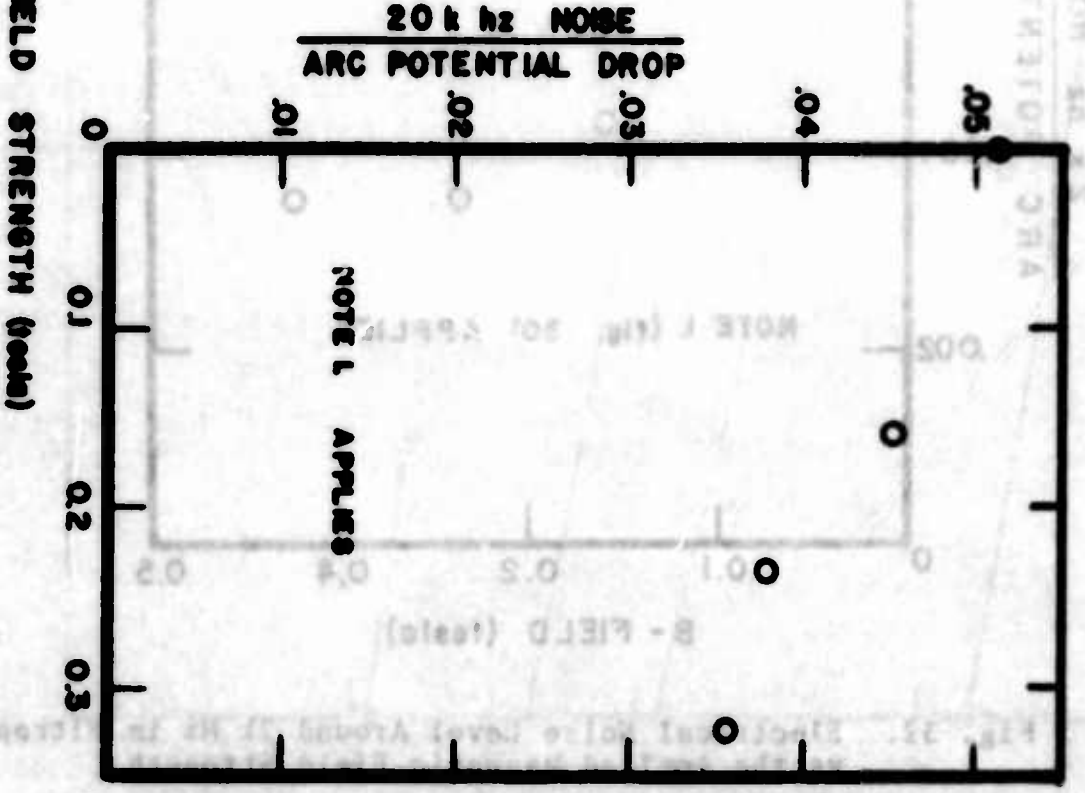

Fig. 31. Electrical Noise Level Around 20k Hz in Nitrogen vs the Applied Magnetic Field Strength

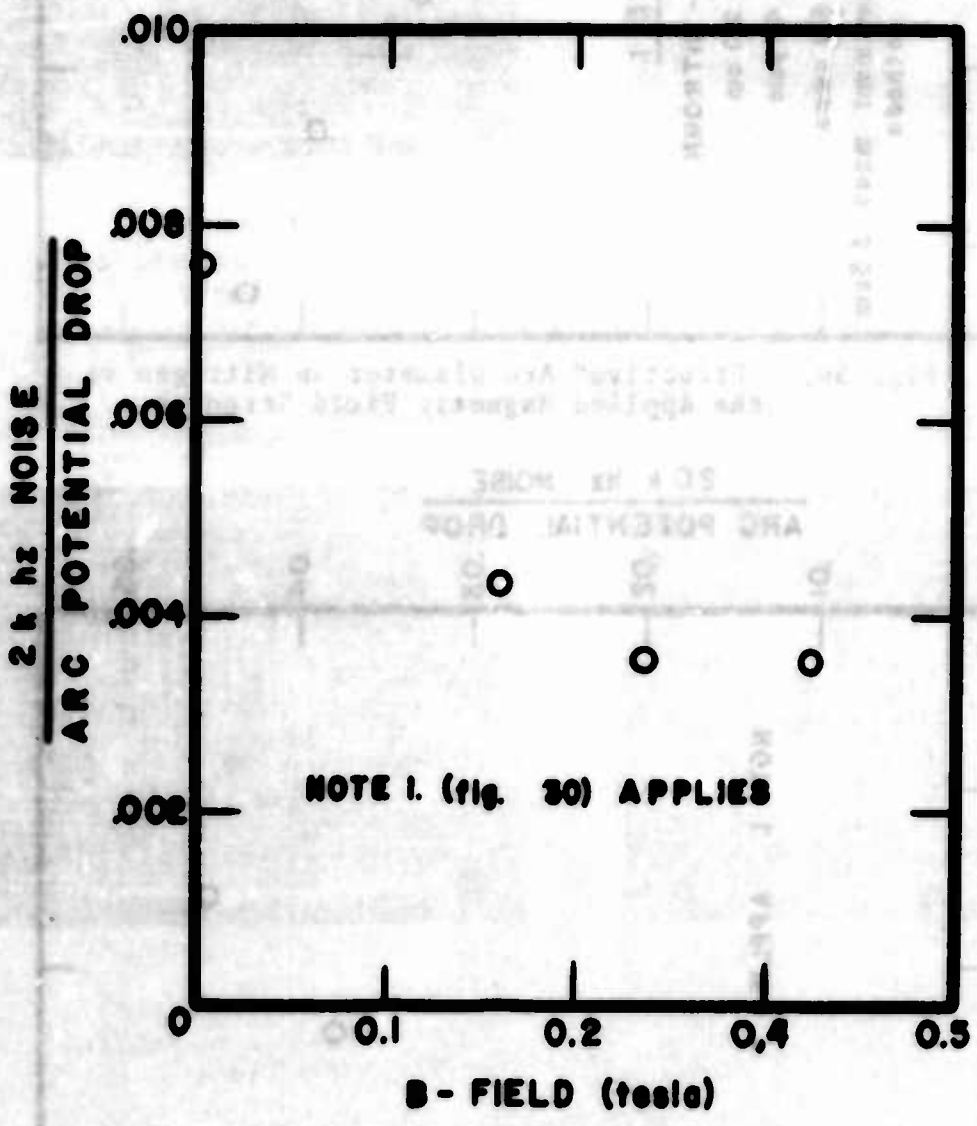

Fig. 32. Electrical Noise Level Around 2k Hz in Nitrogen vs the Applied Magnetic Field Strength

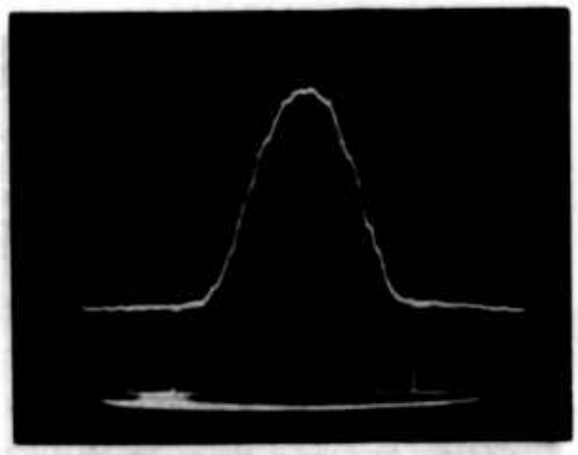

Ordinate 10 m. V/cm
Abscissa 0.2 m sec/cm
B = 0

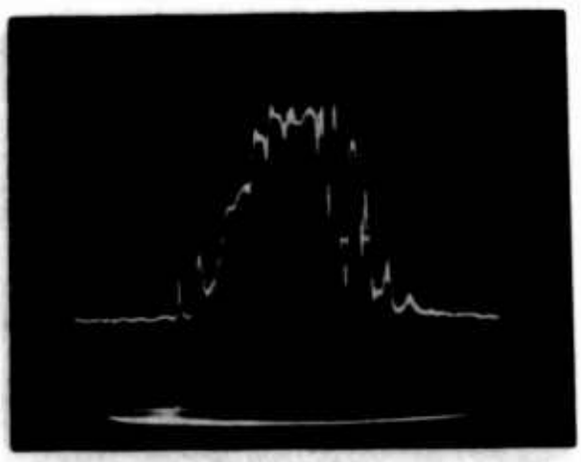

Ordinate 10 m. V/cm
Abscissa 0.2 m. sec/cm
B = 0.0225 Tesla

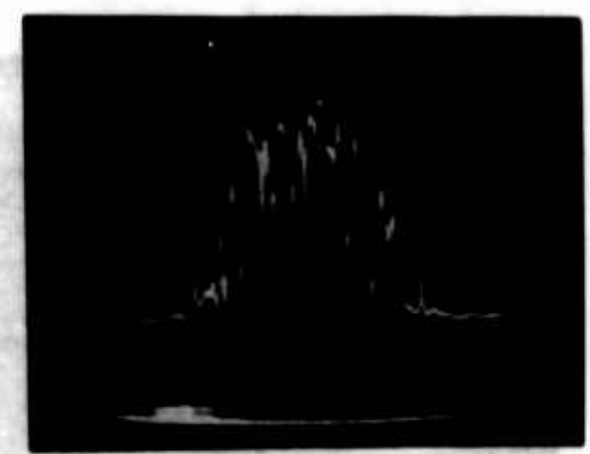

Ordinate 10 m. V/cm
Abscissa 0.2 m. sec/cm
B = .024 Tesla

Ordinate 10 m. V/cm
Abscissa 0.2 m. sec/cm
B = 0.030 Tesla

Figure 33. Oscilloscope Traces from the Fast Pulse in Nitrogen for Several "Negative" Magnetic Field Strengths

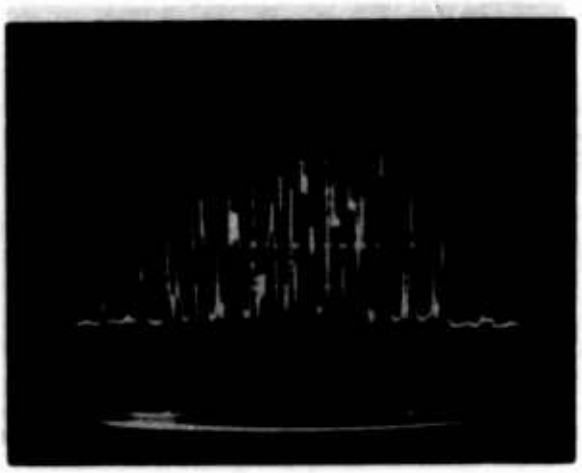

Ordinate 10 mV/cm
Abscissa 0.2 m. sec/cm
B = 0.045 Tesla

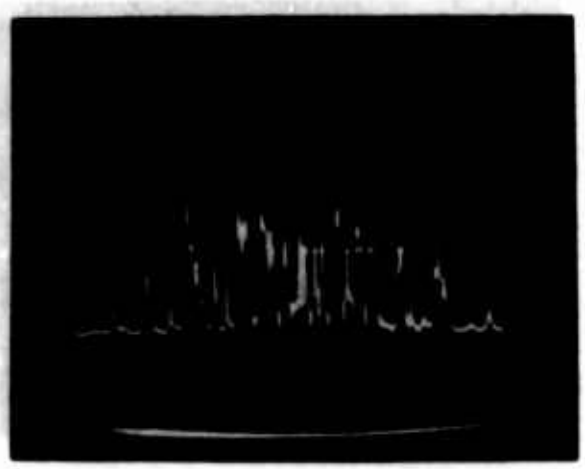

Ordinate 10 m. V/cm
Abscissa 0.2 m. sec/cm
B = 0.060 Tesla

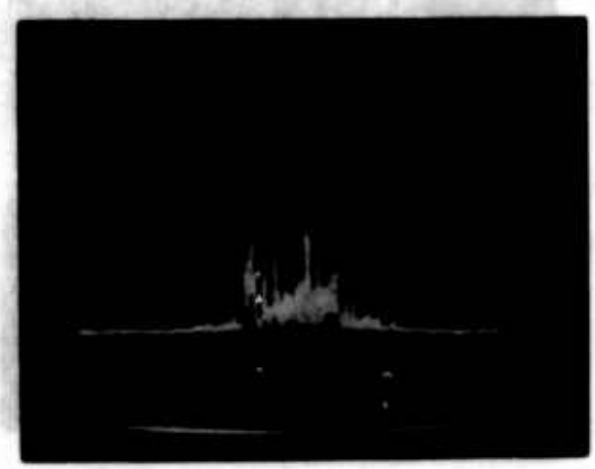

Ordinate 10 m. V/cm
Abscissa 0.5 m. sec/cm
B = 0.075 Tesla

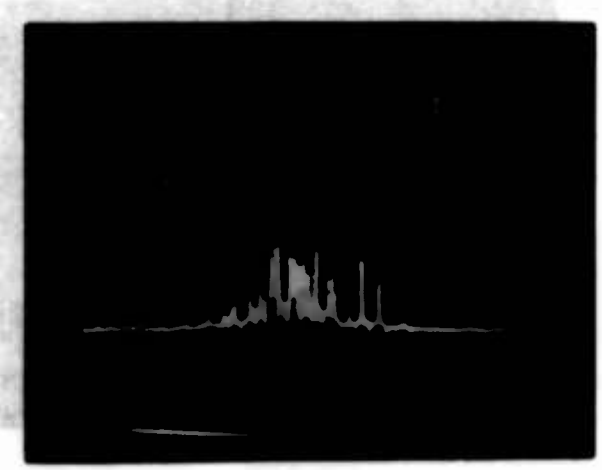

Ordinate 10 m. V/cm
Abscissa 0.5 m. sec/cm
B = 0.090 Tesla

Figure 33 (cont'd)

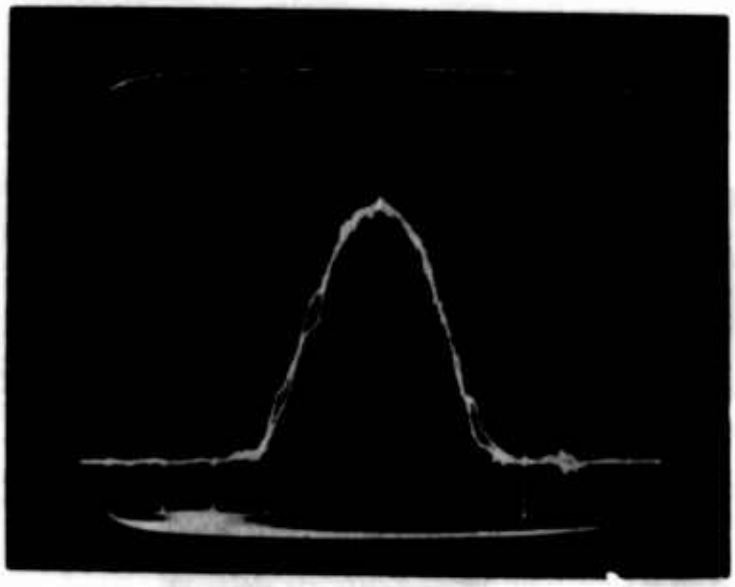

Ordinate 10 m. V/cm
Abscissa 0.2 m. sec/cm
B = 0

Ordinate 10 m. V/cm
Abscissa 0.2 m. sec/cm
B = 0.105 Tesla

Figure 34. Oscilloscope Traces from the Fast Disc in Nitrogen for Several "Negative" Magnetic Field Strengths

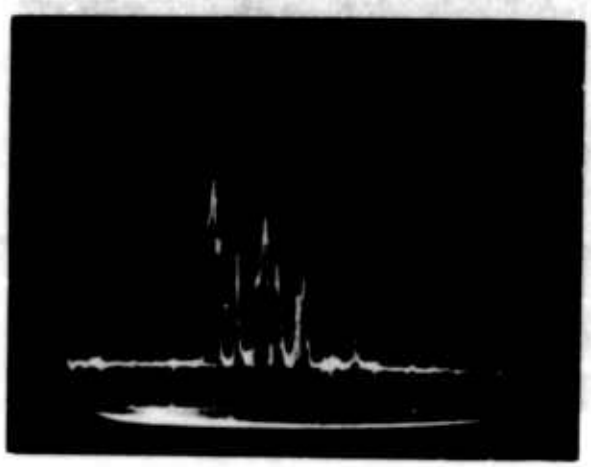

Ordinate 10 m. V/cm
Abscissa 0. 5 m. sec/cm
B = -0. 0195 Tesla

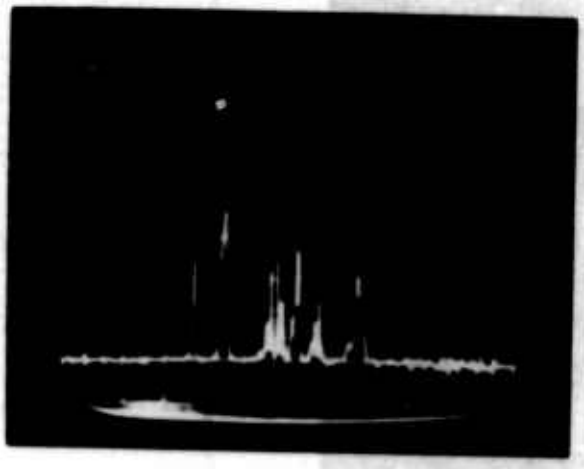

Ordinate 10 m. V/cm
Abscissa 0. 5 m. sec/cm
B = -0. 030 Tesla

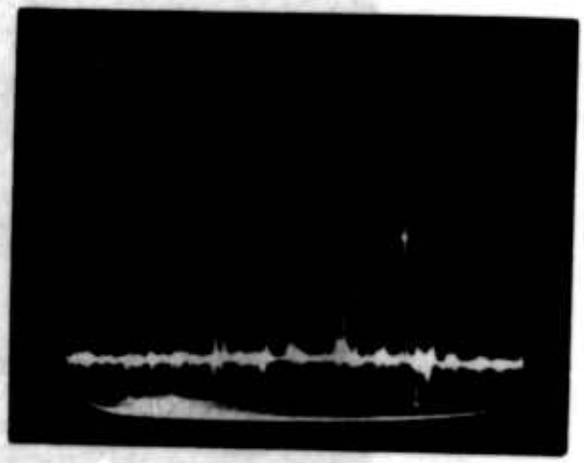

Ordinate 10 m. V/cm
Abscissa 0. 5 m. sec/cm
B = -0. 045 Tesla

Figure 34. (cont'd)

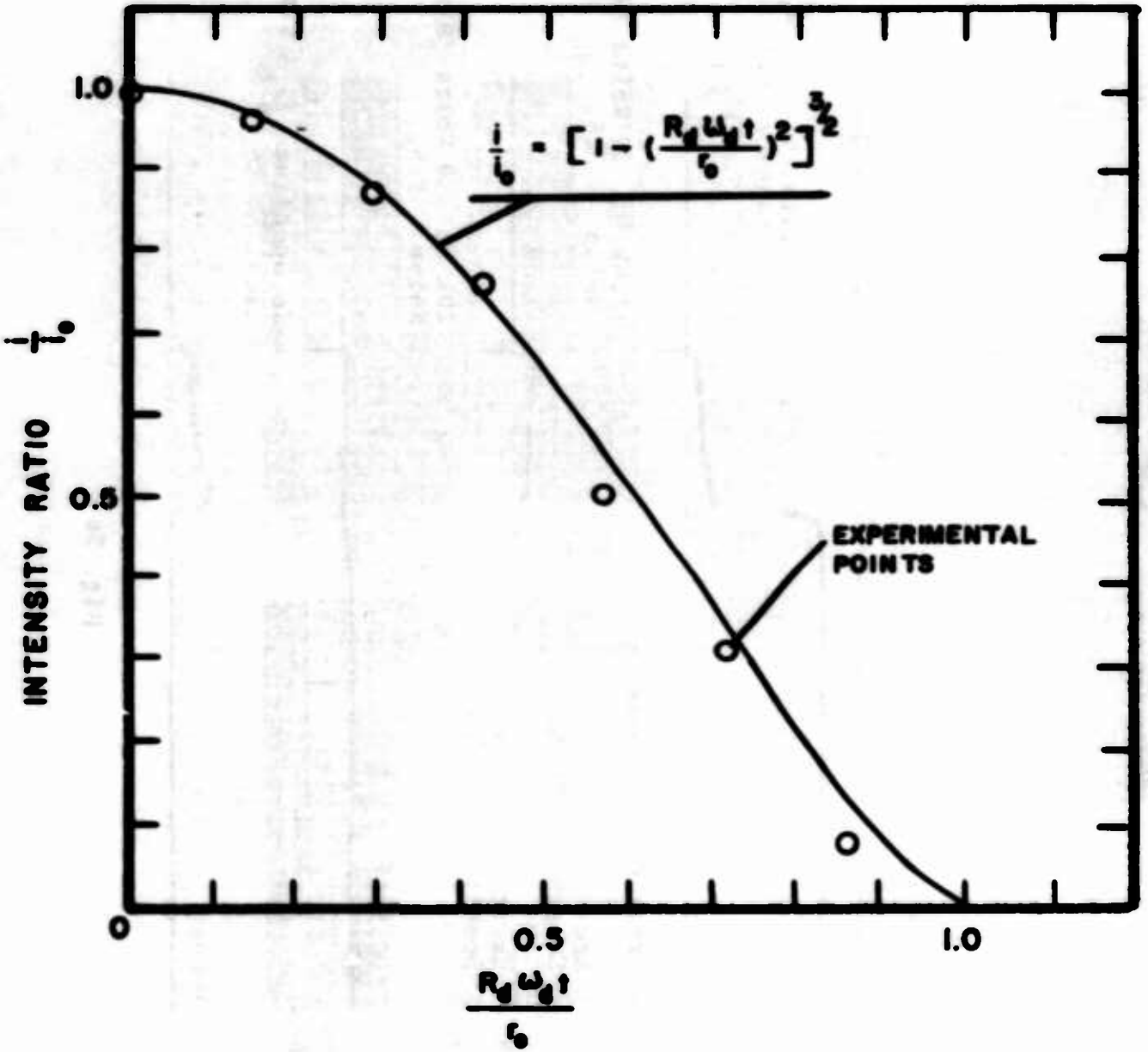

Fig. 35. Computed and Measured Light Intensity Ratio from Arc

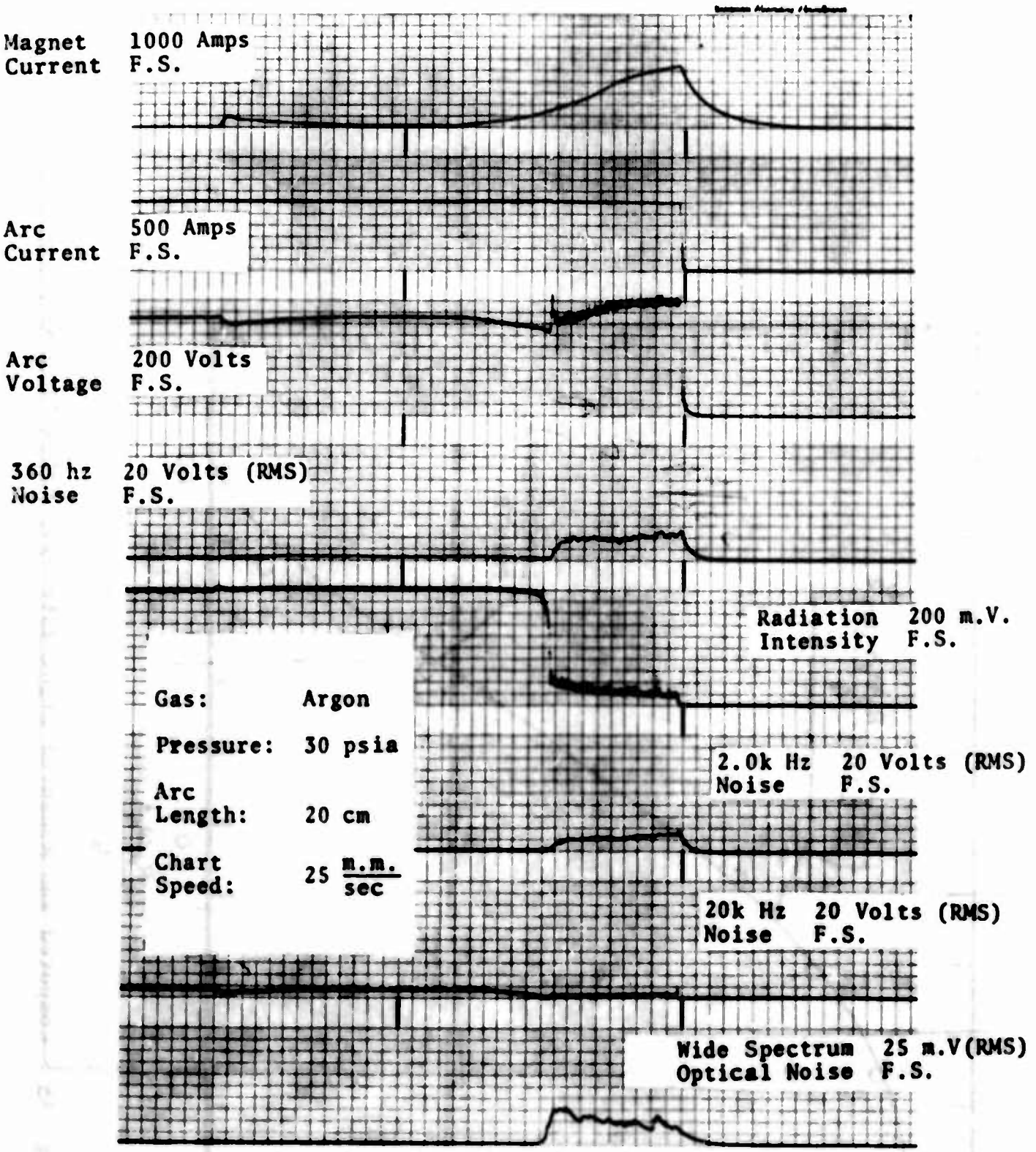
Magnet Current
1000 Amps F.S.
Arc Current
500 Amps F.S.
Arc Voltage
200 Volts F.S.
360 hz Noise
20 Volts (RMS) F.S.
Radiation Intensity
200 m.V. F.S.
Gas: Argon
Pressure: 30 psia
Arc Length: 20 cm
Chart Speed: 25 m.m./sec
2.0k Hz Noise
20 Volts (RMS) F.S.
20k Hz Noise
20 Volts (RMS) F.S.
Wide Spectrum Optical Noise
25 m.V(RMS) F.S.

Fig. 36

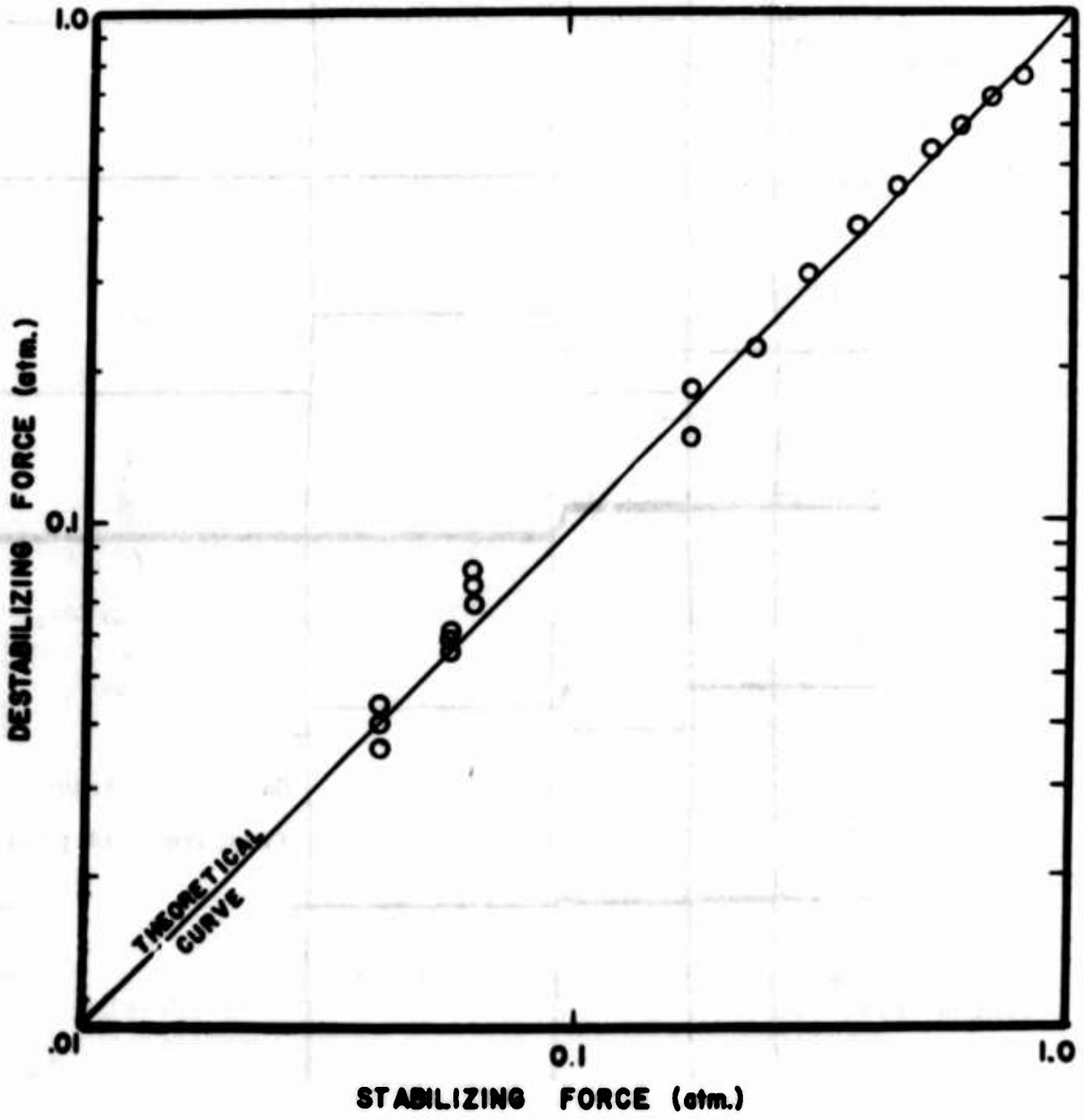

Fig. 37. Vortex Stabilization Data

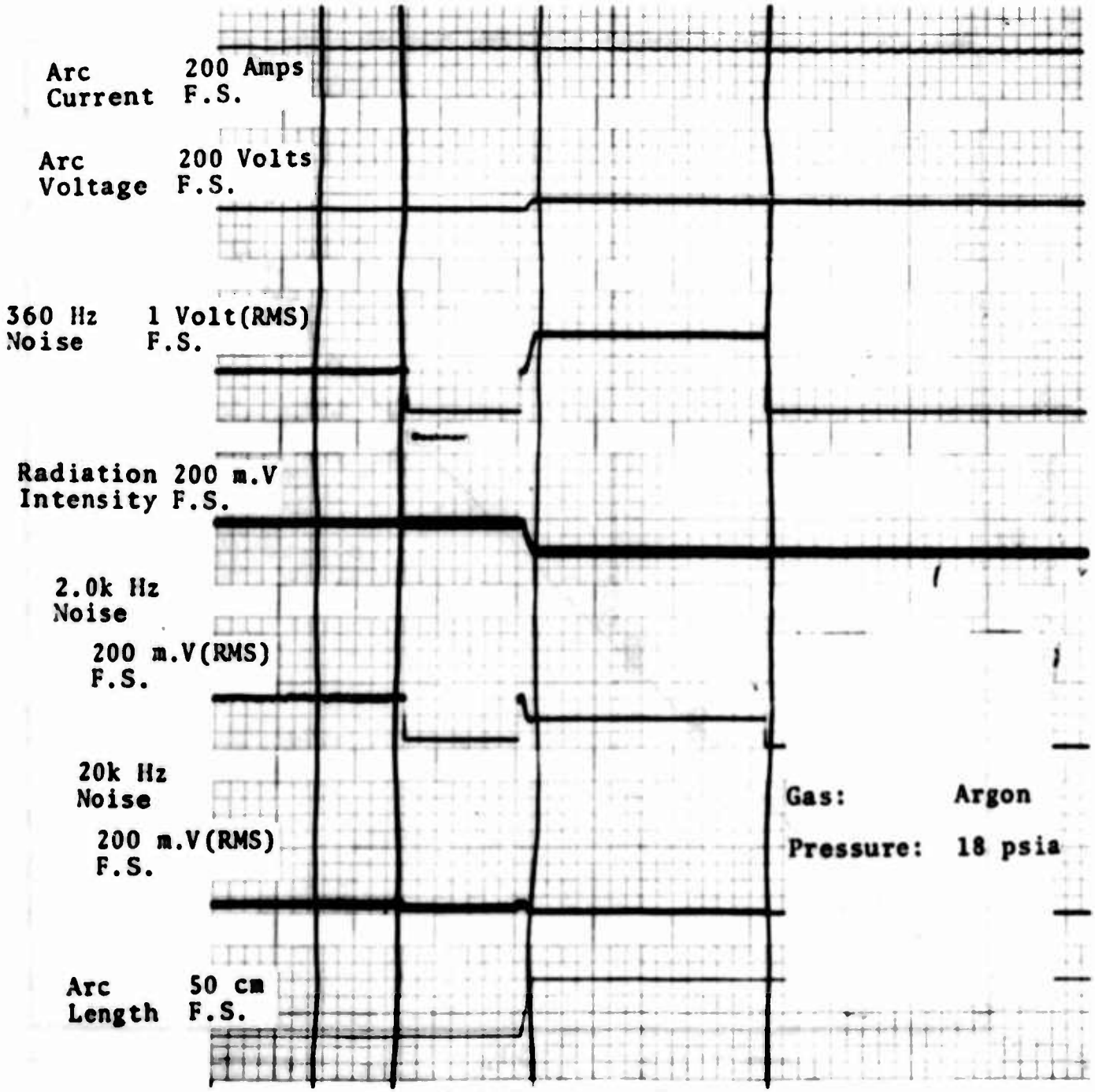
Arc Current 200 Amps F.S.
Arc Voltage 200 Volts F.S.
360 Hz Noise 1 Volt(RMS) F.S.
Radiation Intensity 200 m.V F.S.
2.0k Hz Noise 200 m.V(RMS) F.S.
20k Hz Noise 200 m.V(RMS) F.S.
Arc Length 50 cm F.S.
Gas: Argon
Pressure: 18 psia

Fig. 38

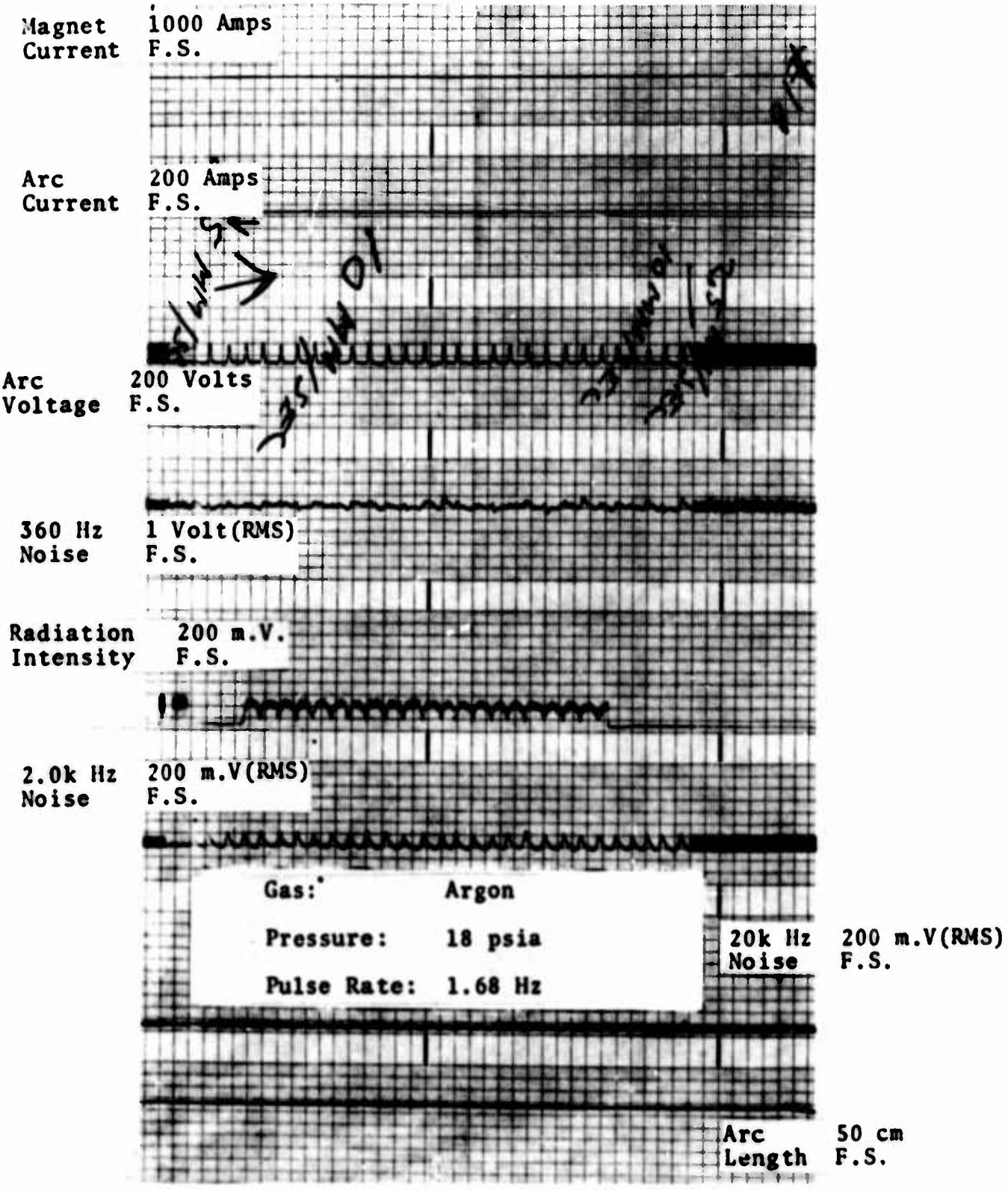
Magnet Current
1000 Amps F.S.
Arc Current
200 Amps F.S.
Arc Voltage
200 Volts F.S.
360 Hz Noise
1 Volt(RMS) F.S.
Radiation Intensity
200 m.V. F.S.
2.0k Hz Noise
200 m.V(RMS) F.S.
Gas: Argon
Pressure: 18 psia
Pulse Rate: 1.68 Hz
20k Hz Noise
200 m.V(RMS) F.S.
Arc Length
50 cm F.S.

Fig. 39

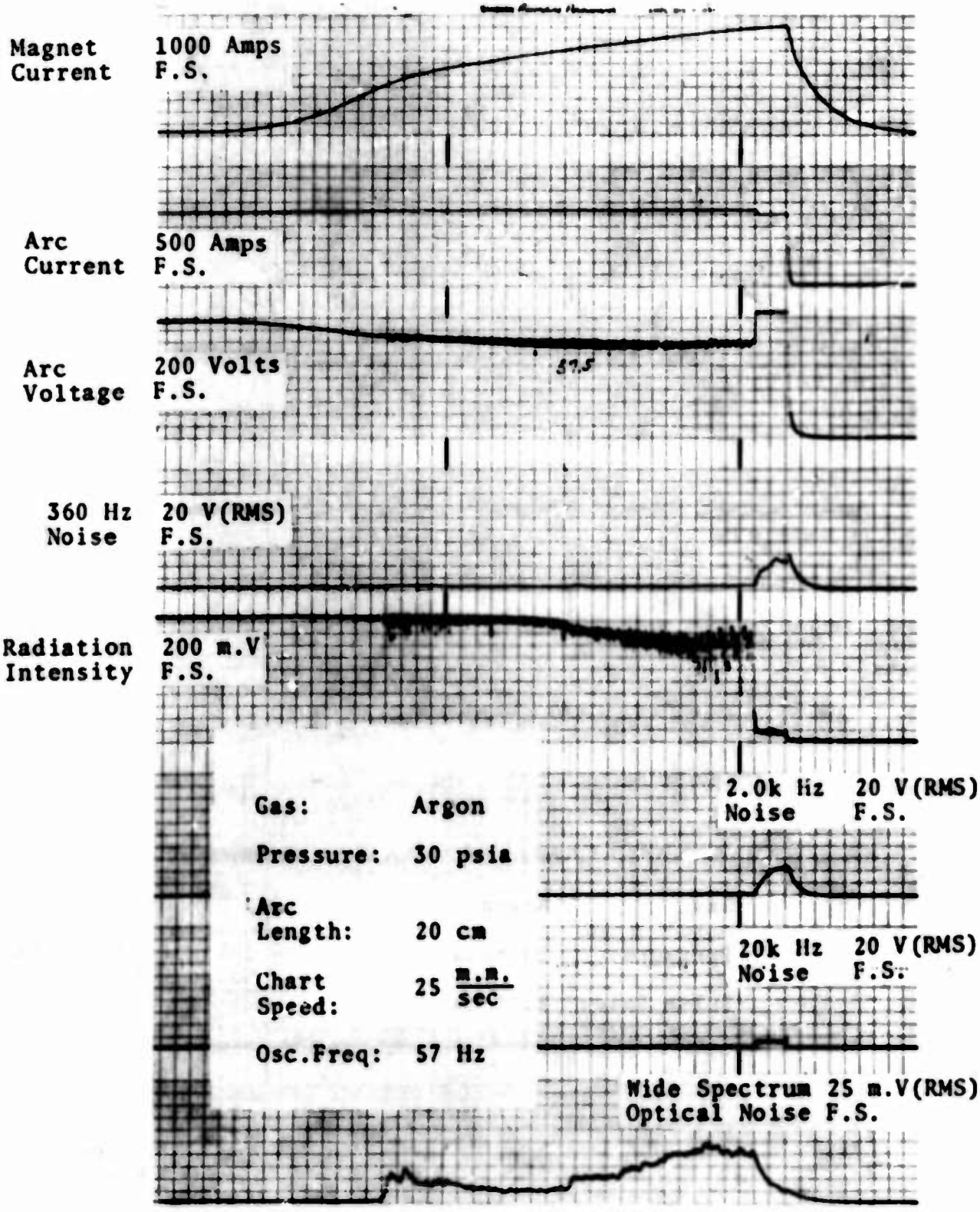
Magnet Current
1000 Amps F.S.
Arc Current
500 Amps F.S.
Arc Voltage
200 Volts F.S.
360 Hz Noise
20 V(RMS) F.S.
Radiation Intensity
200 m.V F.S.
Gas: Argon
Pressure: 30 psia
Arc Length: 20 cm
Chart Speed: 25 m.m./sec
Osc.Freq: 57 Hz
2.0k Hz Noise
20 V(RMS) F.S.
20k Hz Noise
20 V(RMS) F.S.
Wide Spectrum Optical Noise
25 m.V(RMS) F.S.

Fig. 40

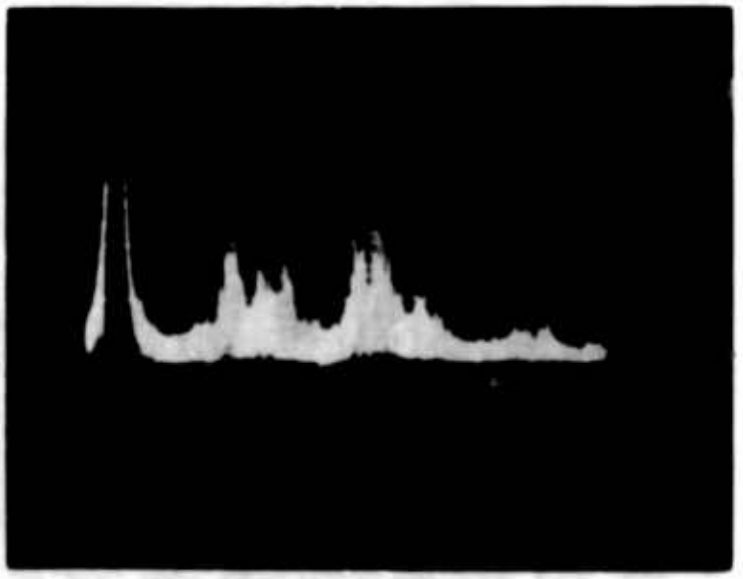

Fig. 41

Centerline Freq. = 5 k hz; 2V/cm
Arc Off
Output from Hotwire

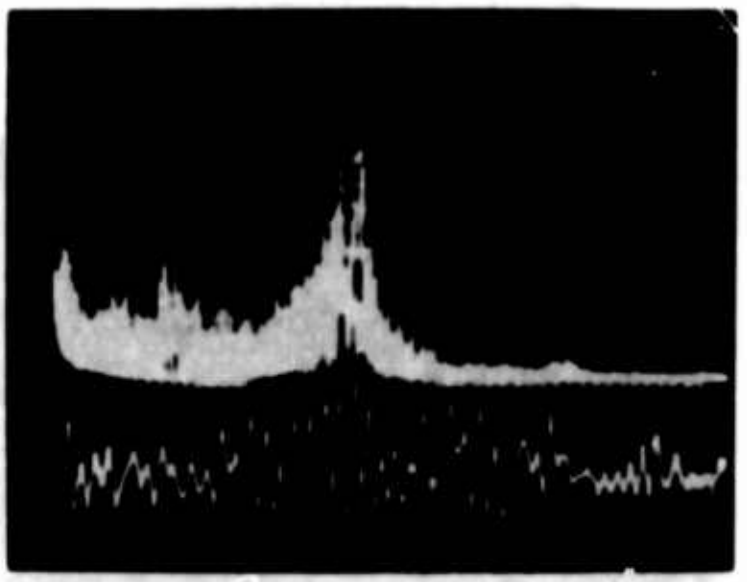

Fig. 42

Upper Trace
Centerline Freq. = 5 k hz; 0.5V/cm
Lower Trace
1 m. sec/cm ; 10 m. V/cm
Arc On
Output from Microphone

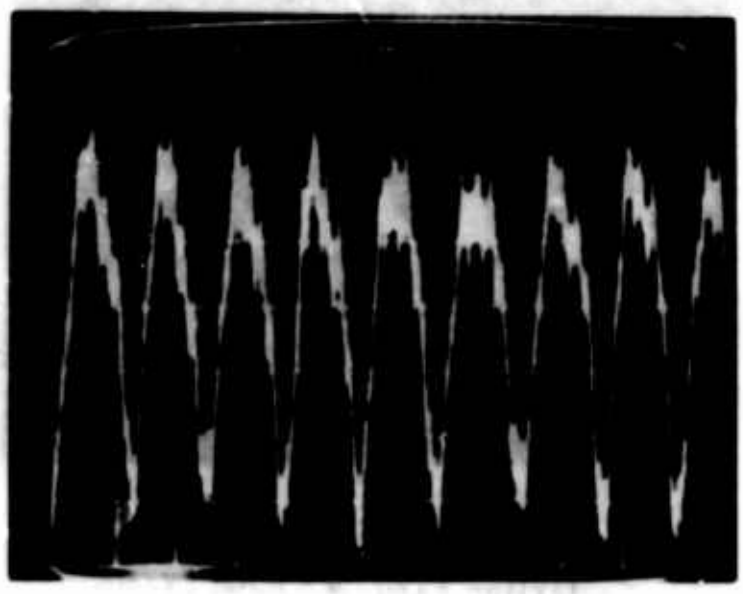

ig. 43

Ordinate 50 m. V/cm
Abscissa 50 m. sec/cm
Signal Across Electrodes

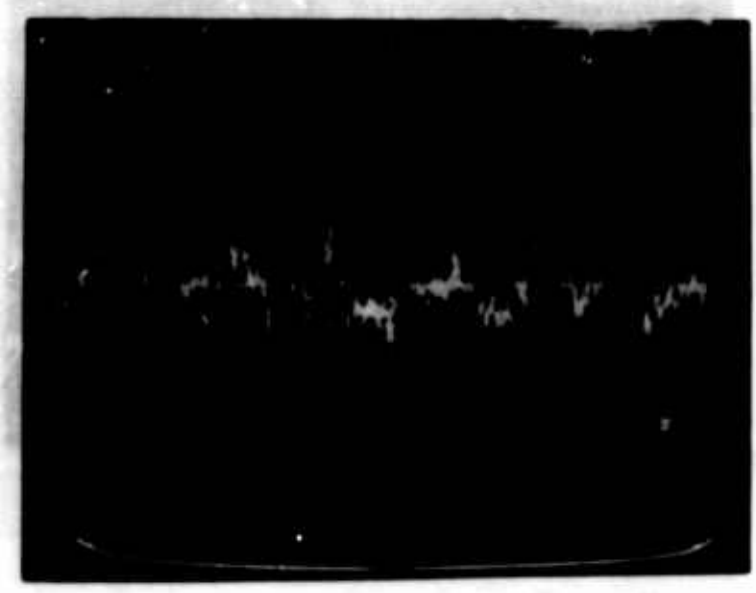

Fig. 44

Ordinate 5 m~~v~~/cm.
Abscissa 2 m. sec/cm
Peizo Gauge Output

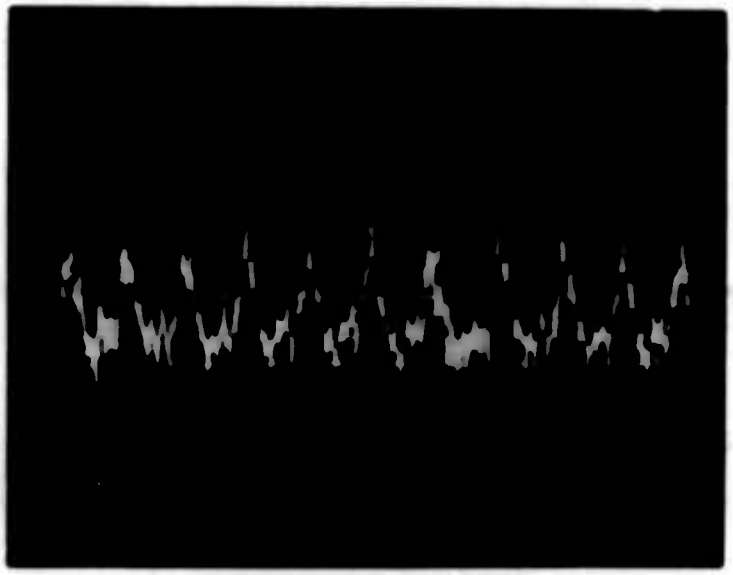

Fig. 45

Ordinate 10 m. V/cm
Abscissa 50 m. sec/cm
Photo Cell Output

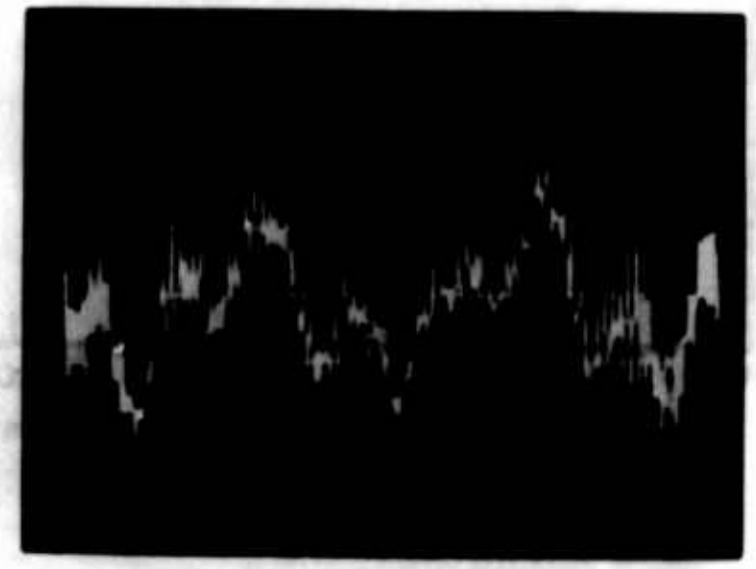

Fig. 46

Ordinate 5 m. V/cm
Abscissa 2 m. sec/cm
Microphone Output

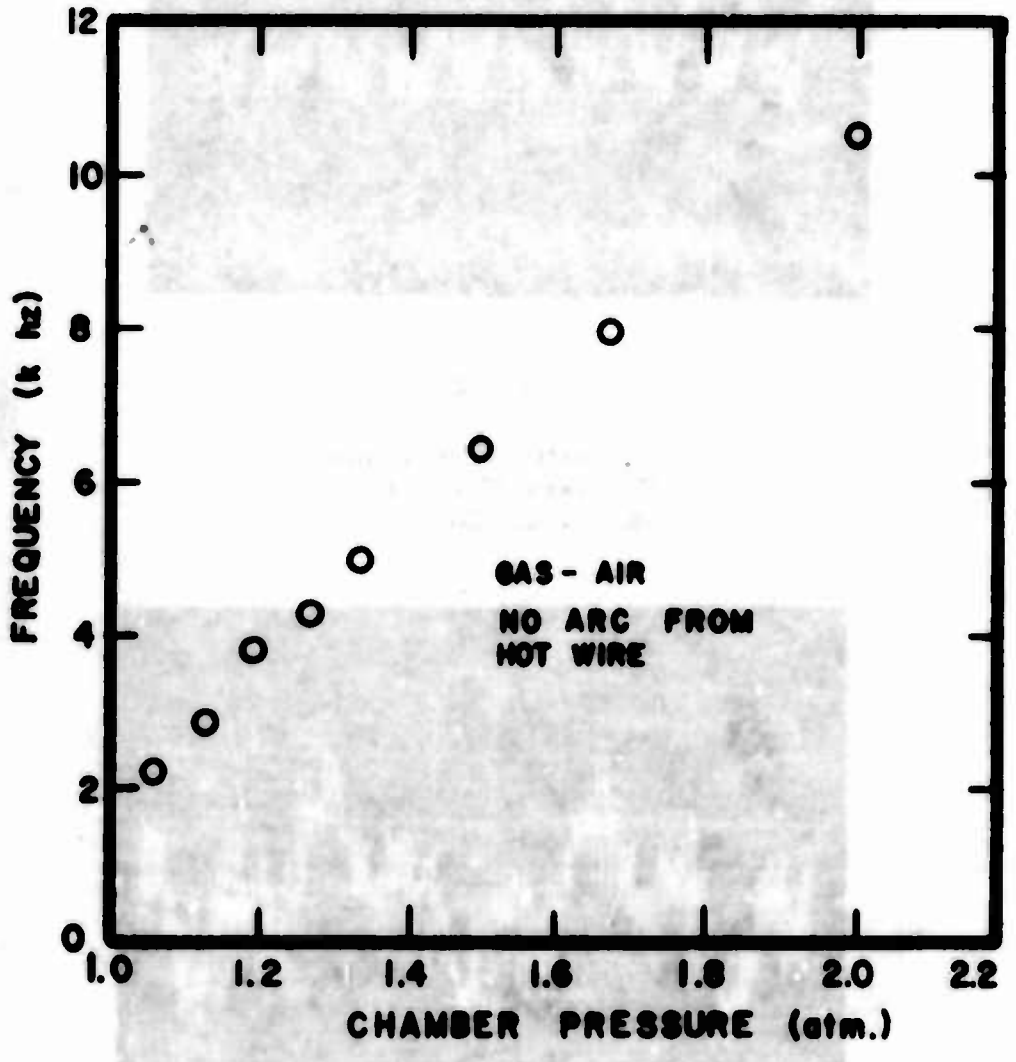

Fig. 47. Audio Frequency vs Chamber Pressure

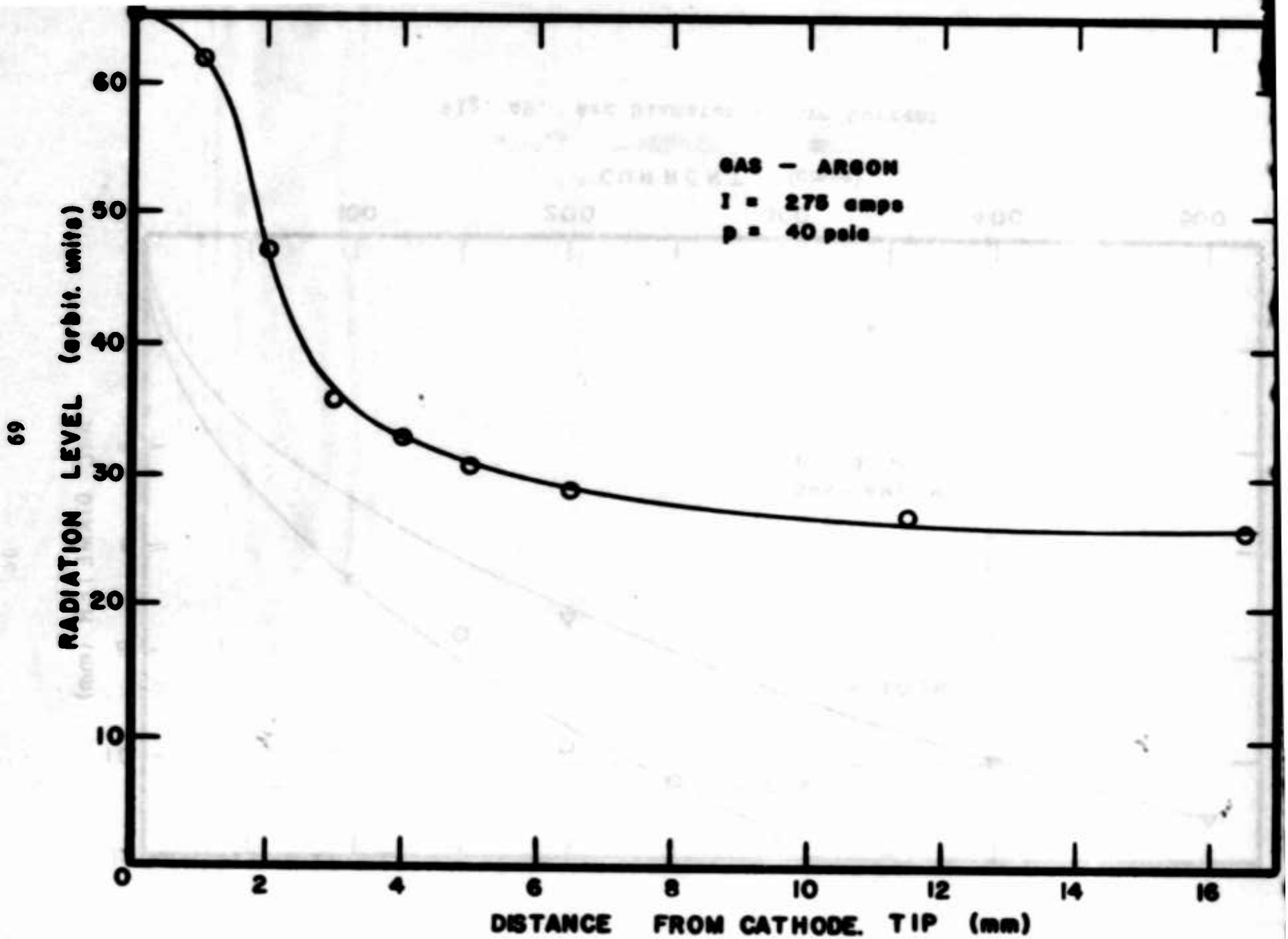

Fig. 48. Radiation Level Near the Cathode Attachment Point

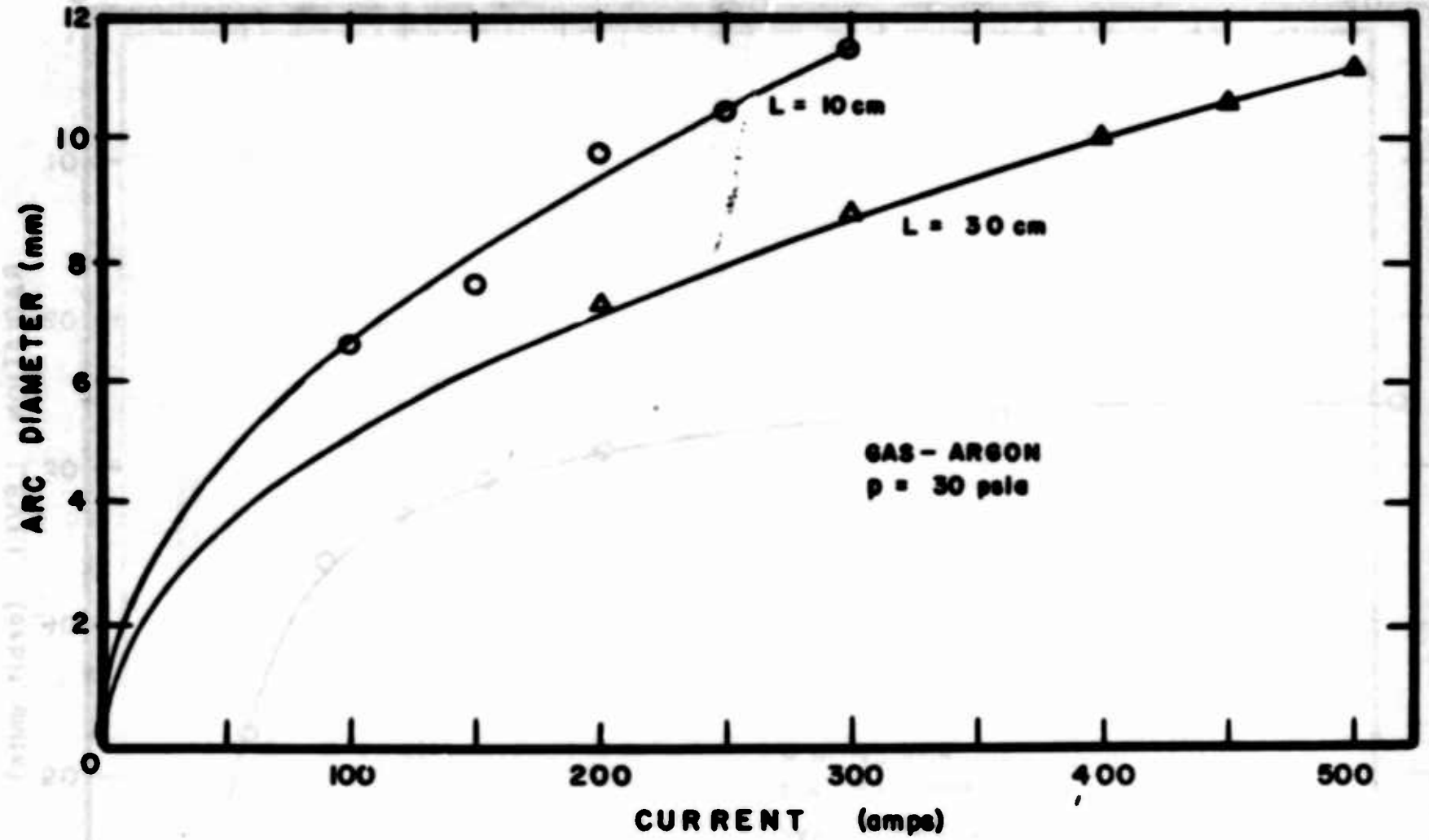

Fig. 49. Arc Diameter vs Arc Current

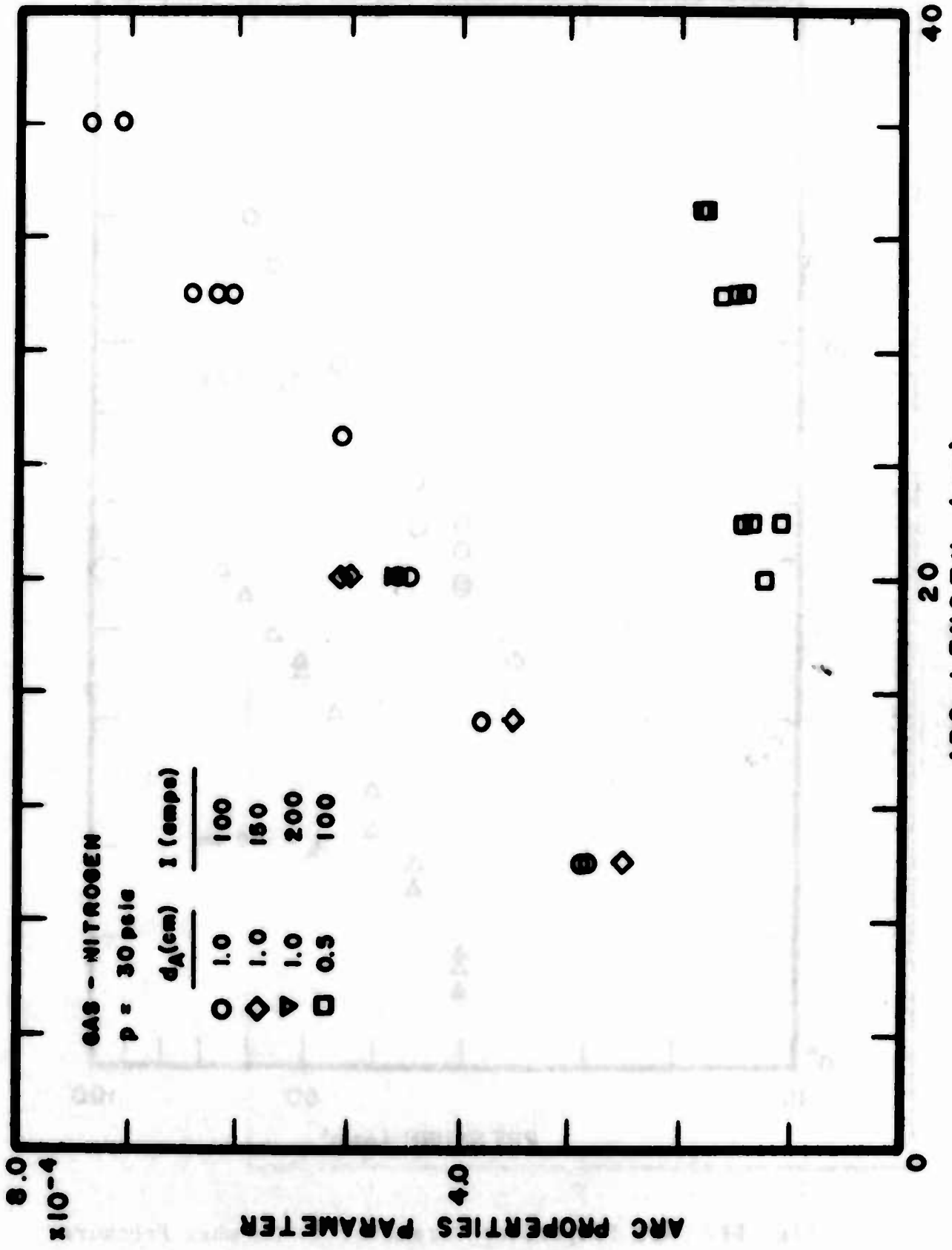

Fig. 50. Arc Properties Parameter vs Arc Length in Nitrogen

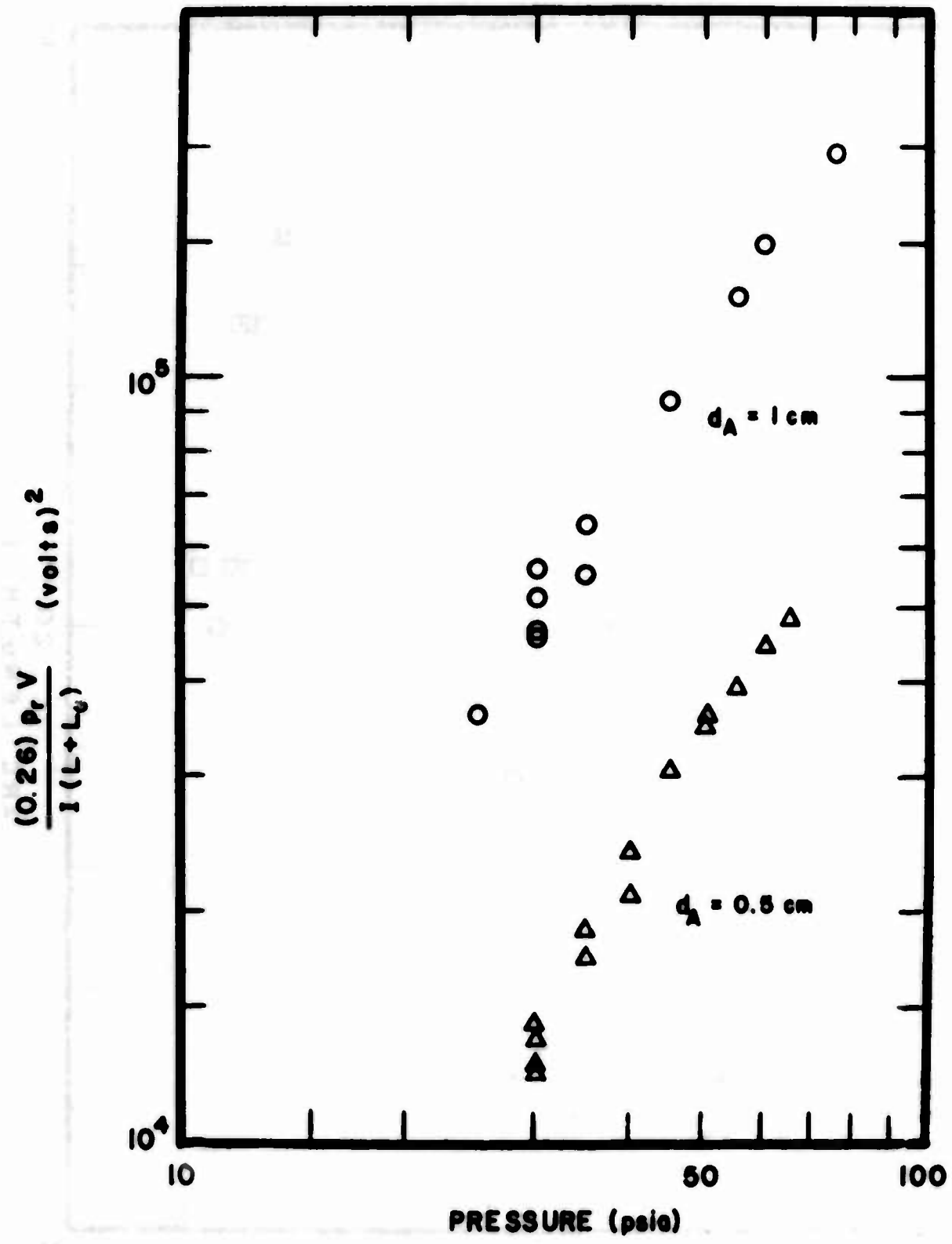

Fig. 51. Arc Properties Parameter vs Chamber Pressure

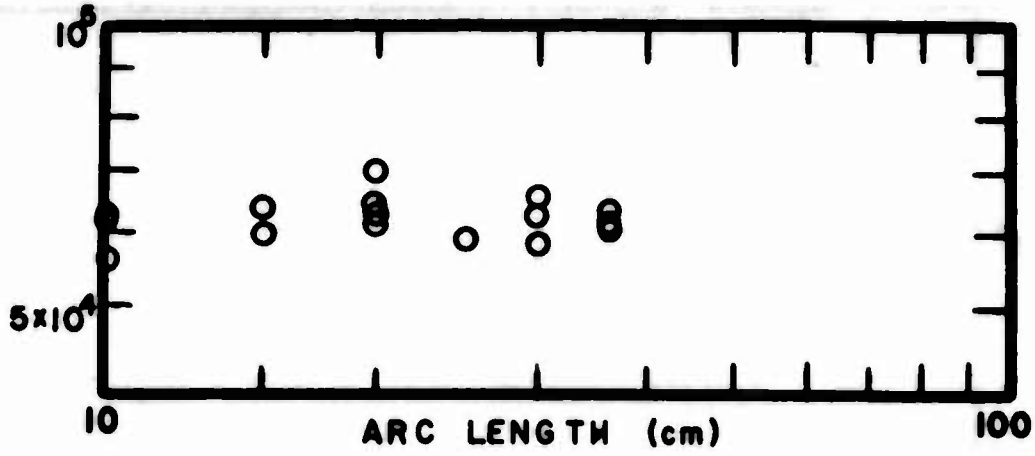

Fig. 52. Arc Properties Correlation Parameter vs Arc Length

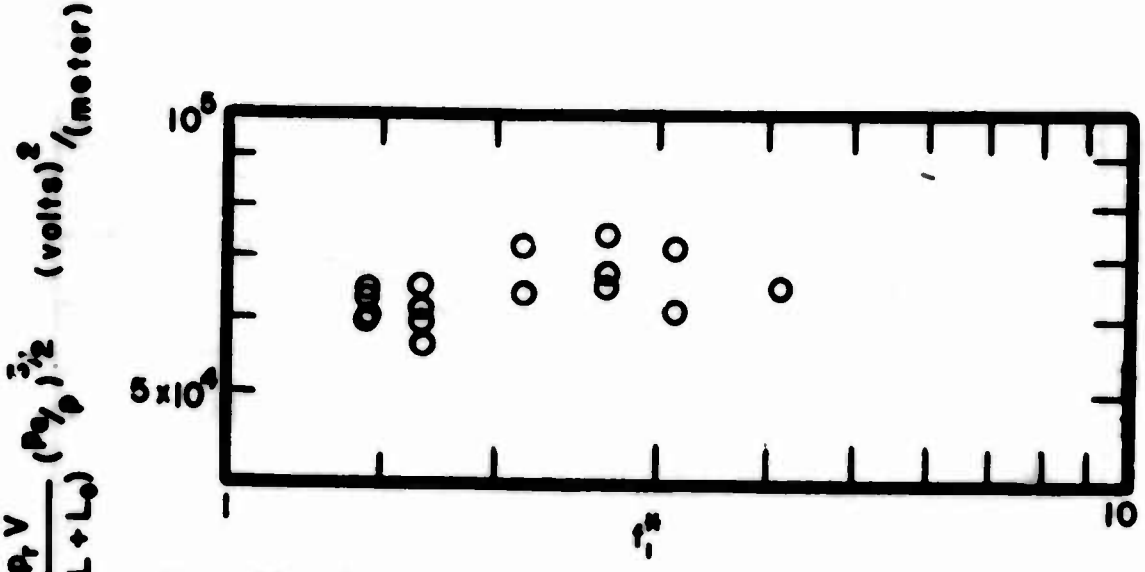

Fig. 53. Arc Properties Correlation Parameter vs Circulation in Gas

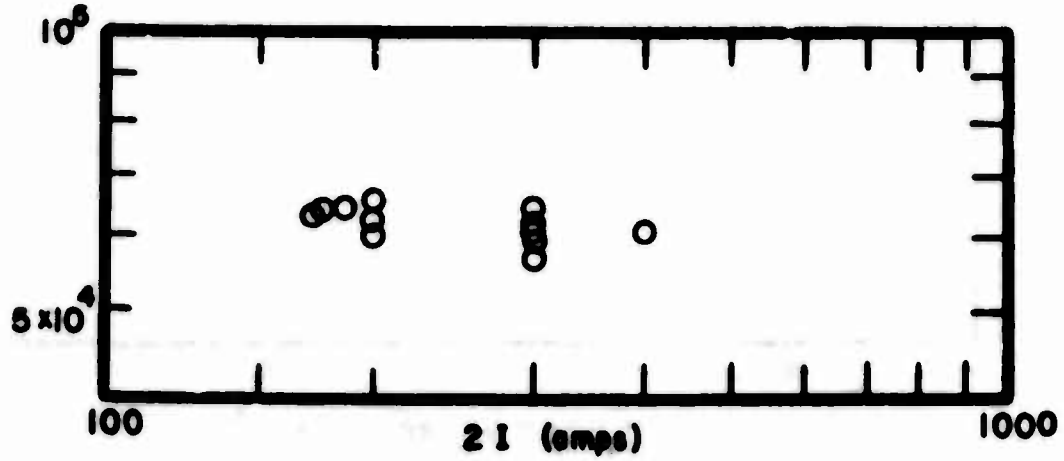

Fig. 54. Arc Properties Correlation Parameter vs Arc Current

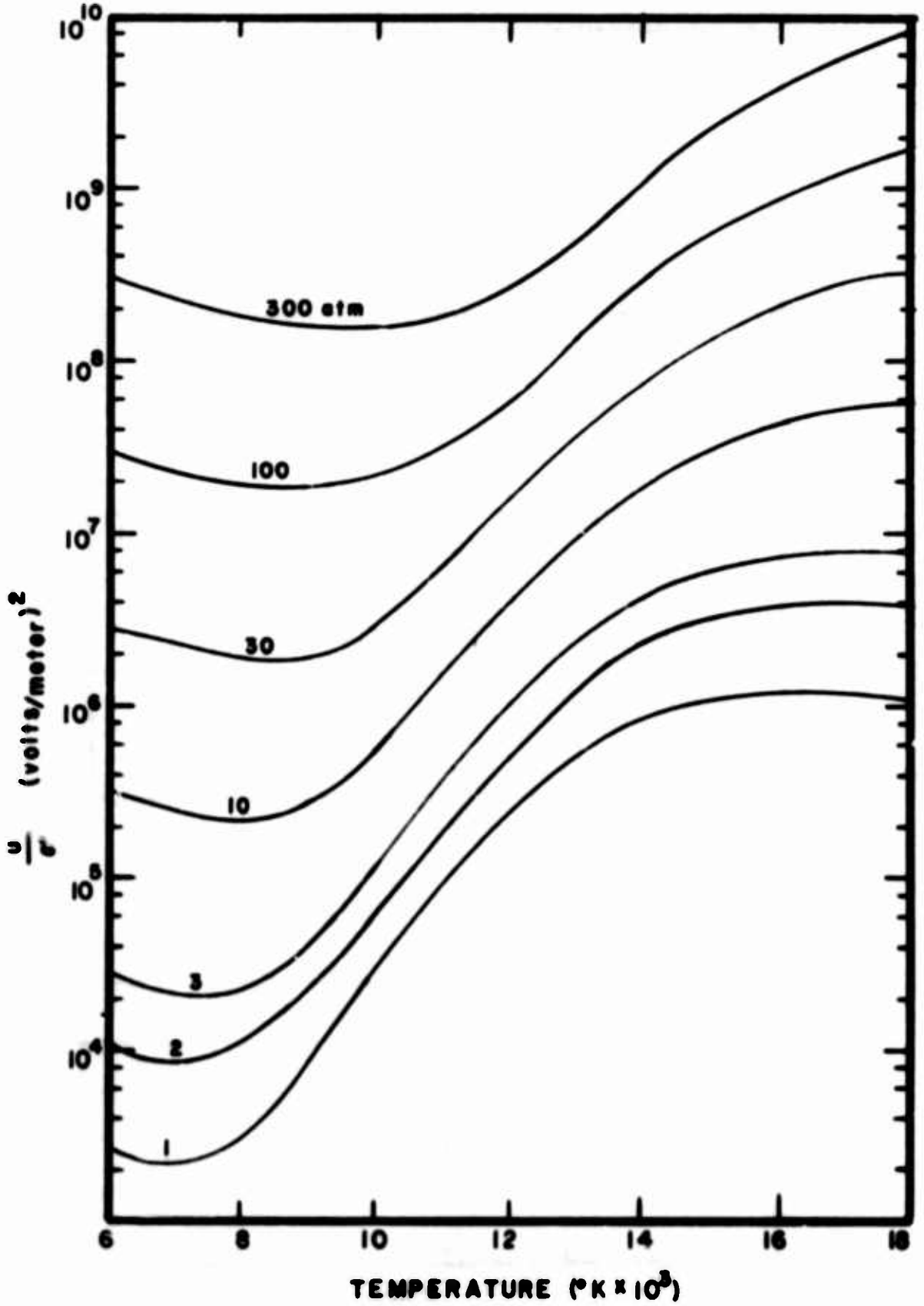

Fig. 55. Theoretical Values for the Function C(T,p) for Nitrogen Taken From Reference 13.

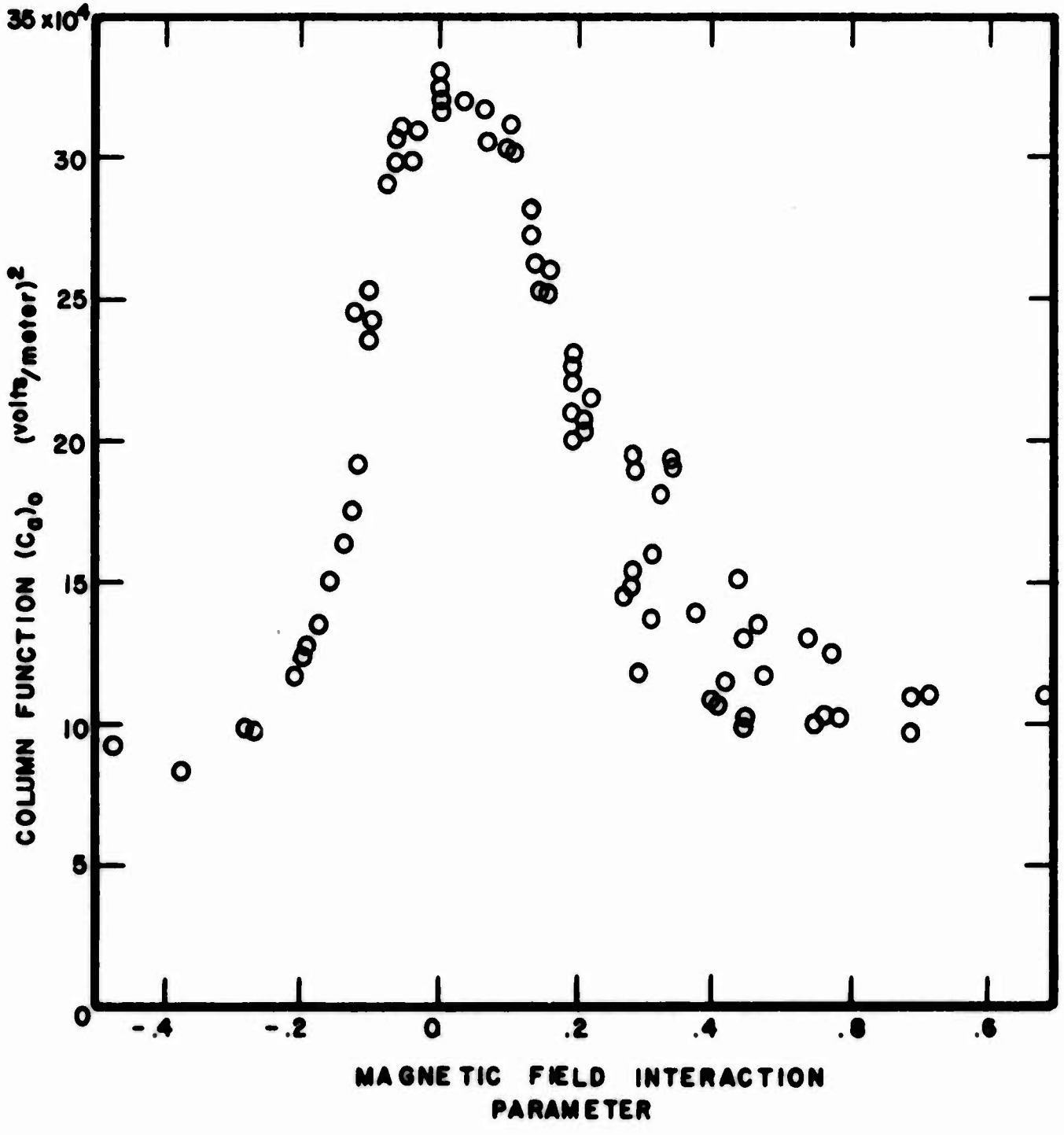

Fig. 56. Correlation of the C-Function with the Magnetic Interaction Parameter

APPENDIX I

RADIATION INTENSITY OBSERVED BY SCANNING A SPINNING AND CONVECTING HELICAL ARC

The calculation of the light intensity that would be observed from an arc that follows a helical path and is convected both azimuthally and axially can be carried out easily by considering it from a geometric point of view. Figure AI-1 shows the geometric diagram needed. The arc radius is defined by γ_o and R represents the radius of the helix. It is assumed that the cross-sectional area of the detector is very much smaller than the arc radius. Place the detector a distance y from the center of symmetry and now compute the light intensity observed there. Let the radial distribution of specific radiation in the arc be given by $u_{\ell} f(\gamma/\gamma_o)$. The intensity observed from an element of the arc along χ_o is

$$di = \pi/4(\Delta y)^2 \, 2\mu \cdot f(\gamma/\gamma_o) \, d\chi \qquad \text{AI-1}$$

The element Δx can be expressed in terms of angles as follows

$$\frac{d\chi}{R \cos \theta + y} = \sec^2 \alpha \, d\alpha = \frac{d\chi}{\cos^2 \alpha} \qquad \text{AI-2}$$

Using the relation that

$$R \cos \theta + y = \gamma_o \cos \phi$$

the intensity can be expressed as

$$i = \frac{\pi}{2}(\Delta y)^2 \, u_{\ell} \int_0^{\phi} f(\gamma/\gamma_o) \frac{R \cos \theta + y}{\cos^2 \alpha} \, d\alpha \qquad \text{AI-4}$$

Since

$$\frac{\gamma}{\gamma_o} = \frac{R \cos \theta + y}{\gamma_o \cos \alpha} = \frac{\cos \phi}{\cos \alpha}$$

$$i = \frac{\pi}{2} (\Delta y)^2 \, u_{\ell} \, \gamma_o \cos \phi \int_0^{\phi} f\left(\frac{\cos \phi}{\cos \alpha}\right) \frac{d\alpha}{\cos^2 \alpha} \qquad \text{AI-5}$$

If the distribution function $f(\gamma/\gamma_o)$ is parabolic, the integral can be evaluated as follows

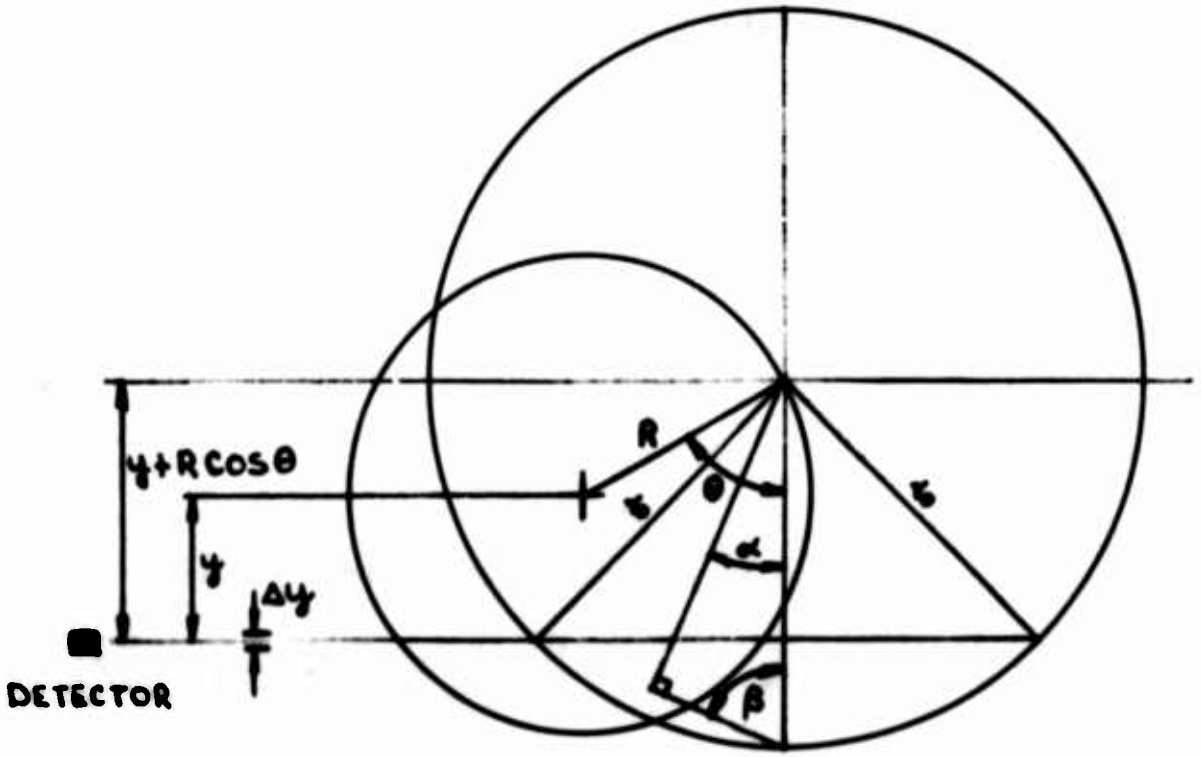

Fig. 57. Geometric Configuration for Computing Observed Light Intensity for a Moving Helical Arc

$$\int_0^{\phi} \left(1 - \frac{\cos^2 \phi}{\cos^2 \alpha}\right) \frac{d\alpha}{\cos^2 \alpha} = \tan \phi - \cos^2 \phi \int_0^{\phi} \frac{d\alpha}{\cos^4 \alpha}$$

$$= \frac{2}{3} \sin \phi \left\{ \frac{1}{\cos \phi} - \cos \phi \right\}$$

The intensity then becomes

$$i = \frac{\pi}{\gamma} (\Delta y)^2 \gamma_o \mu_{\ell} |\sin^3 \phi| \qquad \text{AI-6}$$

Using the expression AI-3, this becomes

$$i = \frac{\pi}{\gamma} (\Delta y)^2 \gamma_o u_{\ell} \left\{ 1 - \left(\frac{\gamma + R \cos \theta}{\gamma_o} \right)^2 \right\}^{3/2} \qquad \text{AI-7}$$

Now the spin rate of the discharge is given by $\langle \omega \pm \rangle$ hence

$$\theta = \langle \omega \pm \rangle \qquad \text{AI-8}$$

The parameter y represents the position of scan and can be represented by

$$y = R_d \sin \omega_d t \qquad \text{AI-9}$$

or when $\omega_d t \ll \frac{\pi}{\gamma}$

$$y = R_d \omega_d t \qquad \text{AI-9a}$$

The final expression for the intensity of the light is

$$i = \frac{\pi}{\gamma} (\Delta y)^2 \gamma_o u_{\ell} \left\{ 1 - \left(\frac{R_d \omega_d t + R \cos \langle \omega \pm \rangle t}{\gamma_o} \right)^2 \right\}^{3/2} \qquad \text{AI-10}$$

This expression is evaluated for several values of

$$\frac{R_d \omega_d}{\gamma_o}, \quad \frac{R}{\gamma_o} d\omega \pm$$

The reference intensity is called i_o where

$$i_o = \frac{\pi}{\gamma} (\Delta y)^2 \gamma_o u_{\ell}$$

Figures 58 through 70 show plots of the function in Figure 66 vs. the time.

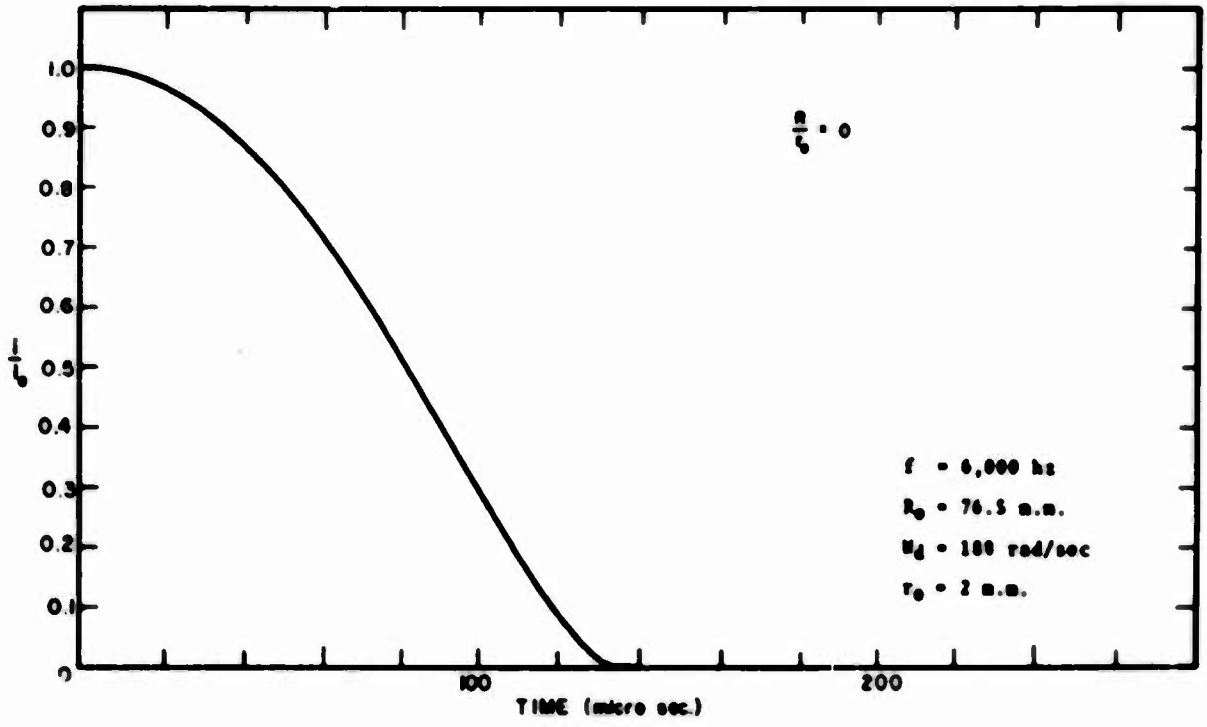

Figure 58. Light Intensity Observed by Scanning a Convecting Helical Arc

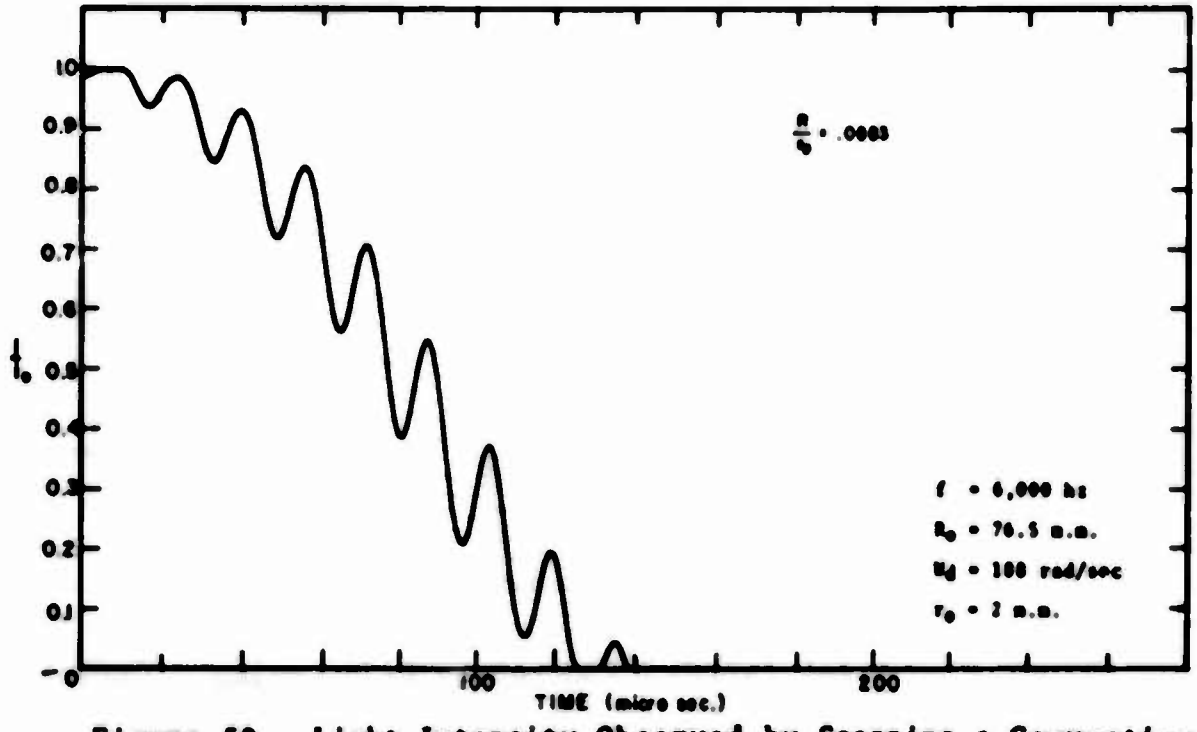

Figure 59. Light Intensity Observed by Scanning a Convecting Helical Arc

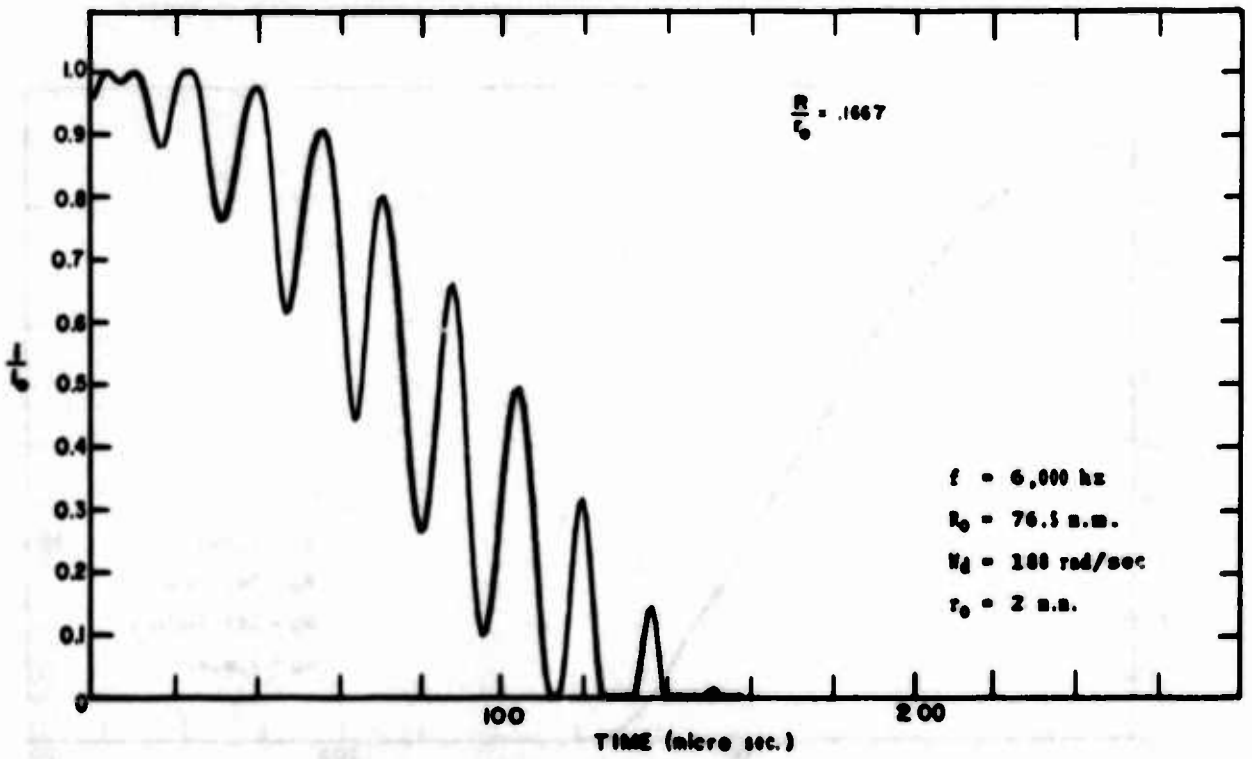

Figure 60. Light Intensity Observed by Scanning a Convecting Helical Arc

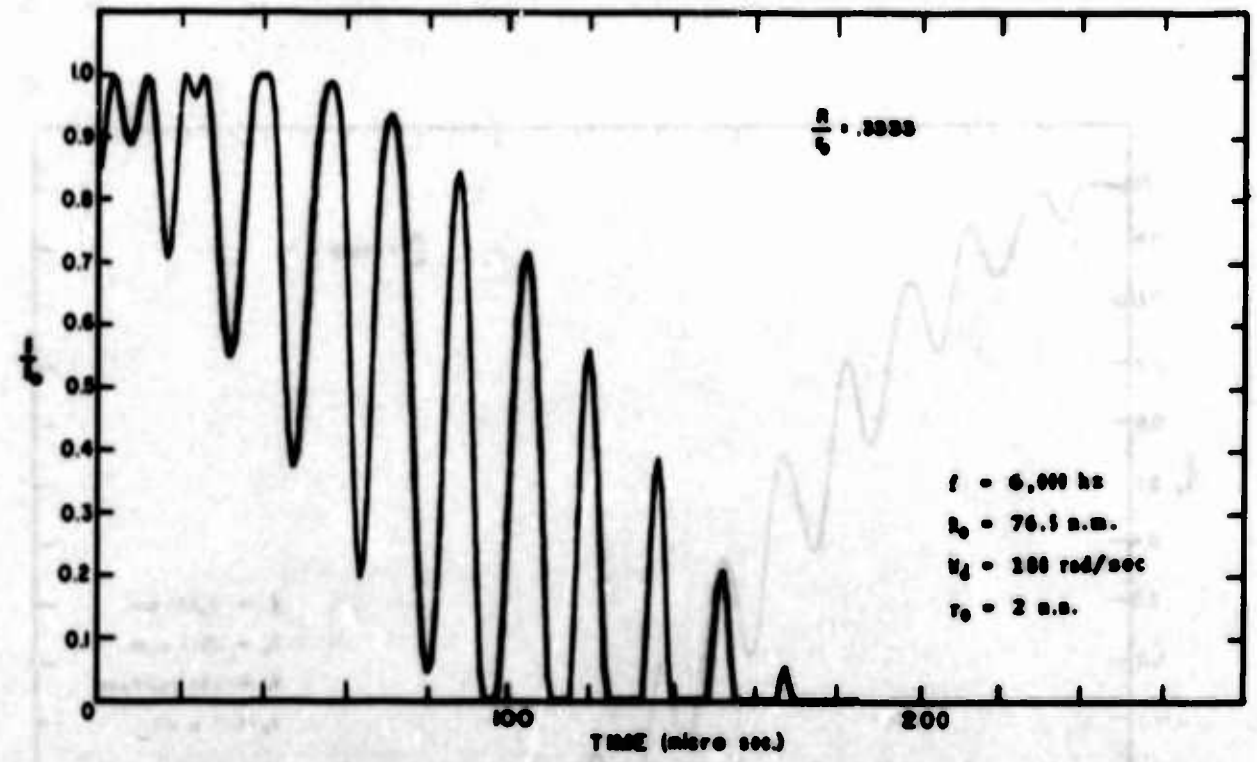

Figure 61. Light Intensity Observed by Scanning a Convecting Helical Arc

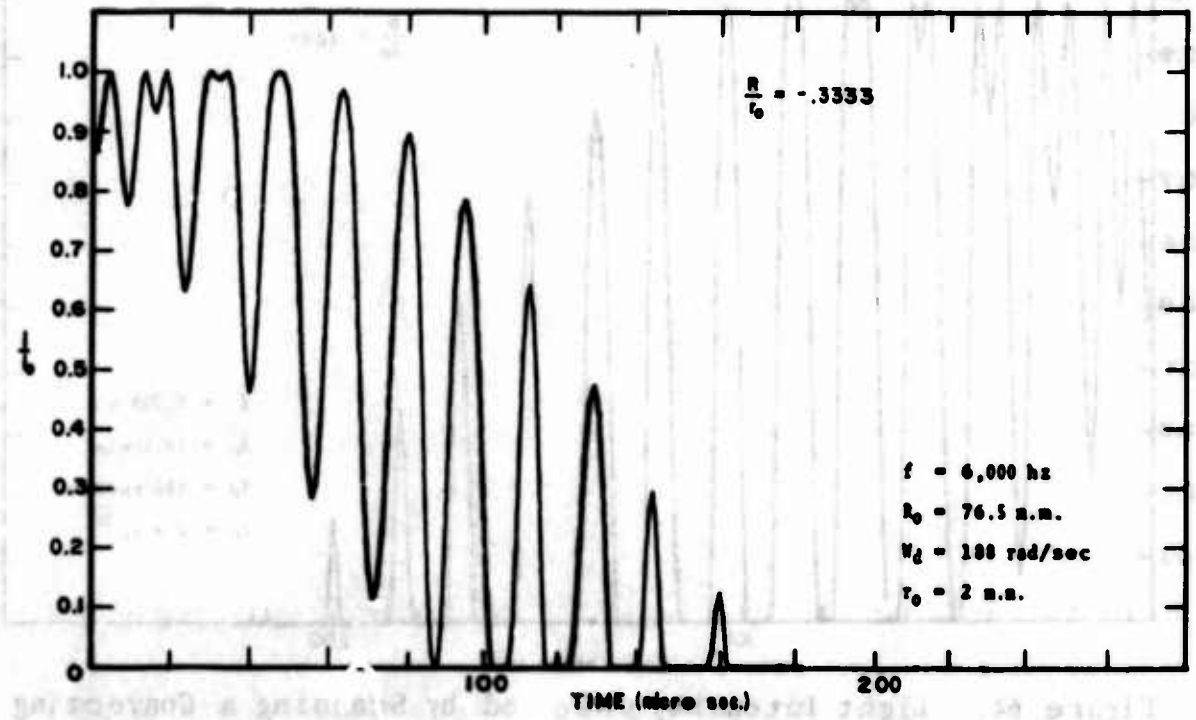

Figure 62. Light Intensity Observed by Scanning a Convecting Helical Arc

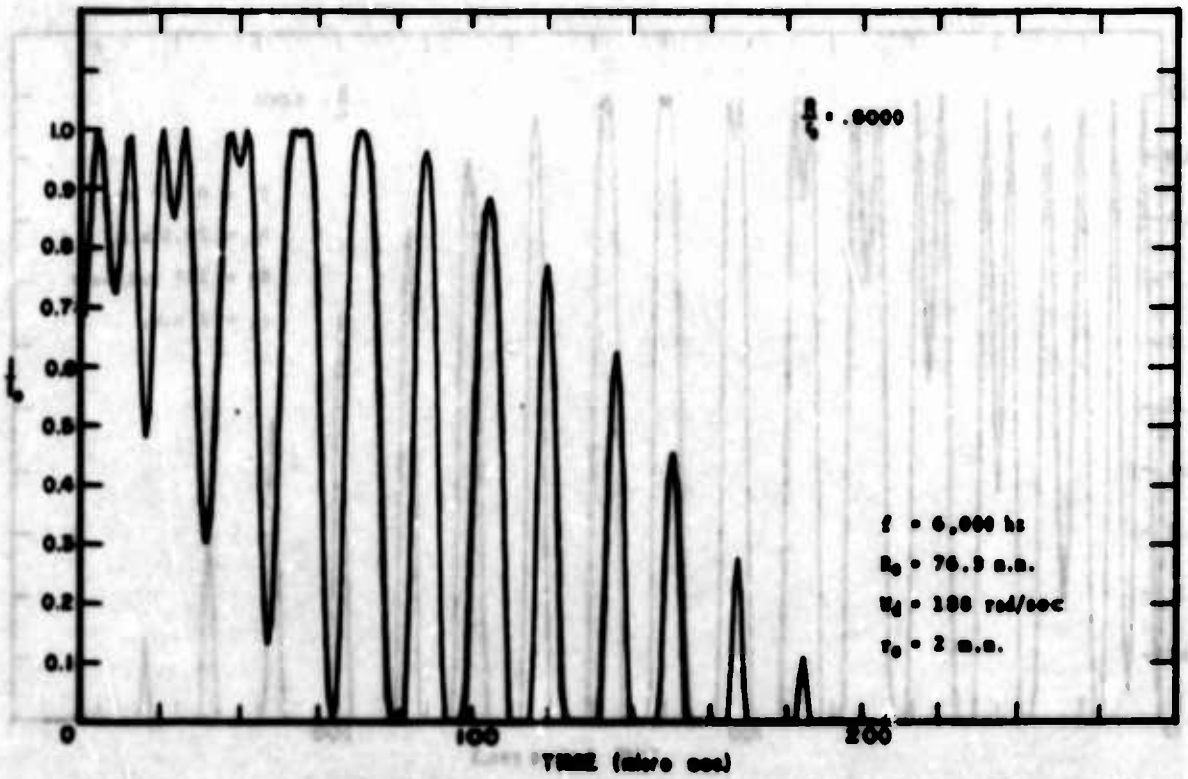

Figure 63. Light Intensity Observed by Scanning a Convecting Helical Arc

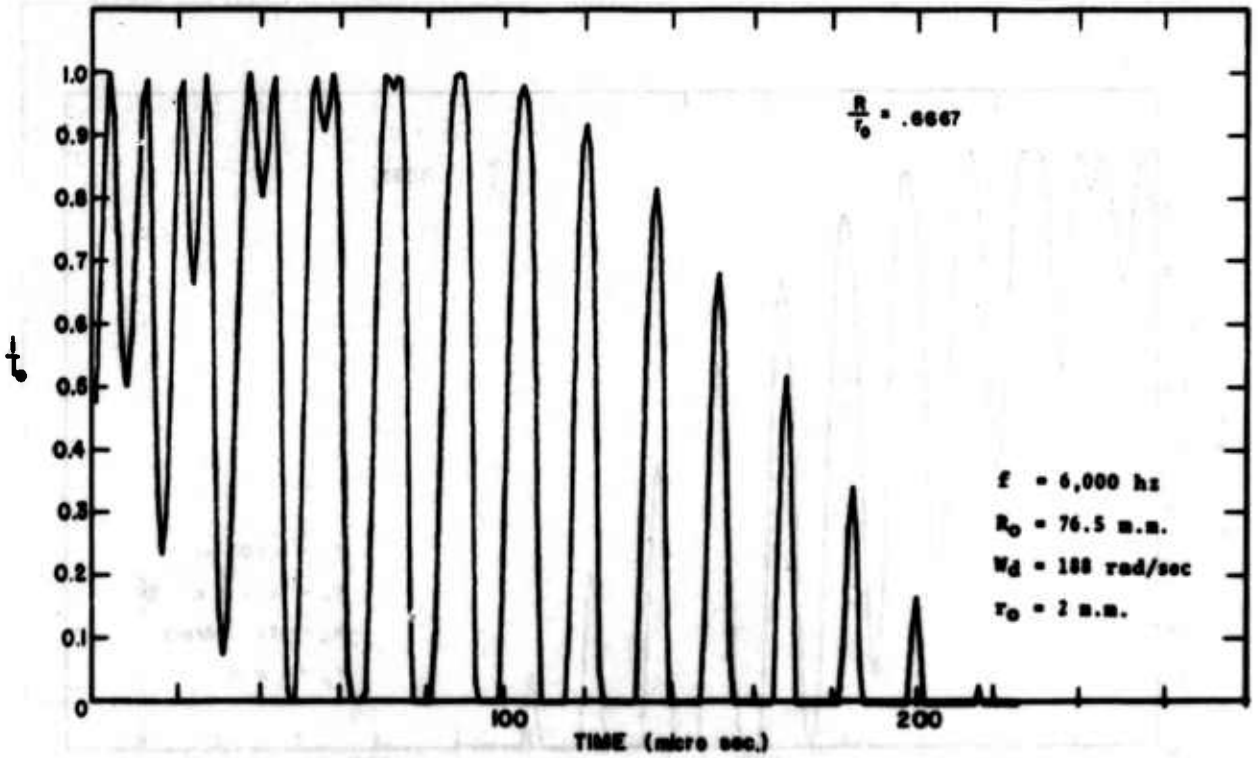

Figure 64. Light Intensity Observed by Scanning a Convecting Helical Arc

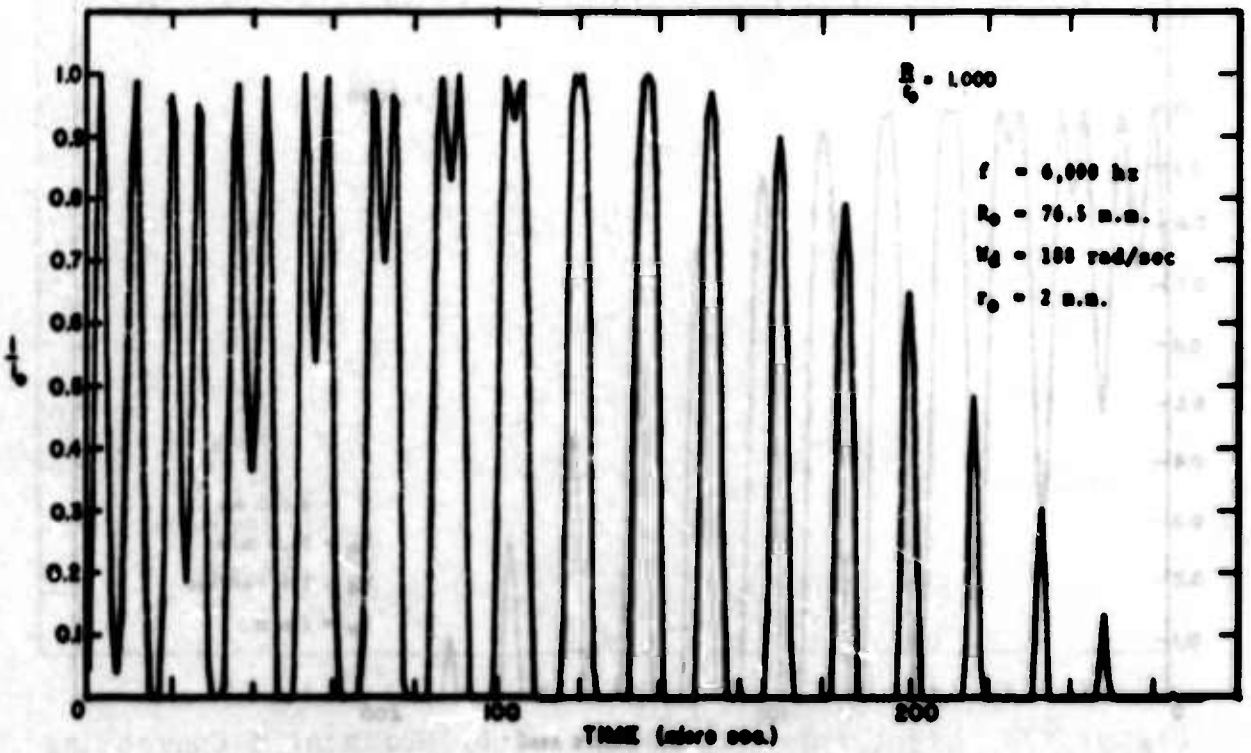

Figure 65. Light Intensity Observed by Scanning a Convecting Helical Arc

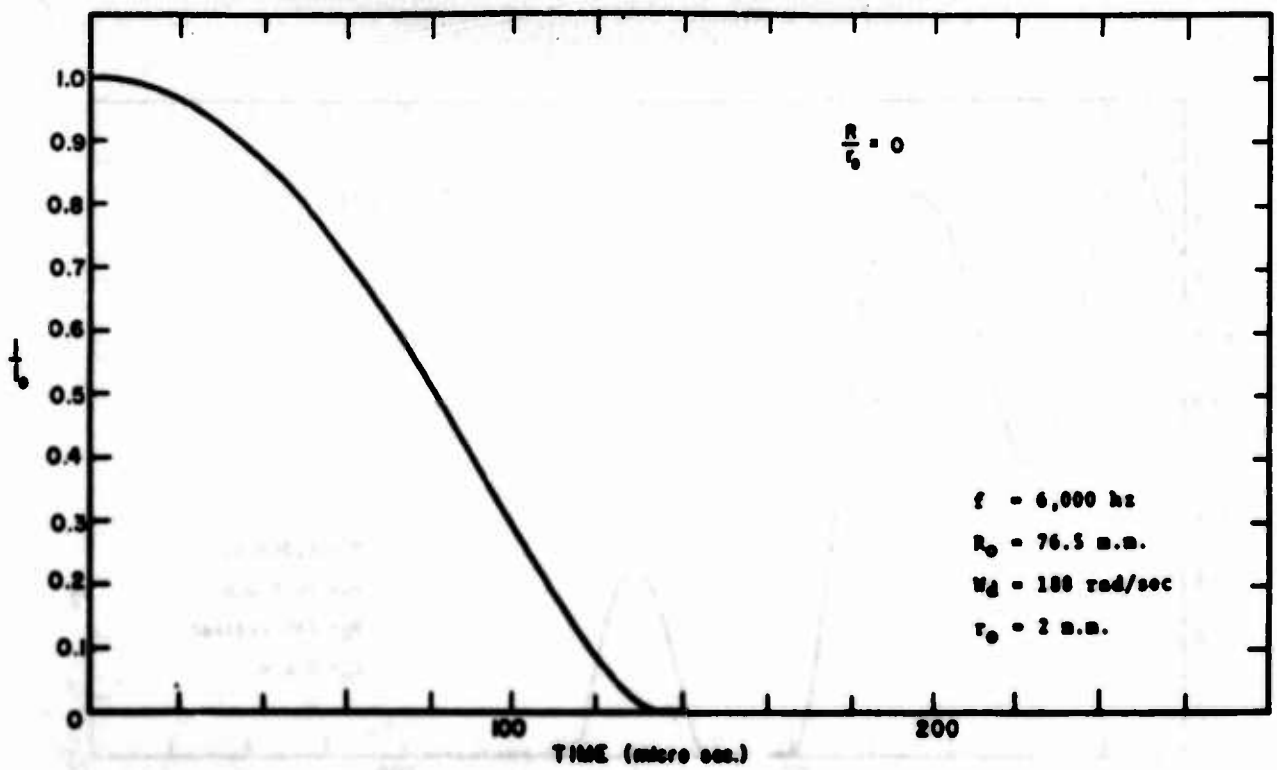

Figure 66. Light Intensity Observed by Scanning a Convecting Helical Arc

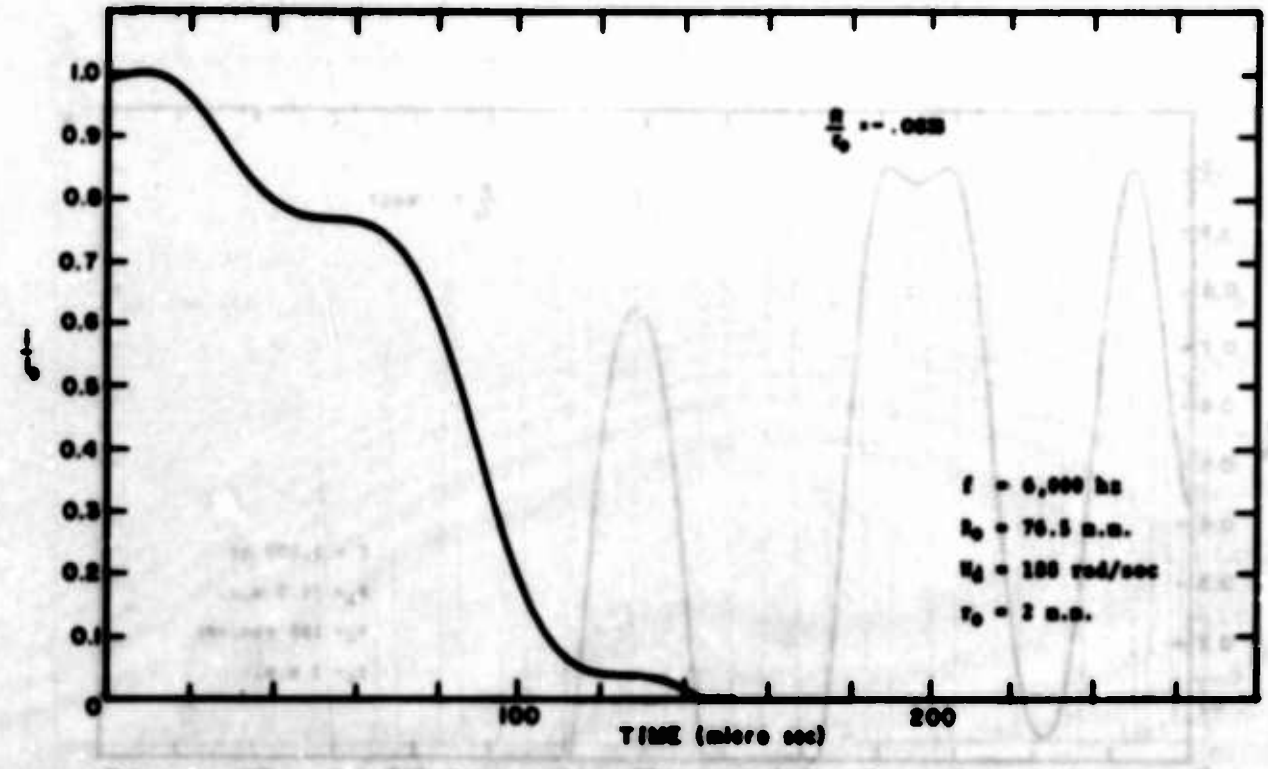

Figure 67. Light Intensity Observed by Scanning a Convecting Helical Arc

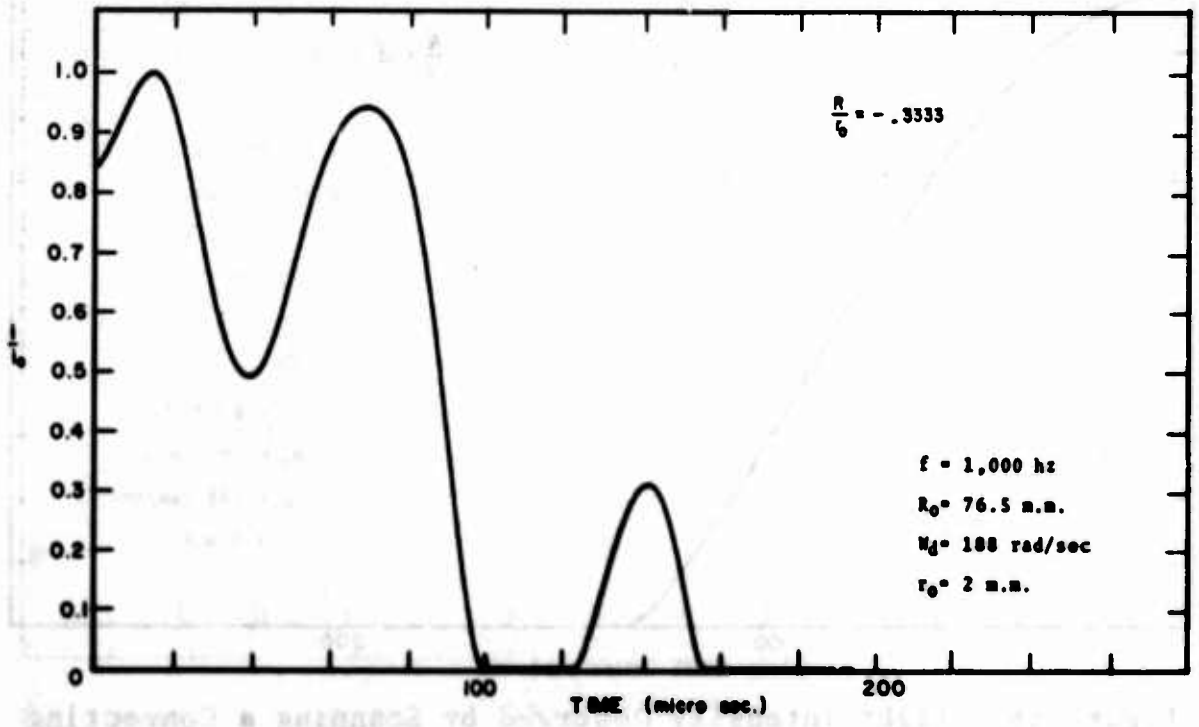

Figure 68. Light Intensity Observed by Scanning a Convecting Helical Arc

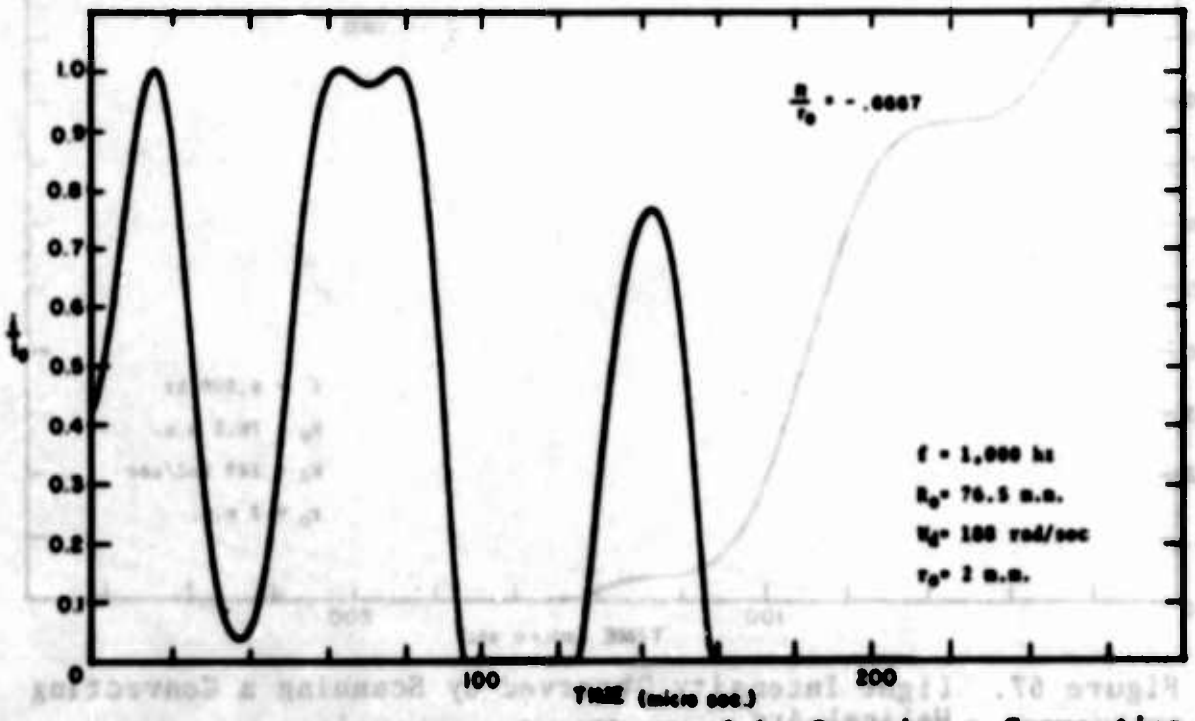

Figure 69. Light Intensity Observed by Scanning a Convecting Helical Arc

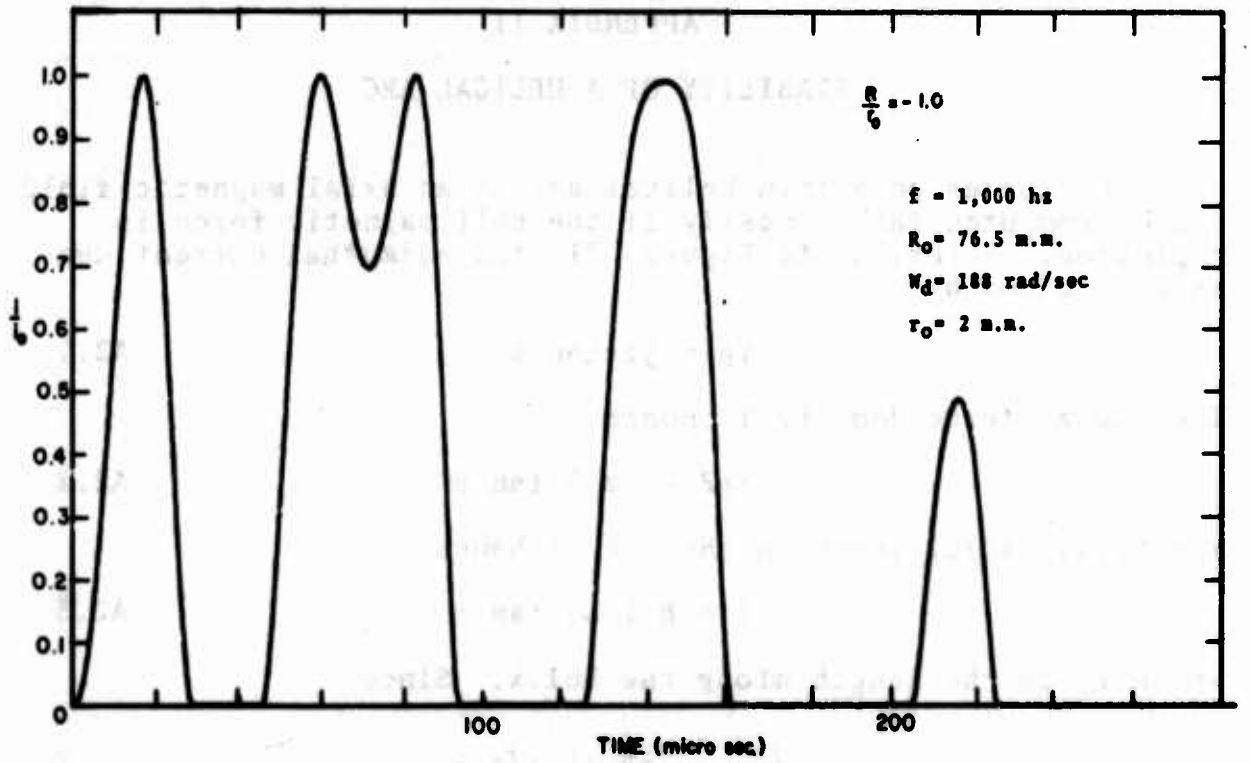

Figure 70. Light Intensity Observed by Scanning a Convecting Helical Arc

APPENDIX II

STABILITY OF A HELICAL ARC

The forces on a thin helical arc in an axial magnetic field can be computed rather easily if the self magnetic force is neglected. Referring to Figure 71 the azimuthal current density is given by

$$j_\theta = jz \tan \theta \qquad \text{A2.1}$$

The radial force density is hence

$$j_\theta B = jz\ B \tan \theta \qquad \text{A2.2}$$

The total radial force on the arc is hence

$$F = B\ I\ L, \tan \theta \qquad \text{A2.3}$$

where L_2 is the length along the helix. Since

$$L_2 = L \left\{1 + \left(\frac{2\pi R}{\lambda}\right)^2\right\}^{1/2} \& \tan \theta$$

$$= \frac{2\pi R}{\lambda} \qquad \text{A2.4}$$

the total force outward on the arc is

$$F_o = 2\pi \frac{B\ I\ L\ R}{\lambda} \left\{1 + \left(\frac{2\pi R}{\lambda}\right)^2\right\}^{1/2} \qquad \text{A2.5}$$

The restoring inward force due to the gas spin can be computed for a discontinuous density model arc. If the density in the arc is ρ_A and the outside density is ρ where the density change takes place at an "arc radius" of γ_A then the radial inward force on the arc is

Mass defect x centripetal acceleration

$$F_i = (\rho - \rho_A)\ \pi \gamma_A^2\ L_1 \frac{v^2}{R} \qquad \text{A2.6}$$

where v is the average gas spin velocity at the radian position R.

$$F_i = (\rho - \rho_A)\ \pi \gamma_A^2 \frac{v^2}{R} L \left\{1 + \left(\frac{2\pi R}{\lambda}\right)^2\right\}^{1/2} \qquad \text{A2.7}$$

For stability, the following inequality must hold

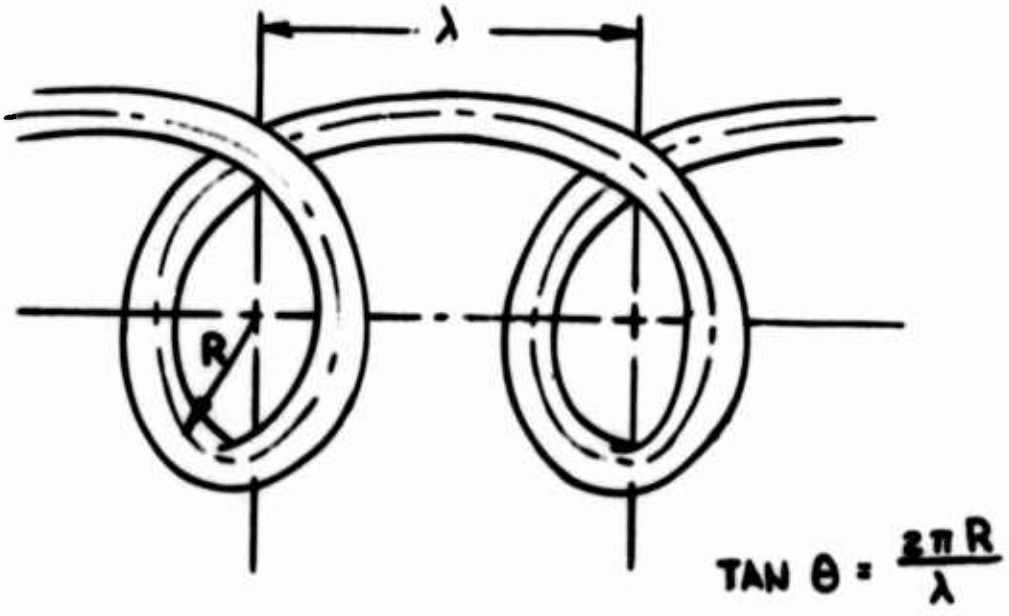

Figure 71. Helix Geometry for Computing Radial Force on the Arc in an Applied Magnetic Field

$$\frac{2\pi B\ I\ L\ R}{\lambda}\ \left[1 + \left(\frac{2\pi R}{\lambda}\right)^2\right]^{1/2} \leq (\rho - \rho_A)\ \pi \gamma_A^2\ \frac{v^2 L}{R_2}$$

$$\left\{1 + \left(\frac{2\pi R}{\lambda}\right)^2\right\}^{1/2} \qquad \text{A2.8}$$

or

$$\frac{BI}{\lambda} \leq (\rho - \rho_A)\ \left(\frac{\pi \gamma_A^2}{\pi R^2}\right)\ v_R^2 \qquad \text{A2.9}$$

This derivation is essentially the same as that given in Reference 11.

REFERENCES

1. Painter, J.H. and J. Ehmsen, "Development of a High Performance Arc Heater for Ground Testing Advanced Strategic Re-entry Vehicle Components," McDonnel Douglas Research Laboratories Report 71-1 Presented at the 6th Aerodynamic Testing Conference of the American Institute of Aeronautics and Astronautics, Albuquerque, New Mexico, 10-12 March 1971.

2. Smith, R.T. and J. L. Folck, "Operating Characteristics of a Multi-Megawatt Arc Heater Used with the AFFDL Fifty Megawatt Facility," Proceedings of the 15th Annual Technical Meeting, Institute of Environmental Sciences, 1969, pp 281-294.

3. Richter, R., "Ultra-High Pressure Arc Heater Studies," AECD TR 69-180, September 1969, Arnold Engineering Development Center, Arnold Air Force Station, Tennessee.

4. Richter, R., "Ultra-High Pressure Arc Heater Studies, (Phase III)," AEDC TR 70-106, March 1970, Arnold Engineering Development Center, Arnold Air Force Station, Tennessee.

5. Harder, R.L. and G. L. Cann, "Correlation of High Pressure Arc Heater Results," AIAA Journal, Vol. 8, No. 12, December 1970, pp 2220-2225.

6. Marlotte, G.L., G. L. Cann, R. L. Harder, "A Study of Interactions Between Electric Arcs and Gas Flows," ARL Report 68-0049, March 1968, Thermomechanics Research Laboratory, Aerospace Research Laboratories, Wright-Patterson Air Force Base, Ohio. (AD #673368)

7. Man Chuan Yuen, "Stability of a Poiseville Plasma Arc in an Axial Magnetic Field," Physics of Fluids, June 1966.

8. Hall, M.C., "The Structure of Concentrated Vortex Cores," Royal Aircraft Establishment, Technical Memorandum Aero. 869.

9. Alfven, Honnes, "Gas Insulation of a Hot Plasma," Nature No. 4753, 3 December 1960, p 801.

10. Piekaar, H.W., and R. W. Polman, "An Experimental Investigation of a Wall Jet in a Torus." FOM-Instituut voor Plasma. Fysica I.R. 69/024.

11. Morris, J.C., and G. M. Yos, "Radiation Studies of Arc Heated Plasmas," Aerospace Research Laboratories Report ARL 71-0317. (AD #740570)

12. Yos, G.M., "Transport Properties of Nitrogen, Hydrogen, Oxygen, and Air to 30,000°K," AVCO RAD Division, Report RAD-TM-63-7, 22 March 1963.